MSc Thesis Report

Electrochemical Reduction for Metal Recovery in Water Treatment: A Novel Approach

Akhilesh Soodan

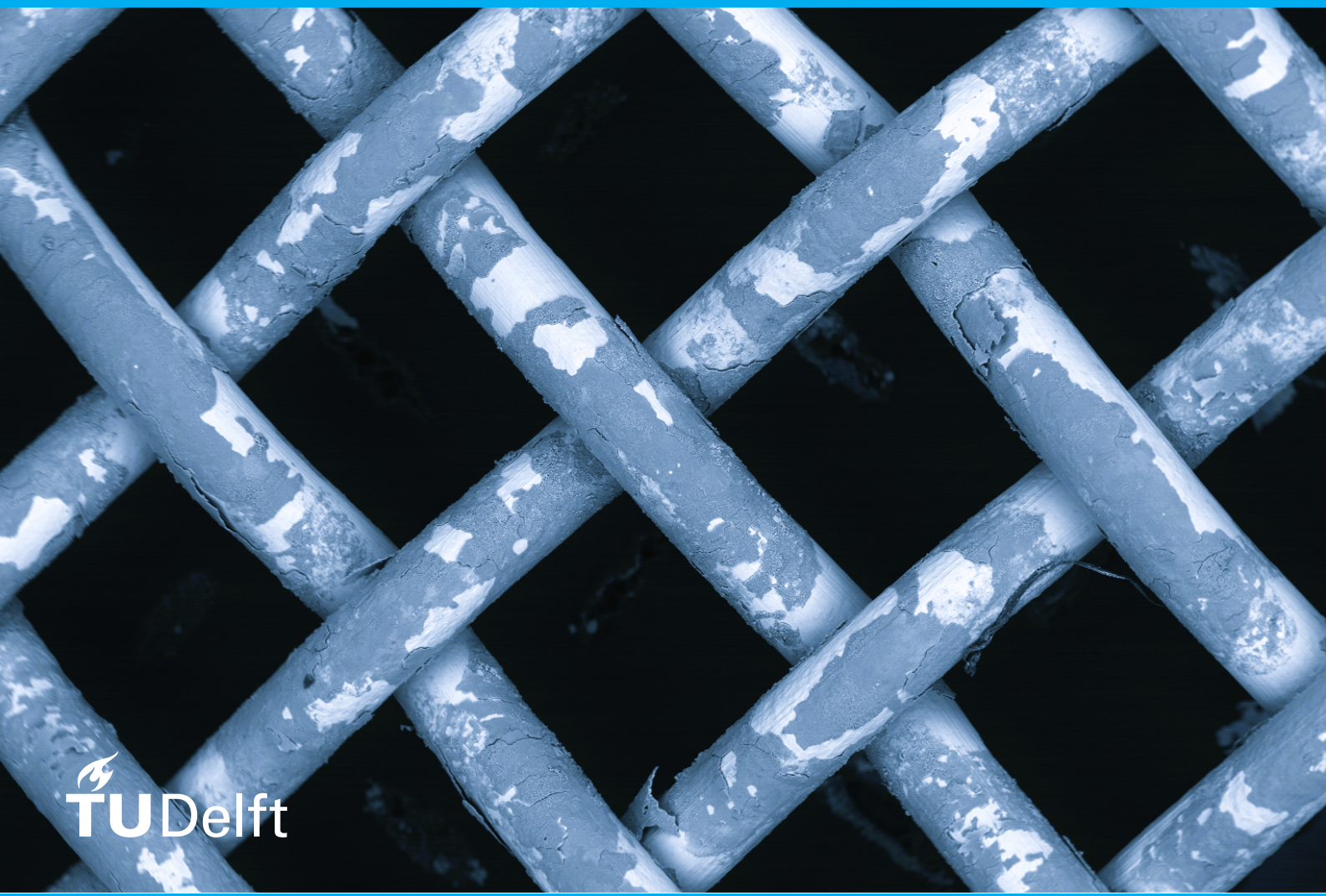

TU Delft

MSc Thesis Report

Electrochemical Reduction for Metal Recovery in Water Treatment: A Novel Approach

Submitted by:

Akhilesh Soodan
Student Number: 5594758
MSc Civil Engineering
(track- Environmental Engineering)
Defended on 22nd August 2023

Supervisors:

Prof. dr. ir. Doris van Halem (Chair)
Dr. ir. Ralph Lindeboom (External Supervisor)
Ir. Erik Kraaijeveld (Daily Supervisor)

TU Delft

Contents

Acknowledgements

This report encapsulates the culmination of extensive research and efforts towards the MSc thesis study of *'Electrochemical Reduction for Metal Recovery in Water Treatment: A Novel Approach.'* This thesis represents an important milestone in the attainment of a Master's in Science in Civil Engineering (track-Environmental Engineering).

The thesis journey can sometimes feel surreal as we get immersed in the lab experiments, disconnected from the bustling world outside. The ups and downs of this thesis experience have taught me the importance of resilience, adaptability, and the ability to embrace both success and failure as integral parts of the learning process. Moreover, it is important to acknowledge that such a journey cannot be undertaken alone. The support, guidance, and collaboration of numerous individuals play a pivotal role in shaping the outcome of the research. I would like to express my sincere gratitude to many influential individuals who have played a significant role in the completion of my thesis.

Throughout this arduous yet rewarding experience, the guidance of my esteemed thesis advisor and chair of the committee, Prof. dr. ir. Doris van Halem, has been indispensable. Her profound knowledge and insightful guidance helped steer me through this study's intricacies, fostering my intellectual growth and pushing me to surpass my limitations. Her unwavering commitment to academic excellence and continuous encouragement for my success was vital.

I am also deeply grateful to Dr. ir. Ralph Lindeboom for agreeing to become my external supervisor. I appreciate his valuable perspectives and expertise during our discussions on my thesis topic.

I have a special appreciation for ir. Erik Kraaijeveld (EngD), who played a crucial role throughout my thesis journey. Erik's dedication, expertise, and support made him an invaluable ally throughout this academic endeavor. He was always available to discuss ideas, brainstorm approaches, and provide guidance, even during the most demanding times. His passion for the field and genuine interest in my work were motivating and inspiring. His friendship and personal touch helped in making this journey more rewarding.

I would also like to thank the TU Delft WaterLab staff for their support throughout the project.

I would also like to extend my heartfelt thanks to my friends and family for their support throughout this journey. Their encouragement, confidence in my abilities, and willingness to lend an empathetic ear during this thesis's ups and downs have given me the strength to persevere. Finally, I would like to acknowledge the support of my partner, Mitali. Her constant presence has made the challenging moments less daunting and the joyous moments even more fulfilling.

I am indebted to these individuals for their contributions and support, without which this thesis would not have been possible.

Abstract

0.1. Highlights

- Fe^{2+} and Mn^{2+} were reduced electrochemically, while no electrochemical reduction was observed in the case of Al^{3+}, showing selectivity of the removal process.
- The electrochemical reduction process strongly depends on the pH, with depositions on the cathode increasing with increasing pH.
- Performance of electrochemical reduction declined with the increasing volume of water treated.
- Faradaic efficiency for removal of metal ions is higher in the water matrices with one type of metal ion than in water matrices with all three types of metal ions mixed simultaneously.

Groundwater is an essential source of drinking water, and it often contains contaminants in the form of dissolved metal ions that pose health risks and affect its suitability for consumption. Removal of these contaminants by conventional treatment methods, such as oxidation and filtration, results in additional treatment steps for managing sludge. New techniques are needed to prevent the formation of low-value sludge and provide better control over the drinking water treatment process. This study focused on understanding the mechanistics of electrochemical reduction for its utility as a groundwater treatment method. It was done by passing artificial groundwater containing dissolved metal ions Fe^{2+}, Mn^{2+}, and Al^{3+} through a stainless steel cathode in an electrochemical cell. It resulted in the removal of these ions through electrochemical reduction and the recovery of metals as deposits. The experiments were performed with very high metal ion concentrations (0.72 mmol/L) to obtain clear and noticeable results from their electrochemical reduction.

It was observed that while Fe^{2+} and Mn^{2+} were removed from the water and deposited on the cathode, Al^{3+} did not get electrochemically reduced. It was due to the system settings adopted for the study being unsuitable for Al^{3+} removal. It highlights the potential of electrochemical reduction as a selective treatment process that offers control by manipulating the system settings. Up to 51.4% removal was observed in Fe experiments, while for Mn experiments, up to 22.22% removal was observed. As the deposits grew with the volume of water treated during an experiment, the electrochemical reduction declined. The removal of metal ions from water became negligible when the volume of water treated reached 6.3 L. It was due to the decrease in the effective surface area of the cathode because of deposits and the changing water composition near the cathode, as the volume of the water treated was increasing, since it was detrimental to the transfer of electrons from the cathode to the dissolved metal ions. It was also observed that the voltage rises continuously as the water is treated, due to increasing cell resistance.

Another observation was that the pH of the water matrix is an essential factor in the electrochemical reduction of the species, with cathodic depositions increasing as the pH increases. Fe depositions increased 5.8 times from 0.109 μm at pH 4 to 0.630 μm at pH 7, while Mn at pH 4 had negligible deposits, which rose to 0.213 μm at pH 7. As the pH decreases, the entropic barrier of H^+ ions decreases, leading to H_2 production and a decline in FE. Further, it was observed that the electrochemical reduction performs better when a water matrix has only one type of metal ion (individual) instead of a water matrix with all three types of metal ions simultaneously (combined). The FE of Fe^{2+} ions in the individual case is 35.05% while it is 11.5% in combined, at pH 7. It is 14.90% for Mn^{2+} in individual and 1.75% in combined. This could be from the decreased availability of the free metal ions in the combined case - due to the formation of bonds between the ionic species and changes in the thermodynamic feasibility of electrochemical reduction resulting from changes in the water matrix composition.

Further investigations are required to check performance with natural groundwater samples, optimize the system settings and find cathode material that best fits the desired contaminant removal.

0.2. Graphical Abstract

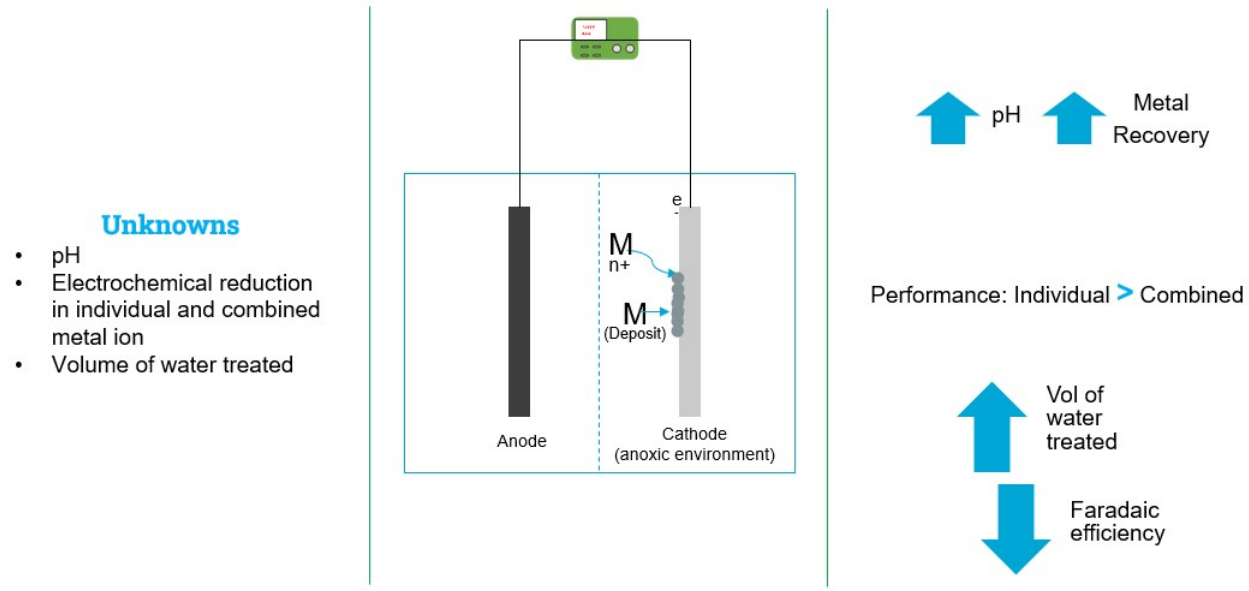

Figure 1: Graphical abstract of the study

List of Figures

List of Tables

Abbreviations

Al : Aluminum

As : Arsenic

Cd : Cadmium

DO : Dissolved Oxygen

E : Cathodic Potential

F : Faraday constant

FE : Faradaic Efficiency

Fe : Iron

ΔG : Gibbs free energy change

HRT : Hydraulic Retention Time

I : Cathodic Current

i : Current density

m : Mass of the deposit

Mn : Manganese

O : Oxygen

Pt: Platinum

Q : Flow rate

q : Charge dosage

SEM-EDS : Scanning Electron Microscopy - Energy Dispersive Spectroscopy

SHE : Standard Hydrogen Electrode

V : Voltage

1 Introduction

1.1. Groundwater as a source of drinking water

Water security, that is accessibility to affordable, abundant, and clean water for day-to-day activities is a necessity for every individual on earth and has been incorporated as a part of important global goal - 'Clean Water and Sanitation for All' (SDG 6) under the United Nations' Sustainable Development Goals 2030 (United 2023). While great developments have been made recently in the drinking water sector with 74% of the world's population now having access to safely managed drinking water services (UNESCO 2022), the fight for global access to clean drinking water is long and gets progressively difficult with rising population and climate change, putting stress on the potable water sources. According to estimates, just 3% of the total amount of water on Earth is freshwater, and only 0.5% of that freshwater can be utilized for human consumption with the rest of the water being stored in glaciers, ice caps, atmosphere, and soil (USBR.gov 2023). Groundwater is an important component of freshwater and a source of drinking water for at least 50% of the world's population (Deltares 2022).

The groundwater may contain many impurities either due to anthropogenic sources or naturally because of the interaction of water with rocks in the aquifer, impacting the general geochemistry. The concentrations of these impurities often exceed recommended values for potability and general use, resulting in widespread health and acceptability problems. As per previous studies, nine major species: HCO_3, Na, Ca, SO_4, Cl, NO_3, Mg, K and Si invariably make up over 99% of the solute content of natural waters at pH 7 (Appleton et al. 1996). Alongside this, there are minor and trace elements, under 1% of the total, such as Arsenic (As), mercury (Hg), zinc (Zn), cadmium (Cd), nickel (Ni), copper (Cu), chromium (Cr) and lead (Pb); which could be present in groundwater as a result of natural and man-made leaching processes. Although present in very low amounts in water, trace elements are extremely hazardous and can result in serious health issues for living organisms including cancer (Qasem et al. 2021). Further, man-made activities have led to the leaching of chemicals such as organic solvents and organic micro-pollutants, causing severe groundwater contamination.

Iron (Fe) and manganese (Mn) minerals are extensively found in the rocks and soil, seeping into the groundwater through contact over a long period. Fe and Mn concentrations greater than 0.3 mg/L and 0.02 mg/L respectively, compromise the water's utility (WHO 2022). This results in a metallic taste of the water, discolouration, and staining of laundry and plumbing fixtures (McFarland & Dozier 2023). Exposure to Mn in drinking water has been associated with neurological issues and lack of coordination and movement control in infants and children (WQA 2022). Aluminum (Al) although not very extensively found in the groundwater, may be present in it due to exposure to aquifer bedrock containing Al-rich minerals or leaching of water from commercial activities such as construction. Al concentrations in groundwater have been known to frequently surpass the threshold for toxicity for aquatic life (Hart et al. 2021). Long-term exposure to high Al levels can cause illnesses in humans and has been hypothesized to result in cognitive impairment in the elderly (WHO 1997). The recommended drinking water limit for Al is less than 0.2 mg/L (EU 1998). Henceforth, humans' high dependence on groundwater and harmful constituents make groundwater treatment necessary before its safe consumption.

The water treatment industry utilizes a plethora of technologies in combined or standalone forms to treat Fe, Mn, and Al in groundwater before supplying it to households. Some of these established technologies include ion exchange, adsorption, chemical precipitation (Wołowiec et al. 2019), column filtration, pressure-driven membrane-based methods such as reverse osmosis, ultrafiltration and microfiltration, biofiltration, and electrochemical methods (Grimm et al. 1998). These technologies have been found to be effective in the removal of Fe, Mn, Al, and other harmful contaminants from the groundwater. However, since they require additional post-treatment steps such as sludge management for oxidation-based methods (chemical precipitation) (Ruj et al. 2021) and disposal of solid waste related to membrane-based treatment (Ezugbe & Rathilal 2020). This results in additional economic and environmental concerns that need to be taken into consideration while planning the treatment systems.

1.2. Electrochemical reduction as a groundwater treatment method

Electrochemistry as a field of study examines how electrical energy affects the chemical changes in the system. It deals with the interrelationship of the energy and movement of electrons with chemical reactions. Electrochemical methods for treatment are becoming widely popular due to their lower resource utilization, selectivity in removal, and flexibility offered as a result of the choices in electrode material and electrolytes, membrane system, and the potential supplied. In an electrochemical system, oxidation occurs at the anode resulting in the release of electrons consumed at the cathode surface, causing the reduction of species at the cathode (Ahmad 2006). The transfer of electrons between the electrodes- anode and cathode, occurs via an ionic conductor (electrolyte). The electrochemical treatment methods have been found to be effective for water treatment and are in the process of widespread adoption in the drinking and waste-water treatment industry. Electrocoagulation has been efficient in various drinking water treatment processes such as pathogen reduction (Ghernaout et al. 2019), arsenic removal (van Genuchten et al. 2012) and coagulation processes (Vik et al. 1984). Electrodialysis has been used widely for desalination and works well in removing inorganic ions such as nitrates, bromides, As, as well as recovering proteins from the waste streams (Tufano & Fendorf 2008). Electrochemical advanced oxidation process offers a unique way of ·OH radical production, a powerful oxidant, by using an electron as a reagent and, therefore, foregoing the requirement of adding expensive chemicals such as H_2O_2, O_3 when providing advanced oxidation treatment (Sirés et al. 2014).

However, it is essential to explore more tenets of electrochemistry that can be successfully exploited for efficient and sustainable water treatment. One such method could be electrochemical reduction. In electrochemical reduction, the chemical species in the cathode chamber are reduced as a consequence of the transfer of electrons from an external source in the form of electrical energy, resulting in the conversion of the chemical species into a different product (Cambridge nd). Therefore, an electron is the reducing agent in the process. Previous research on electrochemical reduction has shown potential benefits in its usage for drinking water treatment processes. It has been proven to remove bromate ions (BrO_3^-), a carcinogenic by-product of disinfection by ozonation, from water at a low pH (Kishimoto & Matsuda 2009). It has also shown good results in the removal of chlorine and bromine-containing haloacetic acids (Korshin & Jensen 2001). By coupling this process with biological treatment, it has been shown to effectively remove antibiotics metronidazole and dimetridazole (Zaghdoudi et al. 2017). Cathodic reduction of nitrates from water has also been observed in the case of zero-valent titanium electrodes (Yao et al. 2019).

Using electrochemical reduction as a treatment method offers the distinct advantage of the recovery of materials such as pure metal and metal hydrides. Groundwater rich in metal ions when passed to the cathode will result in the reduction of the metal ions, causing the deposition of metals on the cathode (Jartych et al. 2002). The electrochemical reduction method can be used to selectively target contaminants by modulating the cathode potential and current settings in the system. It can provide more control over the drinking water treatment process since the treatment system can be monitored and adjustments can be made for a targeted removal. Another important advantage that this method offers is that no sludge is produced at the cathode compared to anode-based oxidation methods. This can help make the water treatment process more sustainable and affordable since fewer resources are utilized to dispose off the harmful sludge. Further, the recovered metals and metal oxides such as Fe from groundwater can be used for forthcoming water treatment steps such as coagulation and removal of BrO_3^- (Xie & Shang 2006). The electrochemical reduction

method can be particularly efficient in directly targeting harmful chemical species such as As, Co, $PO_4{}^{3-}$ in the groundwater by applying specific potentials, which will result in the reduction of the metal ions.

In order to electrochemically reduce a chemical species- metals Fe, Mn, and Al in this study, a reduction potential, E is applied to a cathode. This can be done by supplying a sufficient negative current (I, A or C/s) to the cathode from an external DC power supply. Given the study is from a drinking water treatment point of view, instead of focusing on E, the parameters of interest are the charge dosage (q, C/L) which is the total charge applied per litre of the electrolyte, the current density (i, A/m^2) - the current (I) applied per unit area of the electrode surface, and the mass of the reduced chemical species deposited on the cathode (m, g). q can be calculated with the help of the flow rate Q (L/s) of the cathode-water and is given by:

$$q = \frac{i}{Q} \tag{1.1}$$

The amount of deposition on the cathode is given by:

$$m = \frac{qM}{nF} = \frac{ItM}{nF} \tag{1.2}$$

where t is the time of electrochemical reduction (s), M is the molar mass of the chemical species to be reduced (for instance, M for Fe = 55.85 g/mol and Mn = 54.94 g/mol), F is the Faraday constant (96,485 C/mol), n is the number of electrons transferred (Fe/Mn = 2, Al = 3).

It can be inferred that the electrochemical reduction process can play a multi-faceted role at different steps of the drinking water treatment process and offers distinct advantages in terms of control over the treatment process, low sludge production, and recovery of materials of value.

1.3. Problem and Research approach

While electrochemical reduction can potentially be an asset in the drinking water treatment processes, its performance in terms of the cathodic reduction of the chemical species is dependent on a large number of variables. Table 1.1 enlists the variables which are associated with the electrochemical reduction process (Bard & Faulkner 1980). The high number of unknowns makes it difficult to predict the behaviour of the electrochemical reduction process.

Component	Variables
Electrode	Material Surface area (A) Geometry Surface condition
External	Temperature (T) Pressure {P) Time (t)
Mass transfer	Mode (diffusion, convection, etc) Surface concentrations Adsorption
Electrical	Potential (E) Current (i) Charge dosage (q)
Solution	Bulk concentration of electroactive species (Co, cR) Concentrations of other species (electrolyte, pH,...) Solvent

Table 1.1: Variables affecting electrochemical reduction reaction. (Bard & Faulkner 1980)

Therefore, in order to utilize the electrochemical reduction process method for drinking water treatment processes, more research on the factors impacting its performance is required. This will help in establishing control over the process and achieve the standardization required for commercial water treatment activities. While Table 1.1 enlists many variables, the scope of this study is limited to decluttering three important unknowns which impact the performance of electrochemical reduction. These include the influent feedwater pH, ionic composition of the water matrix, and the volume of water treated. In order to do this, experiments are conducted to remove Fe^{2+}, Mn^{2+}, and Al^{3+} metal ions from artificial groundwater. The recovery of metals by electrochemically reducing these metal ions is analyzed with the electrochemical cell running continuously to treat 6.3 L water. The water matrix is altered by changing the pH, and by changing the ionic composition - firstly by electrochemically reducing a single type of metal ion (individual experiments) and secondly by electrochemically reducing all three types of metal ions simultaneously (combined experiments).

The reactions occurring at the anode and cathode during electrochemical reduction of the metal ions considered in the study are given by:

Anode:

$$2H_2O \rightarrow O_2 \uparrow +4H^+ + 4e^- \tag{1.3}$$

$$2Cl^- \rightarrow Cl_2 \uparrow +2e^- \tag{1.4}$$

Cathode:

$$Al^{3+}(aq) + 3e^- \rightarrow Al(s) \tag{1.5}$$

$$Mn^{2+}(aq) + e^- \rightarrow Mn(s) \tag{1.6}$$

$$Fe^{2+}(aq) + 2e^- \rightarrow Fe(s) \tag{1.7}$$

$$2H_2O + 2e^- \rightarrow 2OH^- + H_2 \uparrow \tag{1.8}$$

The scope of this study is limited to the observations at the cathode side of the electrochemical cell. At the cathode, the electrons supplied for the reduction of a chemical are not completely utilized by the metal ions. A part of the electrons gets transferred to side reactions such as the formation of H_2 side reaction, which is undesirable. This partial utility of the electrons is the basis of Faradaic efficiency (FE), which is a measure of the selectivity of an electrochemical process. FE is the fraction of the total current (electrons) used towards getting the desired product and is calculated in the study using the equation:

$$FE\ (\%) = \frac{Charge\ dosage\ required}{Charge\ dosage\ supplied} \tag{1.9}$$

where the 'Charge dosage required' is calculated by finding the theoretical charge dosage which is required to remove a concentration of the metal (mol/L) that was actually removed by the electrochemical process and the 'Charge dosage supplied' is the actual charge dosage supplied externally resulting in the removal of the above-mentioned concentration.

Since the study is focusing on understanding the mechanistics of the electrochemical reduction process, the concentrations of the metal ions considered for the study are much larger than concentrations of these found in the environment. This way, it can be ensured that clear and noticeable results are achieved. As the concentrations chosen are extremely high, the metal ion removal at low pH can be a field of interest for the treatment of acid mine drainage water (Bigham & Nordstrom 2019). However, the scope of this study does not analyze this technique for application in acid mine drainage. Further, the economics involved in electrochemical reduction to remove the metal ions from water, and the usage of this method for the removal of harmful contaminants such as arsenic has been envisaged. Based on these experiments, recommendations are given to further develop the research and optimize the electrochemical reduction process for drinking water treatment.

1.4. Research Questions

The primary focus of this study lies in developing a profound understanding of the electrochemical reduction process. The study is defined with a broad research question which would further entail sub-questions for covering the objectives of the study. The main research question for the study deals with the aspect of the recovery of metals from the treatment of artificial groundwater by electrochemical reduction. The main research question is:

How can Fe, Mn, and Al be recovered from water through its treatment by an electrochemical reduction process?

Sub questions:

- What is the impact of pH on metal recovery?
- How does electrochemical reduction change with a change in the ionic composition of the water matrix?
- How is electrochemical reduction affected during the continuous operations, as the volume of water is treated?
- What are the energy and economic aspects associated with this method for its application in the drinking water treatment process?
- Can electrochemical reduction be utilized to remove harmful trace metals such as As, which can be of considerable importance?

The first two questions help in developing the understanding of the effect of the water matrix of the cathode feed water on the performance of the electrochemical reduction process. The third question tries to investigate if the experimental setup and apparatus have certain challenges when it comes to the treatment process. It will help in optimizing the system settings in the treatment plant for better removal of metal ions from water. The fourth question throws light into the commercial viability of this method so that the practical implications which will arise during the implementation of this method of treatment are well understood. The fifth question delves into theoretically expanding the utility of this method beyond this study.

2

Methodology

2.1. Experimental set-up

The setup consisted of an electrochemical cell containing a two-compartment electrolytic flow in a perspex frame with dimensions 20 cm X 5 cm X 2 cm (compartment volume: 200 cm^3), separated by a monovalent cation exchange membrane (CXM-200S), as shown in Fig 2.1. The anode chamber contained an anode of Ti mesh coated with IrO_2/RuO_2 (surface area: 100 cm^2), while the cathode chamber contained a stainless steel woven mesh cathode (surface area: 100 cm^2, wire dia 0.26 mm, mesh opening 0.586 mm, material AISI 316). The two electrodes were connected to a DC power supply (30V-3A TENMA 72-10500 bench DC power supply) via crocodile clip cables. The monovalent ion exchange membrane separated the two chambers, preventing the mixing of the anode and cathode solutions while allowing the flow of monovalent cations from the anodic side to the cathodic side. The setup contained a 25 L jerrycan as an anode-feed water tank, connected to a buffer tank to maintain a constant supply of anode-feed water. A peristaltic pump (Watson Marlow Q sci 323) pumped water from the anode feed water tank into the buffer tank and to the anode chamber. Cathode feedwater was kept in a 10 L vessel and directly supplied to the cathode chamber by a peristaltic pump. The cathode feed water was continuously stirred using a magnetic stirrer (Labinco). The effluent from the electrode chambers was directed to separate 25 L waste disposal jerrycans. The cathode feed water tank was kept in an anoxic state to mimic groundwater conditions in the cathode chamber and prevent interference from O_2 with the reduction reaction. The effluent from the cathode chamber was collected through a side duct for further analysis. At the cathode, along with the targeted reduced metal species, H_2 was produced as a side reaction. On the other hand, the anode facilitated the oxidation reaction, primarily resulting in the formation of O_2 and some Cl_2. The gases were not collected and analyzed.

The electrochemical cell used in this study has been previously used for electrochemical advanced oxidation processes experiments (Radjenovic et al. 2011; Rijsdijk 2022). Minor modifications have been made to it to facilitate investigations related to electrochemical reduction. The original set picture from the lab is in the Appendix (1).

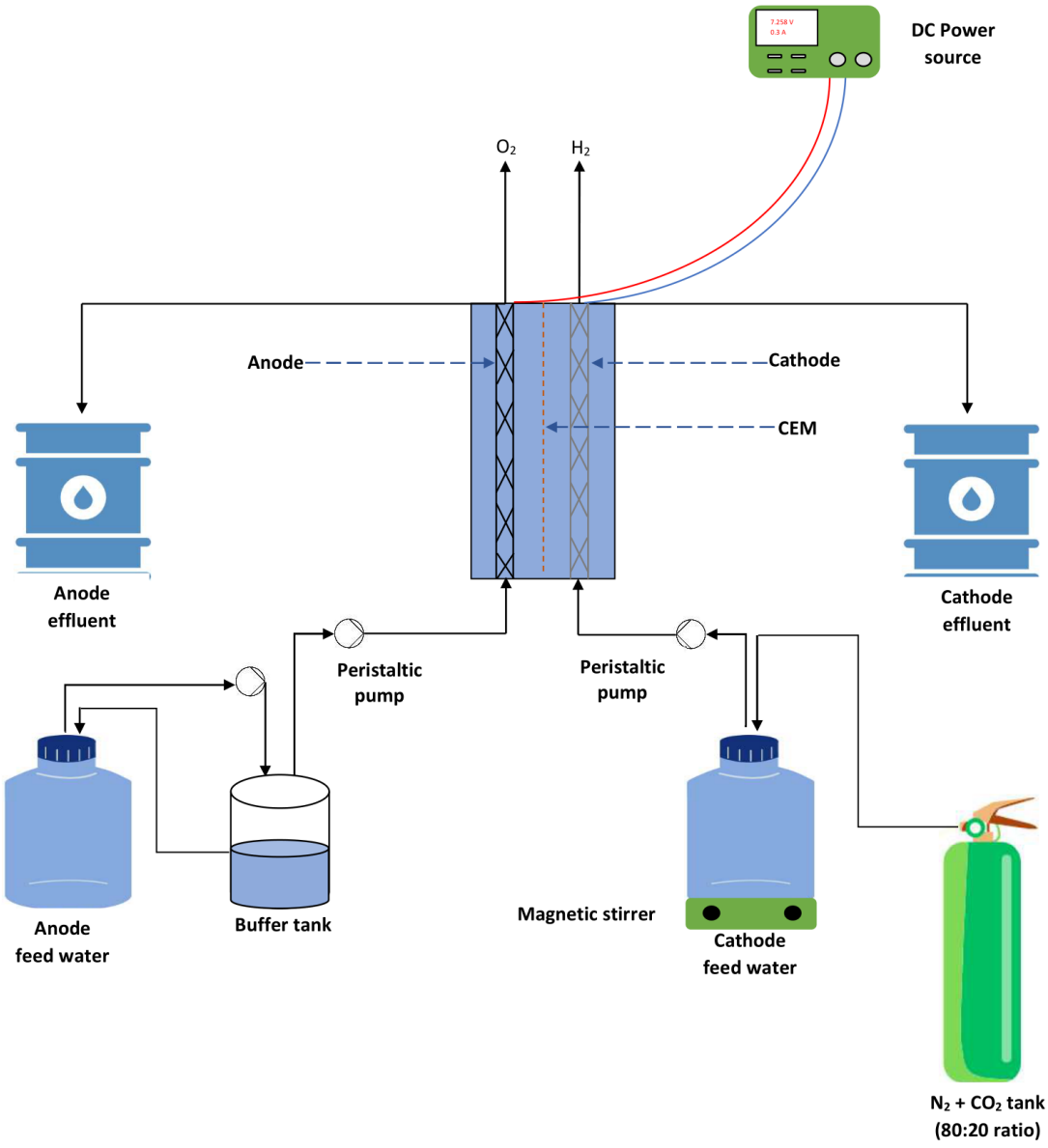

Figure 2.1: Experimental setup for the electrochemical reduction experiment

2.2. Experimental Procedure

2.2.1. Establishing system settings

Given the experimental setup is a flow-through system, a pump curve was made to find the relation between the rpm of a pump and desired flow rate (Fig 36 in the Appendix 5.2). A series of experiments were performed to find an optimal charge dosage and current density at which considerable differences in a metal's influent and effluent concentrations were observed. The associated results of these experiments are available in the Appendix (section .11). Post initial experiments, the following set of settings were adopted for all future experiments:

System Setting	Value
Charge Dosage (C/L)	200
Current Density (A/m^2)	30
Flow rate (L/h)	5.4
HRT (minutes)	2.22
Temperature (C)	19
pH range	4-8

Table 2.1: System settings

2.2.2. Individual and combined experiments

After establishing the system settings, the experiments were carried out in a phased manner, comprising of individual and combined experiments as mentioned in table 2.2.

Experiment	Fe (mmol/L)	Mn (mmol/L)	Al (mmol/L)	System Settings
Individual 1	0.72	-	-	200 C/L, 30 A/m2, pH 4-8
Individual 2	-	0.72	-	200 C/L, 30 A/m2, pH 4-7
Individual 3	-	-	0.72	200 C/L, 30 A/m2, pH 4-6
Combined	0.72	0.72	0.72	200 C/L, 30 A/m2, pH 4-7

Table 2.2: Schematic diagram of the experiments performed during the study.

The step-wise methodology of the experiments is presented in Fig 2.2. The experimental process consisted of first preparing anode feed water and cathode feed water. Anode feedwater was prepared taking demineralized water and adding NaCl as an electrolyte and $NaHCO_3$ as a pH buffer. Cathode feedwater was prepared using ultrapure water and NaCl as an electrolyte and $NaHCO_3$ as a pH buffer, which was then anoxic. The metal sulfates- $Fe_2SO_4.7H_2O$, $Mn_2SO_4.H_2O$, $Al_2(SO_4)_3.14H_2O$, were added to the anoxic cathode feedwater individually or combined, depending on the experiment. This was done only once the dissolved oxygen (DO) of the cathode feed water was 0.1-0.2 mg/L. All the connections in the apparatus were checked, and the DC power supply was turned on at a low current density of 0.02 A/m^2. The water was then pumped into the cathode and the anode chambers of the electrochemical cell from the cathode and anode feedwater tanks, respectively. It was ensured that the water in both chambers was pumped at an equal rate to avoid pressure on the cation exchange membrane which may result in its displacement. Once the chambers were filled with water, the pump setting for the cathode was rechecked for the desired charge dosage of 200 C/L, and the current density in the DC power supply was set at 30 A/m^2. The electrochemical reduction of Fe^{2+}, Mn^{2+}, and Al^{3+} was performed for a volume of 6.3 L (with an equivalent time period of 70 minutes which is approximately 30*HRT). The samples were taken at numerous volumes of the influent of water treated. The volumes were: 0.63 L (at the the time equivalent to 3 * HRT), 1.26 L (6 * HRT), 2.52 L (12 * HRT), 3.15 L (18 * HRT), and 6.3 L (30 * HRT). The sampling above this time stamp was not taken due to the limited capacity of the cathode feed water tank. The collected samples were then analyzed. At each sampling point, the voltage was also measured to help form an estimate of the energy requirements to run the process and the cell resistance developed.

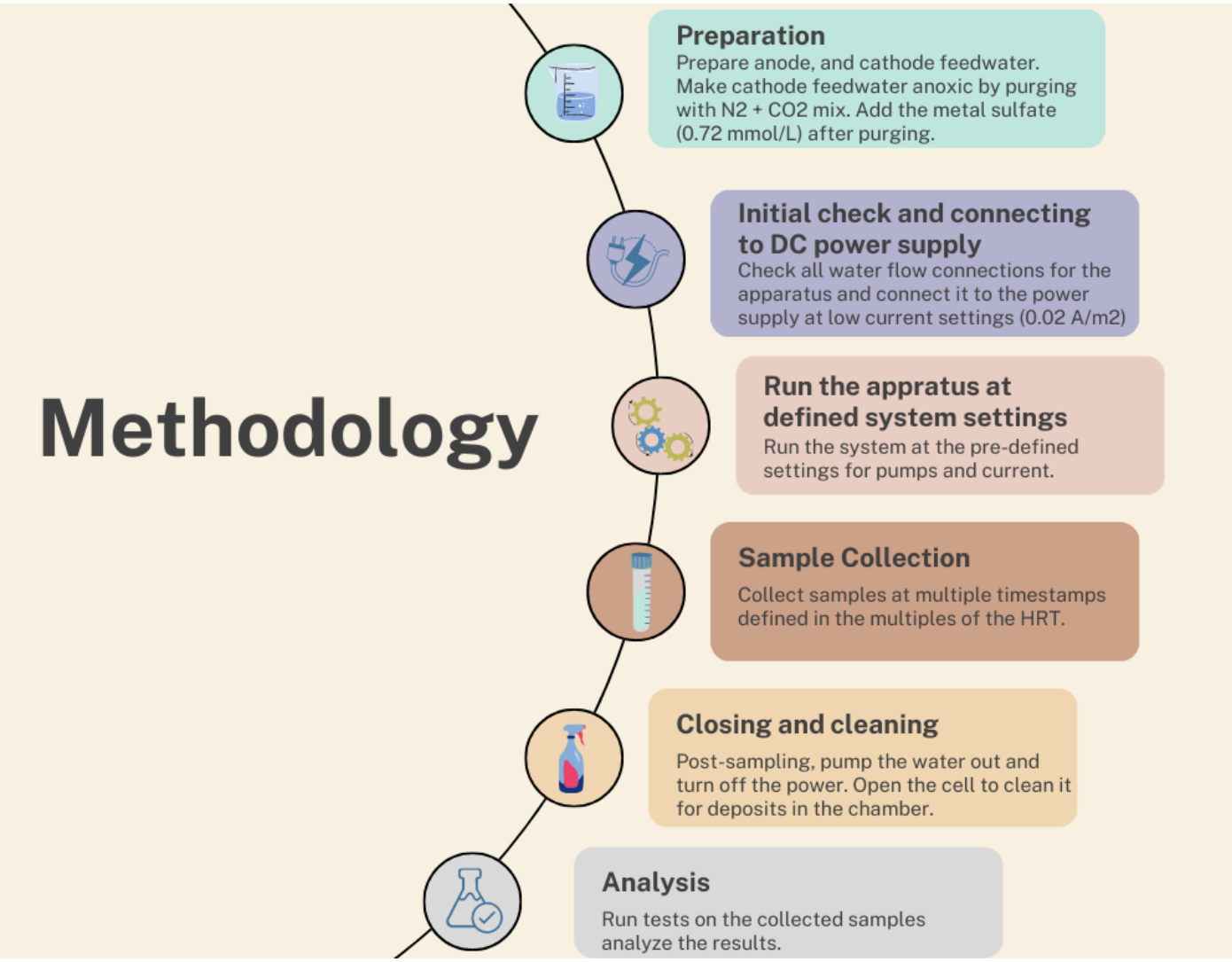

Figure 2.2: Step-wise methodology for the study

2.2.3. Energy and cell resistance measurements

The energy consumption of the electrochemical reduction process in the electrochemical cell (kWh/m^3) and its utility for drinking water treatment can be determined by measuring the voltage (V) of the cell. Energy consumed by the system (kWh/m^3) can be determined by the equation:

$$Energy = V * \frac{I}{Q} \tag{2.1}$$

where I is the current supplied (in A) and Q is the flow rate of the electrochemical cell in m^3/h.

The cell resistance, R, present during the usage of the electrochemical cell can be calculated with the help of voltage measured during the experiment and the constant current supplied. It is given by:

$$R = \frac{V}{I} \tag{2.2}$$

2.3. Sampling and Analysis

Samples were collected from the cathode chamber through an outlet and into 10 mL test tubes at various intervals based on the volume of water treated. Effluent samples were immediately acidified upon collection

using 1% v/v ROTIPURAN Ultra 69% nitric acid (HNO_3) to prevent the formation of precipitates. Additionally, an extra test tube of the sample was collected at the same time stamp for conducting tests using cell test kits and measuring the effluent's pH.

The pH, dissolved oxygen (DO), and electrical conductivity (EC) readings of the feed waters and the collected samples were measured using a multi-meter (MultiLine® Multi 3630 IDS) equipped with probes for pH (SenTix® 940), DO (FDO® 925), and EC (TentraCon® 925). On-spot sample analysis was performed using Fe, Mn, and Al cell test kits. Fe analysis was carried out using the Iron Cell Test (Sigma Aldrich) and measured with the Spectroquant® NOVA 60. Mn was measured using the Manganese Reagent Set LC632 and analyzed with the HACH DR 3900 spectrophotometer. Al was analyzed using the LCK301 cell test and measured with the HACH DR 3900 spectrophotometer. The collected samples were further cross-analyzed for Fe, Mn, and Al using Inductively Coupled Plasma - Mass Spectrometry (Analytikal Jena model PlasmaQuant MS ICP-MS). Acidified samples were diluted by a factor of 10 and filtered through a 0.2 µm filter (Macherey-Nagel GmbH Co. KG) before being sent for analysis with ICP-MS. The nature of deposits on the stainless steel cathode mesh was analyzed using SEM-EDS - Scanning Electron Microscopy - Energy Dispersive Spectroscopy (FEI Quanta FEG 650). The visual inspection of the deposits on the cathode was done with the help of a digital microscope (Keyence VHX-5000).

2.4. Materials

In the experiment, artificial groundwater was created using ultra-pure water (MilliQ 18.2 mω.cm, ELGA PURELAB Chorus) by adding 9 mmol/L sodium chloride (NaCl, J.T. Baker™) to maintain conductivity of the solution in the range of 1400-1500 uS/cm and using 2.14 mmol/L sodium bicarbonate ($NaHCO_3$) from J.T. Baker™ for pH buffer. The materials were weighed using a Mettler Toledo AE 240 Analytical Balance. The pH was controlled with the help of hydrochloric acid (HCl, 3M, Carl Roth) and sodium hydroxide (NaOH, 50% in H_2O, Sigma-Aldrich). The solution was made anoxic by purging with nitrogen (N_2) and carbon dioxide (CO_2) mixed in an 80:20 ratio (Linde Gas Benelux). Iron (II) sulfate heptahydrate ($Fe_2SO_4.7H_2O$, Sigma-Aldrich), manganese (II) sulfate monohydrate ($Mn_2SO_4.H_2O$, Sigma-Aldrich), aluminum sulfate 14-hydrate ($Al_2(SO_4)_3.14H_2O$, Sigma-Aldrich), were used.

3

Results

3.1. SEM-EDS characterization of the deposits on the cathode mesh

SEM-EDS analysis was used to characterize the deposits by combining scanning electron microscopy's imaging capabilities with energy-dispersive X-ray spectroscopy's elemental analysis. SEM gave high-resolution pictures of the deposits, providing the intricate details of their morphology. EDS analysis provided the elemental composition of the cathodic deposits, helping map out the specific elements deposited on the cathode. SEM-EDS was carried out on stainless steel cathode meshes used for Mn^{2+}, Fe^{2+}, and Al^{3+} for individual and combined experiments at pH 7. During the experimentation, separate mesh was used for each type of experiment.

Fig 3.1 is the SEM-EDS analysis of the cathode mesh with deposition, from Fe individual experiments. The EDS map for element Fe in Fig 3.1.a shows changes in the contrast on the surface of the cathode mesh. The stainless steel cathode already has a large percentage of Fe in it. Further, the deposition of Fe is happening on its surface. The EDS map shows light and dark contrasts depending on the percentage of element Fe. In this picture, the brightly lit parts for the Fe element are the parts of the cathode mesh where no deposition happened, and the exposed area of the stainless steel cathode is visible. On the other hand, darker parts refer to regions where depositions of Fe happened. The Fe deposition displays darker regions in the EDS map since along with the deposited Fe, the element oxygen (O) was also present in the deposition (Fig 3.1.b), and this brought down the percentage of Fe in the composition of the deposited region. On comparing Fig 3.1.a and Fig 3.1.b, it is observed that the O element is present only in the dark spots where Fe is deposited and not in the brightly lit parts where the stainless steel cathode mesh is exposed. Further, EDS point scans (Fig 3.1.d) were done at different points on the cathode to find the elemental composition by the percentage of weight at a particular point. In the regions of no deposition (point 1 in Fig 3.1.d), where the stainless steel cathode mesh is exposed, the percentage of Fe element by weight is 73.03%. This is expected since the weight percentage is split among the other elements of the stainless steel alloy, such as Cr, C, Ni, and others. The Fe percentage is closer to the approximate percentage of 68% which the manufacturer provided (Appendix .10). The regions of Fe deposition on the cathode had lesser Fe element percentage by weight (53.64% in point 2 in Fig 3.1.d), since a large percentage share was attributed to element O (14.40%). This aligns with the earlier observed presence of element O in the regions of Fe deposition in the EDS map (Fig 3.1.b). Further information on the results of point EDS for different positions and the element analysis by weight, atom, and compound is available in Appendix .6.1. Fig 3.1.c shows the Fe deposition to be uneven and pointy.

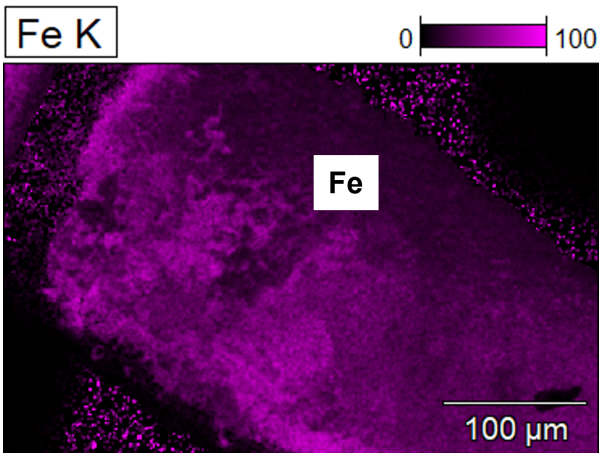

(a) EDS for Fe

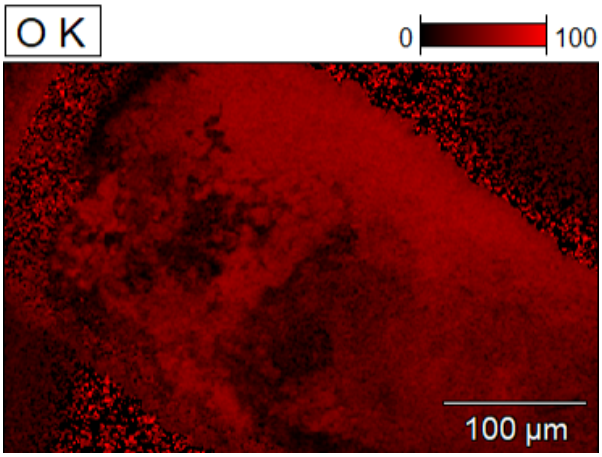

(b) EDS for O

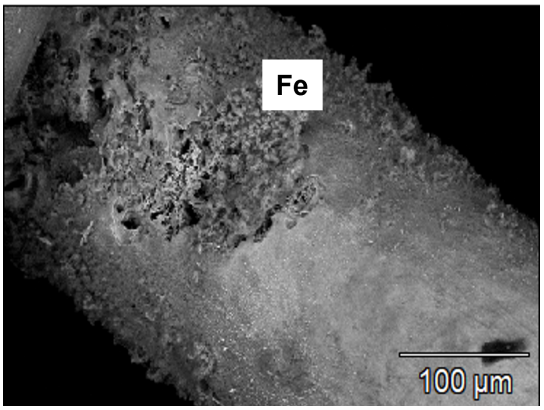

(c) SEM picture for Fe deposits

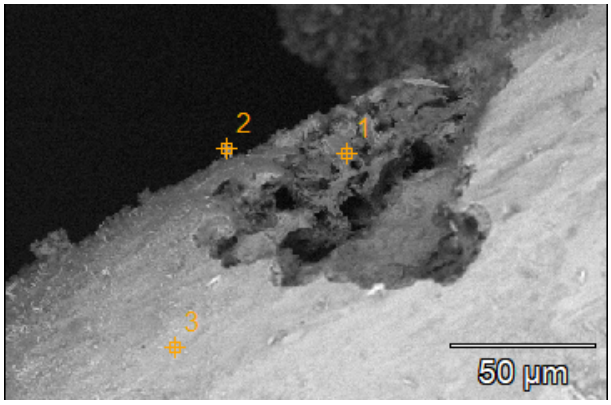

(d) EDS point scan for Fe

Figure 3.1: SEM-EDS for Fe deposits on the cathode in Fe individual experiment at pH 7

The SEM-EDS analysis for Mn in individual experiments provides a clear distinction between the stainless steel mesh cathode area and the Mn deposition, as seen in Fig 3.2. The deposits are of uneven, flaky, and have rough texture (Fig 3.2.c). The presence of element O is detected as seen in Fig 3.2.b. Comparing EDS maps of Fig 3.2.a and Fig 3.2.b, shows that element O is present only in the regions of Mn deposits. Point EDS analysis of the cathode (Fig 3.2.d, point 4) shows element Mn being present as 53.34% by weight on the deposition and element O on the same point being 35.43% by weight. Further information on the results of point EDS for different positions and the element analysis by weight, atom, and compound is available in Appendix .6.2.

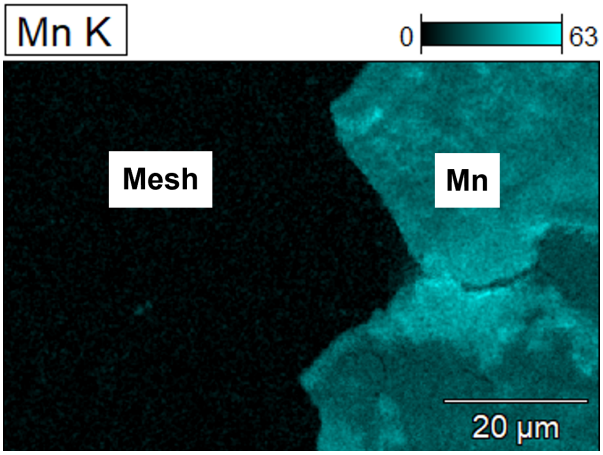

(a) EDS map for Mn

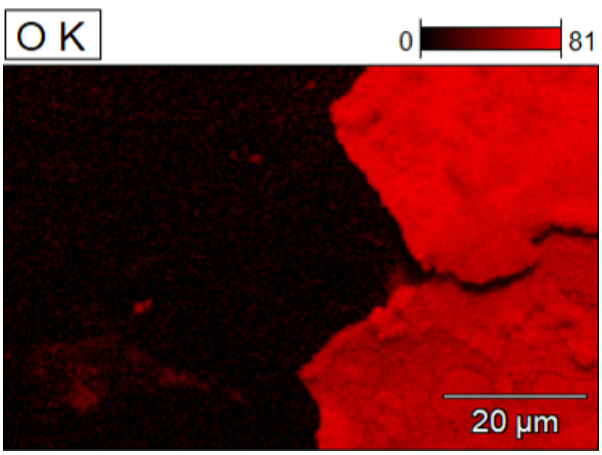

(b) EDS map for O

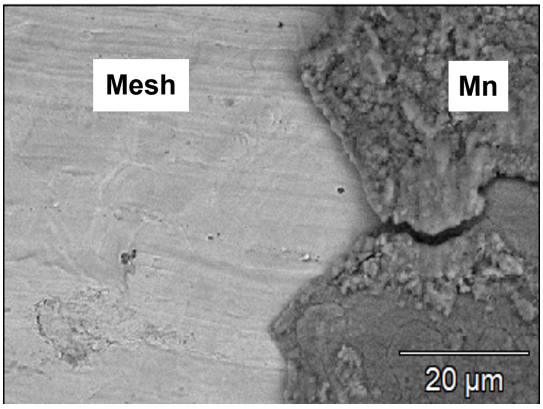

(c) SEM picture for Mn

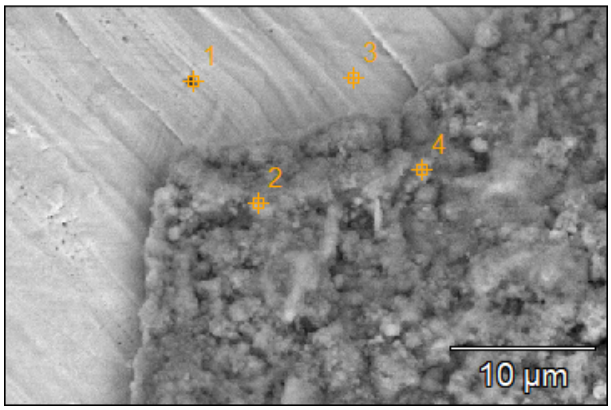

(d) EDS pt scan of Mn

Figure 3.2: SEM-EDS for Mn deposits on cathode

The SEM-EDS analysis of the cathode mesh used for Al in individual experiments did not show any presence of Al deposits. SEM image did not indicate any deposition (Fig 3.3). Further, Point EDS analysis at multiple points of the cathode also failed to reveal any Al. Information on the results of point EDS for different positions and the element analysis by weight, atom, and compound is available in Appendix .6.3.

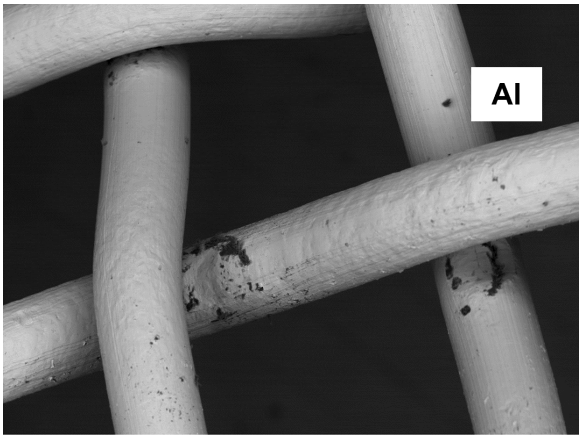

Figure 3.3: SEM picture of Al.

In the combined experiment (Fig 3.4), the SEM image Fig 3.4.e shows the deposition is flaky and occurs in the form of uneven patches. In Fig 3.4.a, Fe deposits are found in the darker regions, while the brighter regions are the exposed parts of the stainless steel cathode with no deposition. Element O is also present and by comparing Fig 3.4.a and Fig 3.4.b, it can be observed that element O is found only in the regions with deposits. EDS maps in Fig 3.4.c and Fig 3.4.d show the presence of Mn and Al on the cathode, respectively. In Mn and Al EDS maps, a lot of background noise is also noticed, affecting the EDS map's sharpness. Point EDS analysis (Fig 3.4.f, point 1) showed the presence of Fe, Mn, O, and Al in the deposition. The weight percentage of Al was found to be 11.54%. At the same point 1, the weight percentage of Fe, Mn, and O was 38.36%, 15.37% and 20.85%. Further information on the results of point EDS for different positions and the element analysis by weight, atom, and compound is available in Appendix .6.4.

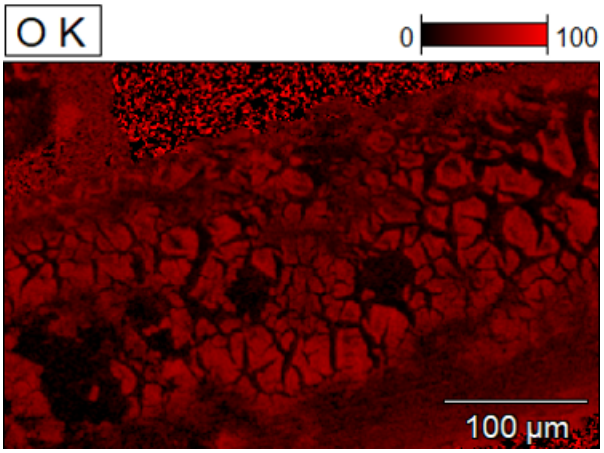

(a) EDS map for Fe

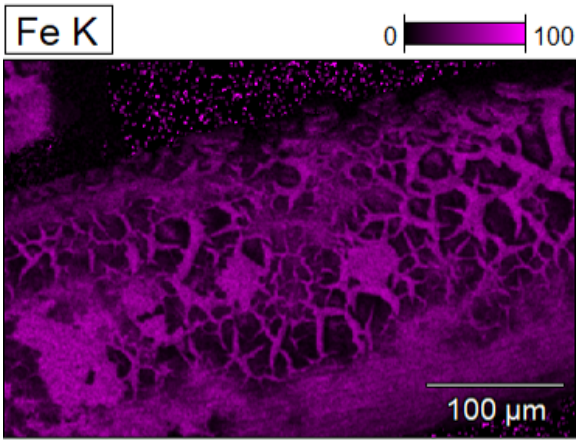

(b) EDS map for Mn

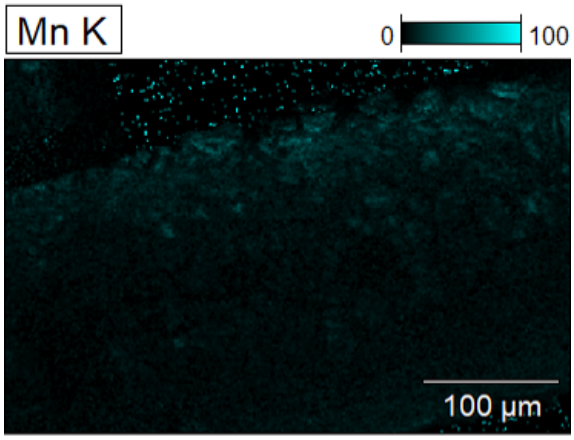

(c) EDS map for Mn

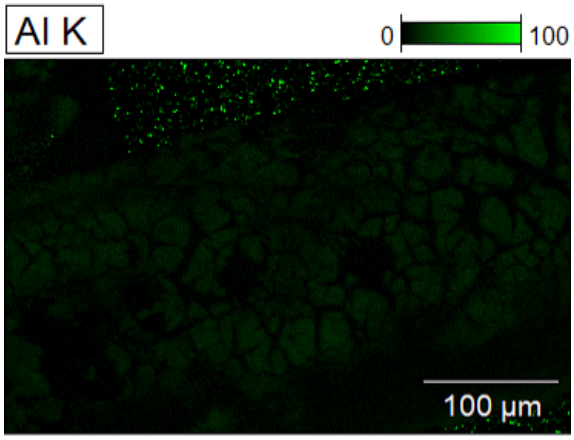

(d) EDS map for Al

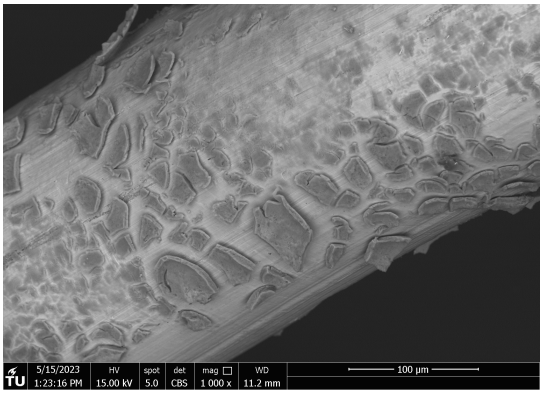

(e) SEM visual of combined deposition

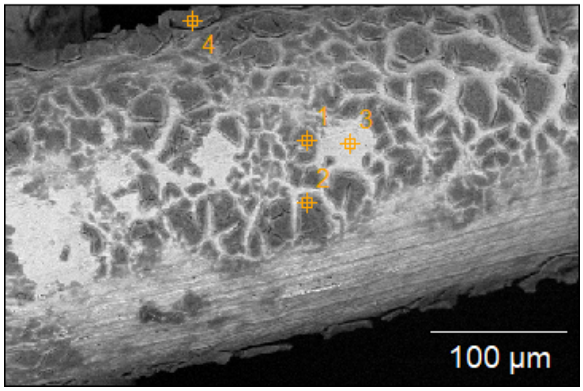

(f) EDS pt scan of combined case

Figure 3.4: SEM-EDS for the deposits on the cathode in a combined experiment

3.2. Thickness of metal deposits

The average thickness (μm) of the metal deposited on the cathode throughout the operation can be calculated at each pH. The calculations of the deposited metal are based on the assumption that all of the electrochemi-

cally reduced metal is deposited uniformly on the entire surface of the stainless steel cathode wire mesh. The method for measuring deposit thickness is provided in the Appendix .2.

In Fig 3.5, we observe a clear deposition trend for Fe at different pH levels in individual experiments. At pH 4, the deposition thickness measures 0.109 μm, increasing to 0.302 μm at pH 6 and, 0.630 μm at pH 7. It indicates a 5.8-fold rise in the deposition from pH 4 to pH 7. In the case of electrochemical reduction of Mn^{2+} during individual experiments (Fig 3.6), pH 6 and pH 7 have deposition of 0.030 μm and 0.213 μm respectively, while negligible deposition is noted at pH 4. In the combined experiments scenario, Fe deposition thickness trends are similar to individual experiments. At pH 4, deposition thickness is 0.067 μm which rises to 0.223 μm at pH 7, resulting in a 3.5-fold increase. The same trend is seen for Mn deposition in combined experiments with depositions increasing from no deposition at pH 4 to 0.034 μm pH 7. Hence in the study, with increasing pH, the deposition of the metal on the cathode increases.

There is a decrease in the deposition in the case of Fe during combined experiments when compared to individual experiments. For instance, at pH 7, the deposition in the combined experiment declines by 64.6% (2.8-fold drop) with respect to the deposition in individual experiments at pH 7 (Fig 3.5). Meanwhile, Mn deposition also decreases for combined experiments when compared to individual experiments (Fig 3.6) with depositions declining by 84% (6-fold drop).

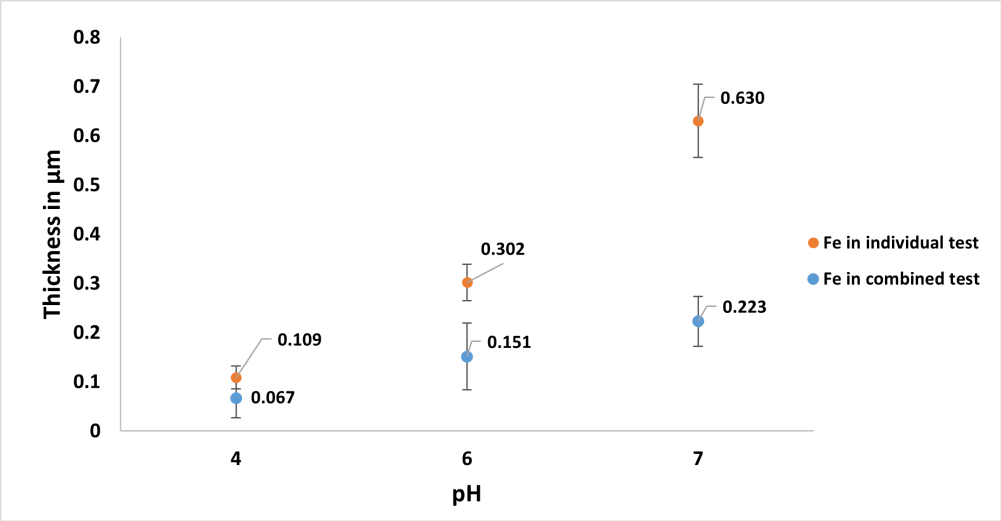

Figure 3.5: Average Fe deposition thickness

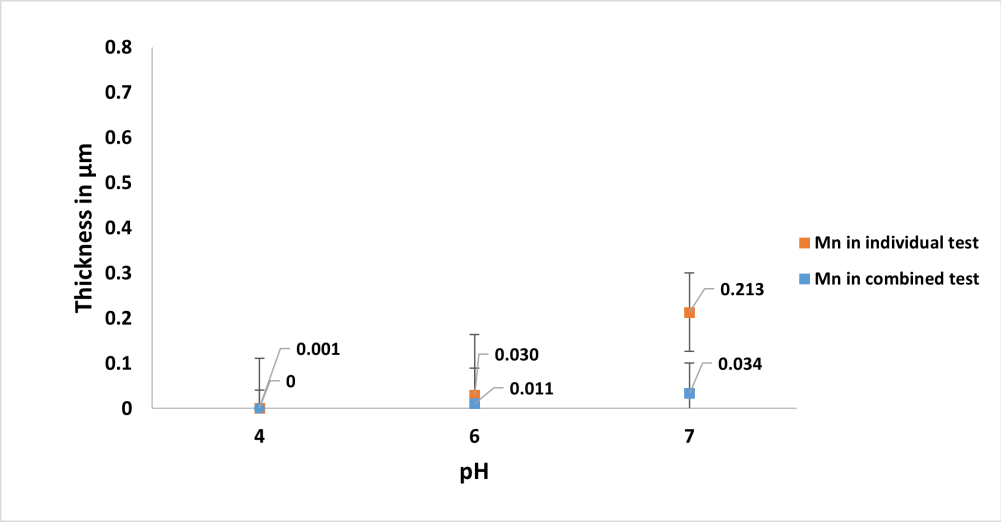

Figure 3.6: Average Mn deposition thickness

3.3. Effluent concentrations over the volume of water treated

The effluent concentrations of Fe^{2+}, Mn^{2+} and, Al^{3+} varied a lot depending on the water matrix of the cathode feedwater and the volume of the water treated. As the deposition on the cathode increases, the effluent concentration decreases and vice-versa. In the case of Mn, water matrices with cathode feedwater pH 4,6 and, 7 were used since rapid precipitation was observed in the cathode feedwater tank at pH 8. In the case of Al, pH 4 and 6 were considered since rapid precipitation was observed at pH 7 and above.

3.3.1. Effluent concentrations during individual experiments

In Fig 3.7, Fe^{2+} in the effluent water increases as the volume of the water treated increases, across all pH. This implies that the electrochemical reduction process is declining with the volume of water passing through the electrochemical cell. It is observed that the effluent concentrations are lowest for pH 7 and pH 8 when the volume of influent cathode feedwater is 1.26 L. Beyond this, as the volume of water treated increases, the effluent concentrations start increasing. The effluent concentrations become almost equal to the influent concentrations (0.72 mmol/L) as the volume of water treated reaches 6.3 L (30*HRT). The lowest effluent concentration of Fe^{2+} in the effluent is 0.35 mmol/L, observed at pH 7 when 1.26 L of water is treated. This is a removal of 51.4% Fe^{2+} from the influent water. At pH 6, the maximum removal is achieved at 0.63 L with 24.1% while for pH 4 the maximum removal of Fe^{2+} is 5.56% when the volume of water treated is 2.52 L.

In the case of Mn^{2+} experiments in Fig 3.8, the effluent concentrations across all pH follow a trend similar to that of Fe^{2+}, with Mn^{2+} increasing in the effluent with the volume of water treated. The minimum effluent content was found at pH 7 for 1.26 L volume of water treated by the system, equal to 0.56 mmol/L. This is a removal of 22.22%. The removal at pH 4 and pH 6 is very low, with maximum removal reaching 3.5% at 0.63 L and 6.2% at 1.26 L respectively.

In the case of Al^{3+} in individual experiments, there were very high effluent concentrations of the metal ions throughout the volume of water treated. Also, no clear trends in the effluent concentrations over the volume of water treated were observed. This indicates a lack of electrochemical reduction of Al^{3+} (Fig 3.9).

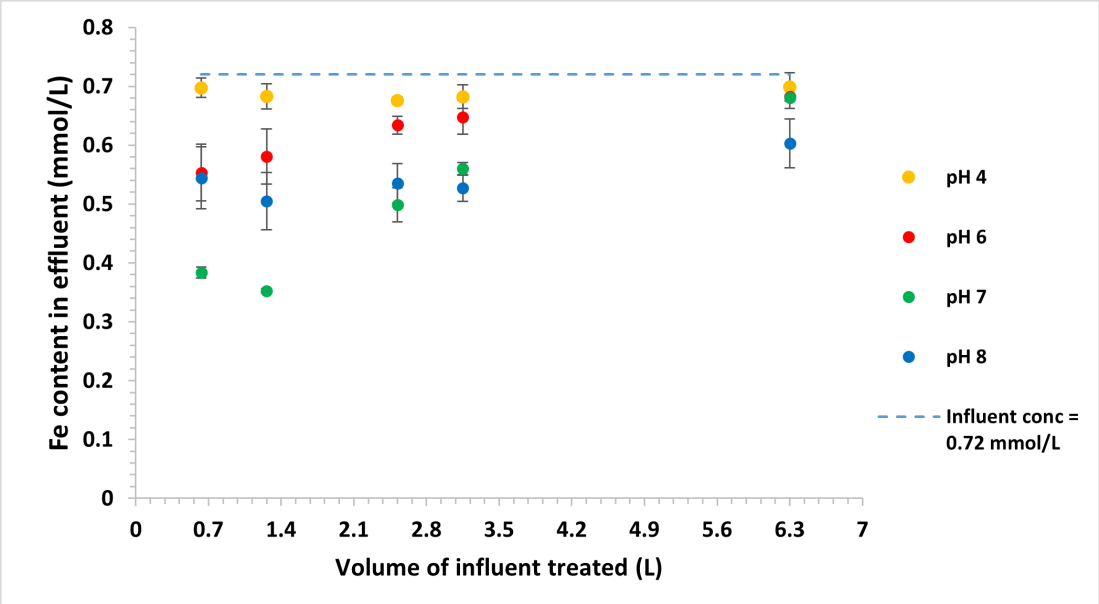

Figure 3.7: Electrochemical reduction of Fe^{2+} with volume of water treated

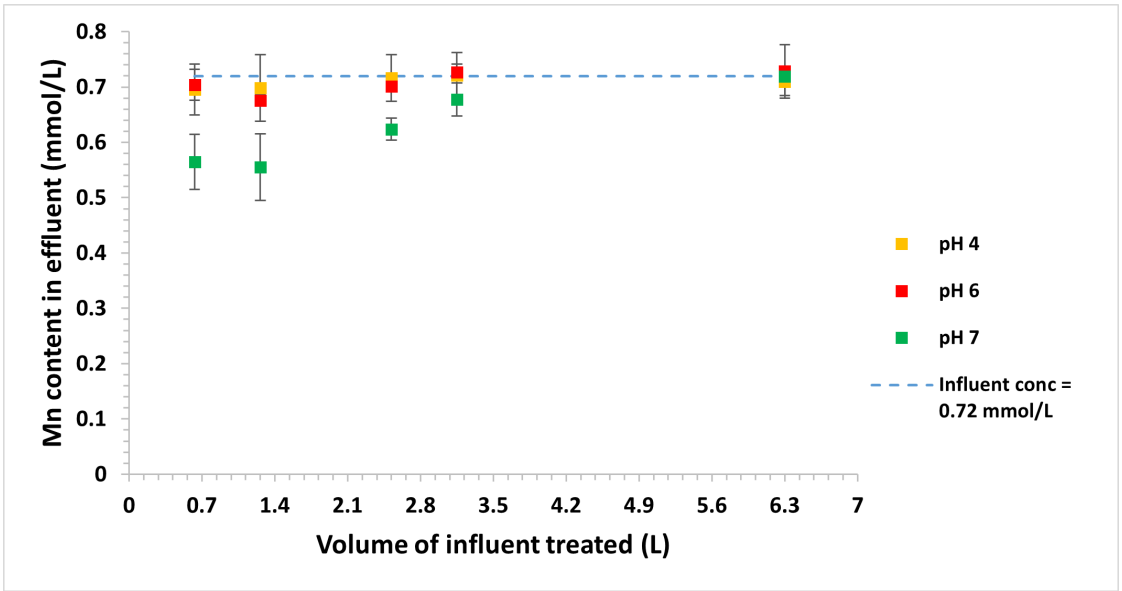

Figure 3.8: Electrochemical reduction of Mn^{2+} with volume of water treated

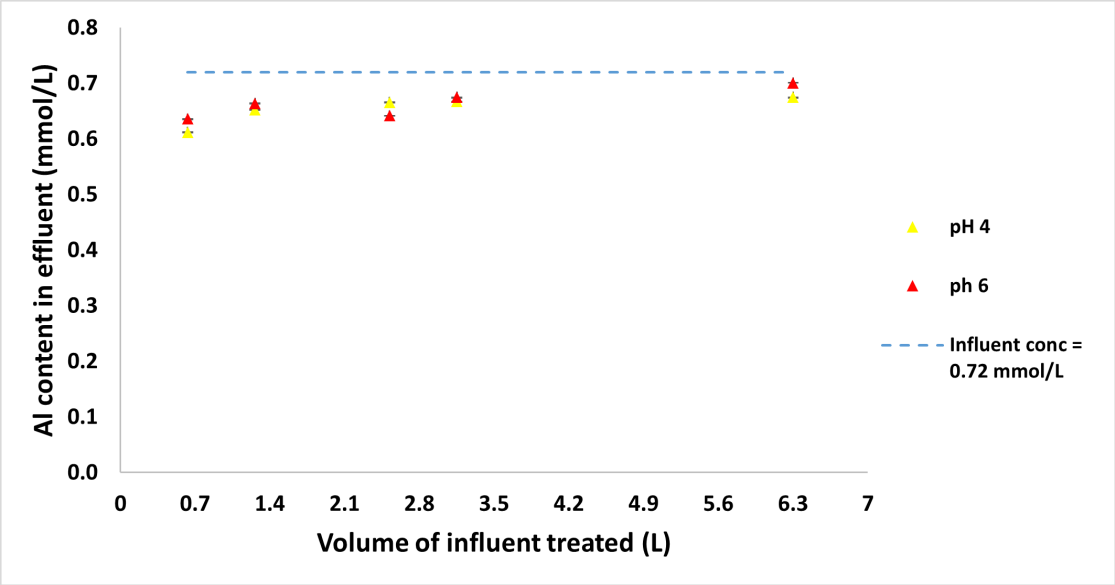

Figure 3.9: Electrochemical reduction of Al^{3+} with volume of water treated.

3.3.2. Combined experiments

Fig 3.10 and Fig 3.11 show the changes in the effluent concentrations of Fe^{2+} and Mn^{2+} respectively, with the volume of water treated at pH 7. Al^{3+} effluent concentrations were not analyzed since no electrochemical reduction was observed in individual experiments. In combined experiments, the effluent concentrations of both Fe^{2+} and Mn^{2+} increases with the volume of water treated. It shows that the general trend of increasing effluent concentrations with volume of water treated is the same in both combined and individual experiments. The minimum Fe^{2+} effluent concentration in combined experiment was 0.59 mmol/L at a volume of 1.26 L, with a removal rate of 18%. For Mn^{2+} the minimum effluent concentration was 0.67 mmol/L at a volume of 0.63 L and removal rate of 6.9%. The effluent concentrations increase as the volume of influent increases, reaching closer to the influent concentration (0.72 mmol/L) around the 6.3 L. The results for effluent concentrations in combined experiments at pH 4 and pH 6 are available in Appendix .3.

It is apparent at each pH that individual experiments have lower concentrations of the metal ions in the effluent in individual experiments when compared to the metal ion concentration in the effluent in the combined experiments. At pH 7 for Fe, the difference in the effluent concentrations at 1.26 L is very high, with 0.35 mmol/L in individual experiments and 0.59 mmol/L in combined experiments, a 1.7-fold rise. Similarly, for Mn, there is a 1.2-fold rise between the effluent concentrations from individual experiments to combined experiments at 0.63 L mark at pH 7.

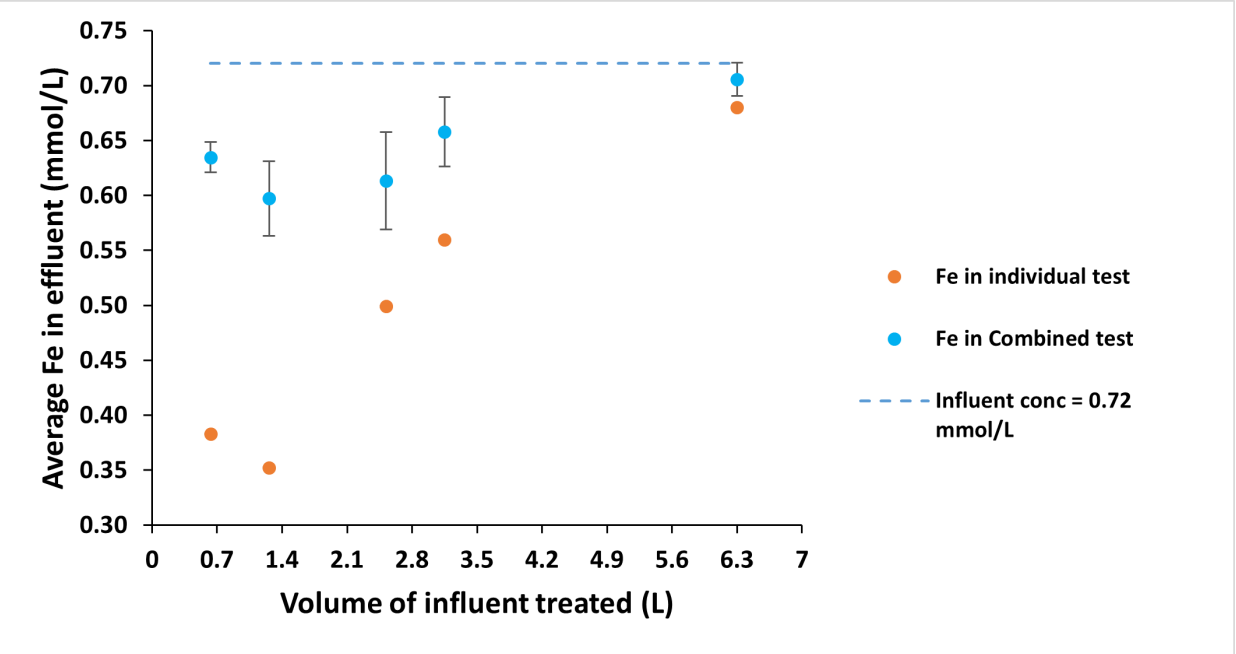

Figure 3.10: Change in the effluent concentration of Fe^{2+} with volume of water treated at pH 7

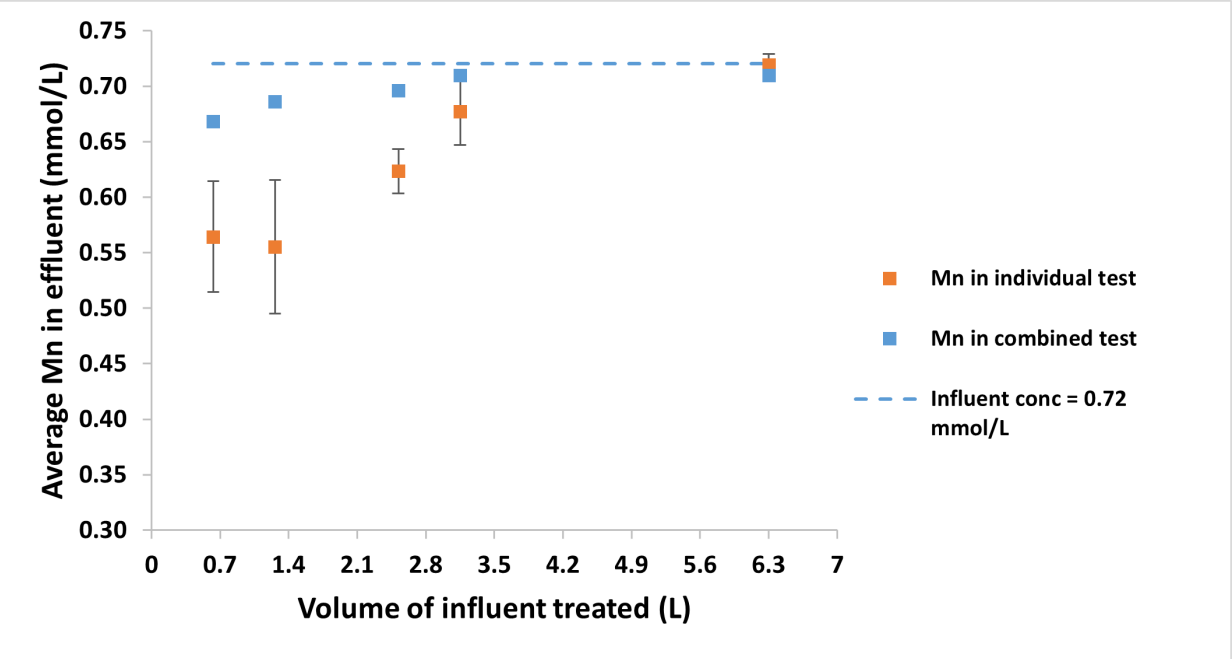

Figure 3.11: Change in the effluent concentration of Mn^{2+} with volume of water treated at pH 7

3.4. Change in Faradaic efficiencies

Fig 3.12 refers to the faradaic efficiencies (FE) in percentages for Fe and Mn in individual experiments and as Fe and Mn together in combined experiments, at data point of pH 7 and 1.26 L volume of treated (6 * HRT). It is observed that the FE is highest for Fe in individual experiments at 35.05%, which was the highest efficiency calculated throughout the study. In the case of Mn, the maximum faradaic efficiency achieved in the study is 14.90%. It shows that for the current study with the standard settings incorporated, the FE for Mn^{2+} is lower than Fe^{2+}. It is assumed that in the case of combined experiments, the number of electrons used for the cathodic reduction of the targeted metal ions (Fe^{2+} and Mn^{2+}) is equal to the sum of electrons Fe^{2+} and Mn^{2+} used during the reduction in combined experiments. This gave the FE in combined case (term 'Combined (Fe+Mn)'), which is 13.25%. The 'Expected combined' FE is calculated based on a scenario in which the number of electrons used for Mn^{2+} and Fe^{2+} electrochemical reduction during combined experiments are same as the number of electrons used in the individual experiments. Fe in this case comes out to be 50.65%.

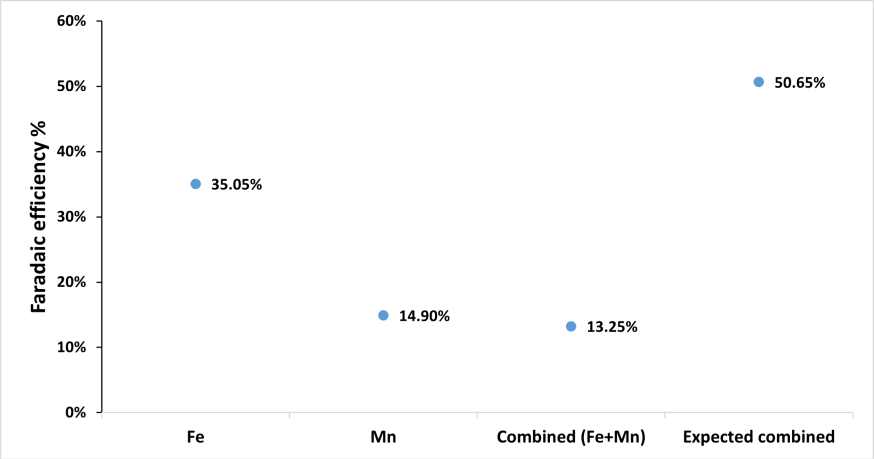

Figure 3.12: Faradaic efficiencies (%) at pH 7 and 1.26 L volume of water treated

3.5. Cell resistance

The resistance of the electrochemical cell with respect to the volume of water treated was drawn for the pH 7 water matrix. The resistance in the cell was found to be increasing with the volume of water treated. Fig 3.13 shows increasing cell resistance for Fe, Mn, and combined experiments. The corresponding cell voltage curve at pH 7 and for the rest of the pH is presented in Appendix .4. Since voltage for Fe, Mn and combined experiments is increasing with the volume of water treated across all pH, there will be a similar trend of increasing cell resistance across all pH due to direct proportionality between the cell resistance and the cell voltage.

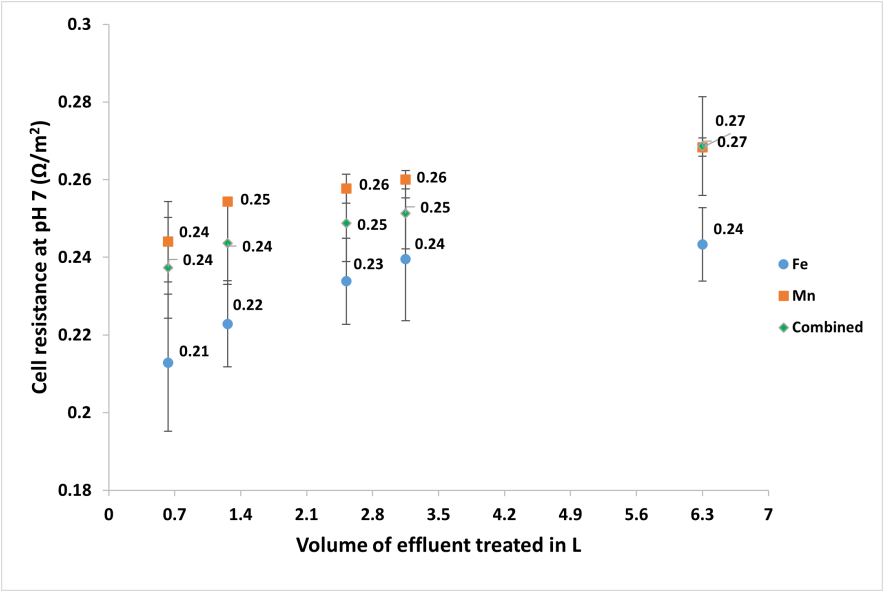

Figure 3.13: Change in cell resistance with volume of water treated at influent pH 7

An examination of the effluent's pH for experiments with different cathode feedwater matrices revealed a noticeable absence of clear trends. Detailed observations of the effluent pH can be found in the Appendix (.5).

4

Discussions

4.1. Selectivity towards electrochemical reduction of metal ions

SEM-EDS results showed the presence of deposits of the metal Fe (Fig 3.1) and Mn (Fig 3.2) after electrochemical reduction. Given the lack of visual proof in the form of deposits of Al (Fig 3.3) and negligible removal of the ions from the cathode feed water, it can be implied that no electrochemical reduction of Al^{3+} occurred in this study in the individual experiments. The system settings standardized for the current study (Table 2.1) were selective towards the electrochemical reduction of Fe^{2+} and Mn^{2+} and not for Al^{3+}. Further, it was also observed that the electrochemical reduction of Fe^{2+} was better than the electrochemical reduction of Mn^{2+}. For instance, the maximum removal of Fe was achieved at pH 7 at 1.26 L volume of water treated, equalling 55.4% (Fig 3.7) while for Mn the maximum removal achieved was 22.2% also at pH 7 at 1.26 L volume of water treated (Fig 3.8). It showcases that in the study, overall, the system settings favoured the removal of Fe^{2+} ions from the influent cathode feedwater. Henceforth, it highlights the capability of electrochemical reduction as a method for selective, targeted contaminant removal through manipulation of the treatment plant set-up.

Every reduction reaction has a specific negative potential, E, that must be achieved for the reaction to be thermodynamically feasible. E measured with respect to a standard hydrogen electrode (SHE) has been presented in Table 4.1 in the form V vs SHE (LibreTexts 2021). The potentials in the table indicate that out of the three metal ions in consideration, Fe^{2+} requires the least negative potential to reduce while Al^{3+} requires the highest negative potential. Since Al^{3+} did not get reduced, it was hypothesized that the lack of Al^{3+} reduction could be caused by the fact that the negative potential at the cathode was not 'negative enough.' However, potentiostat measurements were not performed to support this hypothesis. Therefore, a negative current density greater than 30 A/m^2 needs to be applied to achieve Al deposition. This will result in a higher negative potential and make Al^{3+} reaction thermodynamically feasible.

Half-reaction	E (vs SHE)
$Al^{3+}(aq) + 3e^- \rightarrow Al(s)$	-1.68
$Mn^{2+}(aq) + e^- \rightarrow Mn(s)$	-1.18
$Fe^{2+}(aq) + 2e^- \rightarrow Fe(s)$	-0.44

Table 4.1: E vs SHE for the metal reduction half-reactions

This is because E determines the energy of the electrons which are present on the cathode surface. High negative potential helps electrons in reaching a high enough energy state to get transferred into the vacant electronic states of the metal ions in the electrolyte as shown in Fig 4.1 (Bard & Faulkner 1980).

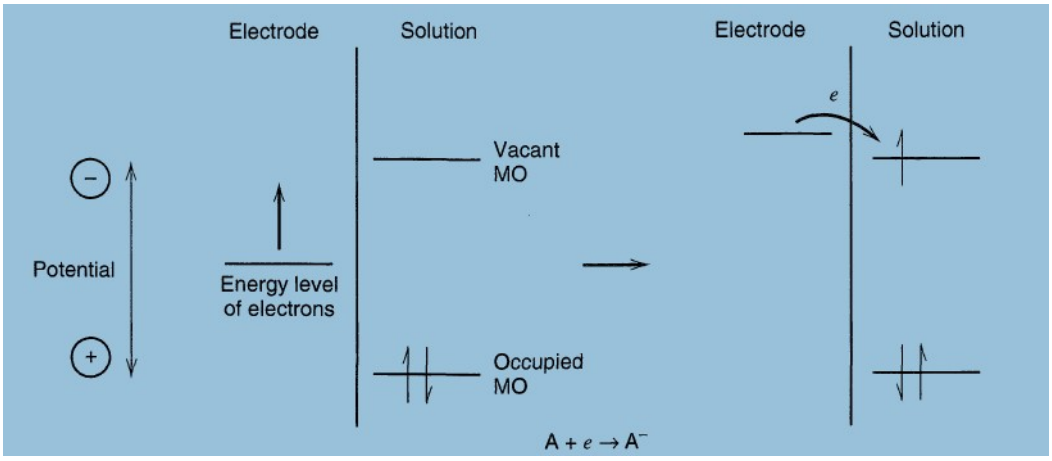

Figure 4.1: Representation of reduction process of a species, A, in solution. The molecular orbitals (MO) of species A shown are the highest occupied MO and the lowest vacant MO. Source: (Bard & Faulkner 1980)

The thermodynamic spontaneity of a chemical reaction is given by Gibbs free energy change (ΔG). The (ΔG) is related to the potential difference (E) at the cathode-solution interface by the relation:

$$\Delta G = -nFE \tag{4.1}$$

where n is the number of electrons transferred in the reaction, and F is the Faraday constant (96485.3 C/mol).

In order for a reaction to be thermodynamically viable, ΔG associated with the reaction should be negative (Kelly et al. 2003). It can be deduced that the Gibbs free energy change for electrochemical reduction of Al^{3+} did not achieve a negative value in the individual experiments. The pourbaix diagrams providing a relation between the E and the pH of the water matrices for Fe, Mn, and Al are in the Appendix (.8).

4.2. Depositions from the electrochemical reduction process

4.2.1. Nature of deposits

The EDS-SEM results of the cathode show the deposition of Fe and Mn elements in individual (Fig 3.1, Fig 3.2), and combined experiments (Fig 3.4). The element oxygen (O) was also detected in the deposits. Given the experiments were conducted in anoxic conditions, O in the deposit entered due to the exposure to the atmosphere, which happened on removing the cathode from the electrochemical cell for SEM-EDS analysis. The wet deposits interacted with the atmospheric oxygen, causing oxidation of the metal deposit. The oxidation process was confirmed visually by observing the formation of orange rust coating on the deposits. Fig 4.2 is the optical microscopic image of a section of stainless steel mesh showing the developing rust on the Fe deposits.
The rusting of Fe is given by:

$$2\,Fe\,(s) + O_2 + 4\,H^+\,(aq) \rightarrow 4\,Fe^{2+}\,(aq) + 2\,H_2O \tag{4.2}$$

$$4\,Fe^{2+}\,(aq) + O_2 + 6\,H_2O \rightarrow 2\,Fe_2O_3 \cdot H_2O\,(s) + 8\,H^+ \tag{4.3}$$

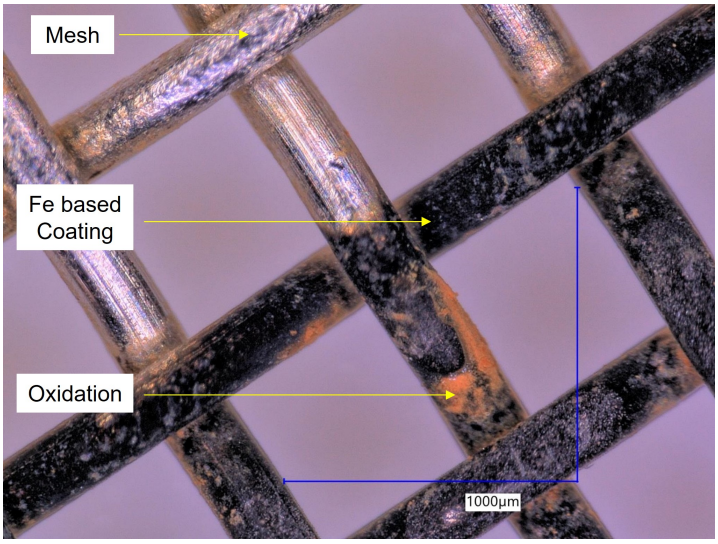

Figure 4.2: Deposition on mesh during electrochemical reduction of Fe^{2+}

Another reason for the presence of O element could be the formation of metal-hydroxyl intermediate, which can get adsorbed onto the cathode (Bard & Faulkner 1980; Hessami & Tobias 1989; Kang & Lee 2023). The studies suggested a build-up of metal-hydroxyl ions on the cathode surface. It is hypothesized that the formation of $Fe(OH)^+$ and $Mn(OH)^+$ ions may occur during the electrochemical reduction process, and could be a contributory factor for the presence of O element in the EDS maps. However, it must be noted that it cannot be ascertained if a metal-hydroxyl formation reaction occurred during this experiment since the studies with metal hydroxide formation were specific to the experimental conditions such as strong alkaline pH, and henceforth more research is required on this topic.

The depositions on the cathode from the electrochemical reduction of Fe^{2+} and Mn^{2+} are expected to be pure Fe and Mn solids. This was ensured through control over the composition of the cathode feed water, containing only the metal ions to be reduced apart from NaCl electrolyte and $NaHCO_3$ buffer in anoxic conditions. Previous studies related to electrodeposition also verify the formation of Fe and Mn deposits, formed by the direct transfer of electrons from the cathode to the metal ions (Bard & Faulkner 1980; Hao et al. 2019; Zou et al. 2015).

4.2.2. Impact of deposits

The study revealed that as deposits accumulate with the increasing volume of water treated by the system, there was a decline in the electrochemical reduction of metal ions (Section 3.3 3). The deposition morphology in the case of Mn was uneven and flaky (Fig 4.3). The removal of Mn^{2+} ions by electrochemical reduction became negligible as these depositions grew and the volume of water treated reached 6.3 L (Fig 3.8). In the case of Fe, pointed depositions were observed on the stainless steel cathode mesh (Fig 4.4). These depositions could be dendrites since these depositions appear visually similar to the pointy Fe deposits described in a previous study (Qiu et al. 2012). Since the electrochemical reduction of Fe^{2+} ions declines with the volume of water treated (Fig 3.7), the formation of deposits is detrimental in these experiments as well. The deposited layers negatively influence the cathodic reduction processes since they reduce the free area of the cathode available to supply electrons to the metal ions. This is in line with previous studies wherein the cathode deposits affected the mass transfer of ions by reducing the effective surface area of the cathode, leading to a decrease in the rate of ion transfer (Subbaiah et al. 2022). This is, however, dependent on the type of deposit and the operating conditions of the electrochemical cell. Also, previous studies have indicated that in cases of excessive H_2 evolution, dendrite formation occurs (Darband et al. 2021; Lotfi et al. 2019; Mostad et al. 2008). The excessive H_2 side-reaction will bring down the FE and therefore, the electrochemical reduction of Fe^{2+}. However, further investigation is required to determine if the dendrite formation also leads to higher H_2 production and the declining electrochemical reduction of Fe^{2+}.

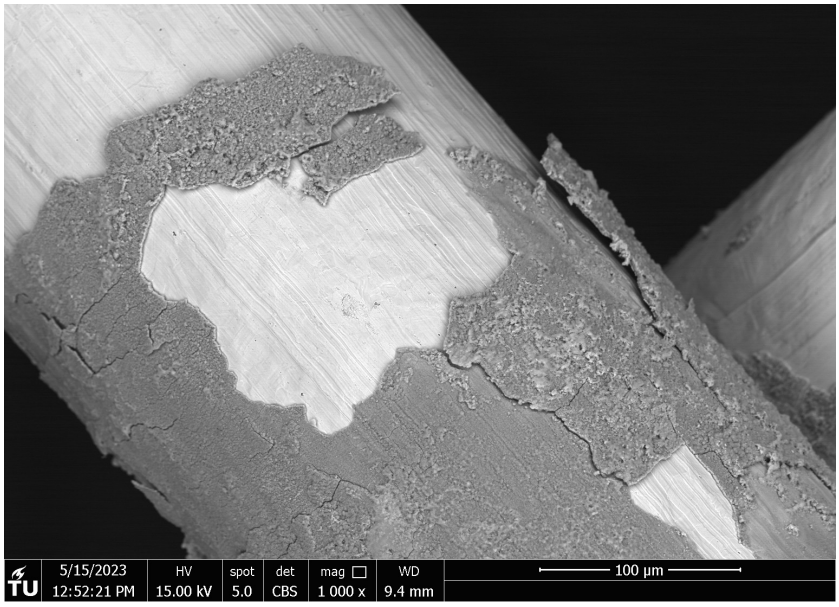

Figure 4.3: Flaky deposits on the mesh during electrochemical reduction of Mn^{2+}

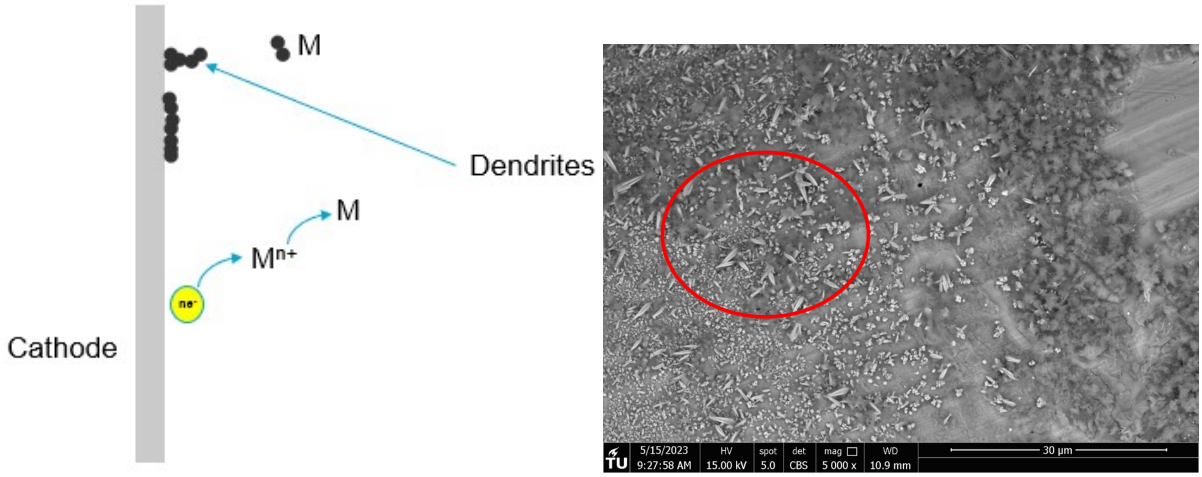

(a) Dendritic growth

(b) Dendritic Fe deposits observed on cathode in SEM

Figure 4.4: Dendritic growth on cathode surface during electrochemical reduction

The deposits do not necessarily occur on the spot on the cathode from where the electron has been transferred (the reaction site). Instead, the reduced atom is understood to diffuse on the cathode surface via terrace and interlayer diffusion (Hao et al. 2019). Such movement of the atoms decides the morphology of the deposition. If the surface diffusion barrier of the cathode is low or surface diffusion is fast, the morphology is smooth (Hao et al. 2019). It was not the case for Fe and Mn deposits since these were uneven. Also, the dendrite formation occurs on exceeding the critical current density, and in case of high concentration of metal ions in the water matrix (Li et al. 2009; Ma et al. 2021). In this study, it could not be deduced whether the current settings or the ionic concentrations exceeded the critical values for the dendrites. The standard settings of this study were not selected while keeping the deposition morphology in perspective. Henceforth, it resulted in conditions that promoted uneven depositions and dendritic growth.

4.3. Impact of water composition on electrochemical reduction

4.3.1. pH effect

In the study, it was observed that the deposition of Fe and Mn declined with decreasing pH (Fig 3.6, Fig 3.5) of cathode feedwater. The Fe deposition declined by 82.7% from pH 7 to pH 4. In the case of Mn, the depositions declined almost by 100% since the deposition in pH 4 was negligible. This indicates that the effect of reducing pH was more severe in the case of Mn than Fe.

The negative effect of the pH decrease on the depositions could be explained by hypothesizing that the entropic barrier of the metal ions and H^+ ion changed with declining pH. It resulted in the entropic barrier of H^+ ion becoming very low and leading to H_2 production, while the entropic barrier of the metal ions stayed high. In an electrochemical cell, there is a formation of a cathode-solution interface in the form of an electric double-layer region between a cathode and the bulk solution (Zhang et al. 2021). The electrostatic environment of the double layer determines the entropic barrier for a particular ion, which becomes the rate-determining step for the electron transfer from the cathode to the metal ion (Rossmeisl et al. 2016). It was previously discussed in the literature that at low pH conditions, the entropic barrier for H^+ is small which causes high H_2 production (Rossmeisl et al. 2016). This will result in H_2 side-reaction dominating over the electrochemical reduction of metal ions and reducing the FE. The side reaction of the H_2 production during acidic conditions and is given by:

$$2H^+ + 2e^- \rightarrow H_2 \uparrow \tag{4.4}$$

The pH of the cathode feedwater matrix also determines the morphology of the depositions and the propensity of the metal ions to get reduced electrochemically. In the present study, the pH range for the experiments for between 4 to 8. The pH at this range makes the depositions susceptible to dendrites in the case of Fe deposits, which was confirmed through SEM pictures (Fig 4.4). A lower pH could have wielded better results in terms of smooth deposition. This can be concurred from a previous study in which at pH > 2.75, the quality of the iron deposits deteriorated, exhibiting increased surface roughness and dendrite formation (Mostad et al. 2008).

The stability of the metal ions in the cathode feedwater matrix was also impacted by pH. In the case of Mn, there was rapid precipitation at pH 8. The precipitation was indicated as $MnCO_3$ by PHREEQC simulation of the cathode feedwater (check Appendix .9). In the case of Fe, slight precipitation was observed at pH 8 and PHREEQC indicated it to be $FeCO_3$. While in for Al, precipitation was observed from pH 7 and above. It was indicated as $Al_2(CO_3)_3$, $Al_4(OH)_10SO_4$ and AlOOH by PHREEQC (check Appendix .9).

It was observed that with an increasing volume of water treated, the removal of the metal ions from water decreases (Fig 3.7, Fig 3.8). A contributory factor towards the decline in the electrochemical reduction performance could be the difficulty in the movement of the electroactive species (metal ions) from bulk solution towards the electrode surface. The metal ions in this cathode-solution interface continuously interact with the cathode to get reduced. In a previous study (Zhang et al. 2021), it was discussed that there is change in the distribution of the metal ions in the interface layer over time due to the formation of electroinactive materials. Electroinactive species such as H_2 and reduced metals interacts with the cathode and the interface through adsorbing and desorbing on the cathode surface, affecting the electrochemical reduction process.

4.3.2. Impact of ionic species

In the current study, the interactions between Fe^{2+}/Mn^{2+}/Al^{3+} and other species in the water matrix in individual experiments, and between the metal ions of Fe^{2+}, Mn^{2+}, Al^{3+}, and other species in the water matrix in combined experiments are occurring. It was observed that there is a significant drop-off in FE (faradaic efficiency) in combined experiments from the individual experiments (Fig 3.12). When comparing individual and combined experiments at pH 7, the FE for electrochemical reduction of Fe^{2+} declined from 35.05% in individual experiments to 11.5% in combined. Meanwhile, for Mn^{2+} the FE declined from 14.90% in individual to 1.75% in combined experiments. The drop in the case of Fe is more substantial than that of Mn. The low

FE values in combined experiments indicate that the electron transfer from cathode to Fe^{2+} and Mn^{2+} ions have reduced. If both the metal ions would have taken the same number of electrons as they did during the individual experiments, FE of 50.65% would have been achieved. However, it did not occur during combined experiments and there is a clear lack of synergy in FE.

In order to gain a better understanding of how these metal ions behave in their water matrices, pourbaix diagrams were developed with the help of the Materials Project (Anubhav et al. nd). In Fig 4.5, the pourbaix diagram of the combined water matrix is provided. It can be observed that a large number of interactions can happen between the three ionic species. There are possibilities for the formation of bonds between Fe^{2+}, Al^{3+}, and Mn^{2+} in different combinations. This may have impacted the performance (or lack of) of the electrochemical reduction in combined experiments since less number of free metal ions would have been available for the electrochemical reduction to take place. This could also possibly indicate why Al was present in the EDS-SEM analysis of the combined experiment. Since at pH 7, there are cases in which Al may join Fe and Mn ($MnAlFe_2$, Al_2FeO_4). It could be hypothesized that Al formed one of these pairs and got adsorbed to the deposits. Additionally, the electrochemical reduction performance of metal ions in combined experiments could have declined from the individual experiments since the water matrix in the cathode chamber was completely altered. This concurs with the previous studies which confirmed that the nature of anions and cations in the system has an effect on the electrochemical reduction process (Mustafa et al. 2020) and its thermodynamic feasibility (Kelly et al. 2003).

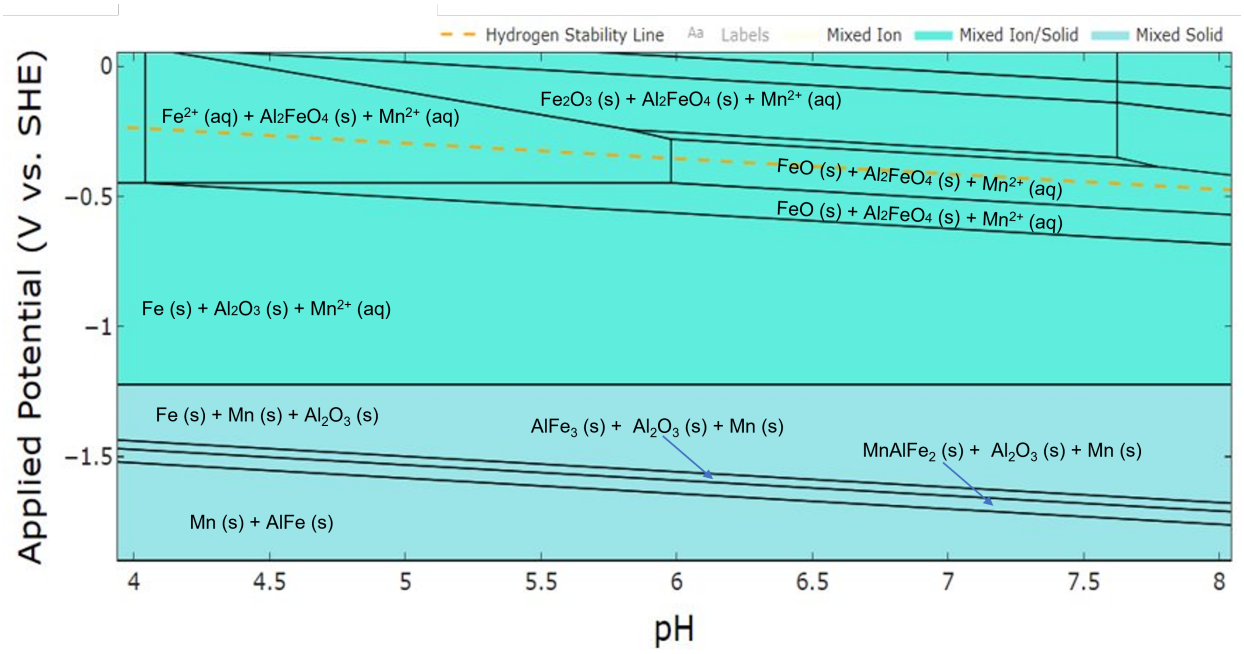

Figure 4.5: Pourbaix diagram for combined water matrix

4.4. Impact of material properties of cathode

4.4.1. Cathode base material

In this study, a stainless steel cathode was used. The peak FE observed throughout the experiment was 35.05% in the case of Fe^{2+} reduction at pH 7 (Fig 3.12). The lower FE of the electrochemical reduction of metal ions is attributed to the higher selectivity of the stainless steel cathode towards the electrochemical reduction of H^+ ions. The stainless steel cathode favoured H_2 evolution reaction and showed a lower preference towards transferring electrons to the metal ions and therefore, brought down the FE of metal ion reduction. This is in line with the previous findings related to stainless steel cathodes in which their higher preference towards H^+ electrochemical reduction was observed (Call et al. 2009). Other instances of stainless steel favouring H_2 production include the dominance of the side reaction of H_2 during electrochemical reduction of CO_2 for producing CO (Hori et al. 1985, 1994; Hussain et al. 2018) reaching FE of H_2 side reaction as high as 94.8%. The cathode material impacts electrochemical reduction since the selectivity of the product formed, i.e., the preference of the cathode towards the formation of a reduced product, is dependent on it.
Another property of stainless steel cathode which has an impact on its performance is its low hydrogen overpotential which results in H_2 side-reaction. In order for the cathode to electrochemically reduce a species, along with the reduction potential of the reaction, activation energy is also required. Activation energy can be considered in terms of high overpotential which is the additional potential, beyond the thermodynamic requirement, needed to drive a reaction at a certain rate (Bard & Faulkner 1980). A cathode should have high hydrogen overpotential so that electrochemical reduction of targeted species is preferred over the side reaction of H_2 production (Müller et al. 2016; Sáenz et al. 2012a). Additional information related to the overpotential of a cathode is provided in the Appendix (.12.1).

As discussed previously, dendritic depositions can form on the cathode. In the study, the stainless steel cathode was found to be susceptible to dendrite formation as seen in the SEM-EDS images. This is in line with the previous study which found that the phenomenon of dendrites formation is typical in stainless steel cathodes and is detrimental to the performance of the cathode (Kovendhan et al. 2019). Also, post-experiment, the stainless steel mesh cathode is difficult to maintain since reproducing its surface and keeping it clean is difficult. The presence of impurities in the solution may result in their diffusion onto the electrode surface and adsorption, which can significantly alter the interfacial properties (Bard & Faulkner 1980). Moreover, the surfaces of the solid electrodes are not atomically smooth and have defects, such as dislocation lines.

4.4.2. Formation of a passive layer on cathode

During the experiments, there is a possibility of the formation of a passive film of Cr oxide layer which could have resulted in poor performance of the cathode. Stainless steel alloy is typically composed of elements Fe, C, Ni, and Cr. It drives its corrosion-resistant properties from the Cr content. When exposed to oxygen, Cr in the steel forms a thin film of Cr_2O_3 that covers the stainless steel surface and protects the underlying iron from rusting. This layer is 1-3 nm thick and passive in nature, affecting the surface of the cathode (Kaun et al. 2004). Regular cleaning of the surface of the cathode or exposure to acids. results in a higher proportion of Cr on the surface, which then oxidizes and forms a uniform oxide-based passive film (Inc. nd). Cathodes made of stainless steel are susceptible to poisoning due to Cr oxide layer. This layer is known to cause high interfacial contact resistance on the surface of the electrode (Myung et al. 2008) and blocked pores on the surface (Tawfik et al. 2007). Further, in a study, a passive film of Cr oxide is also expected to form on the stainless steel cathode in a solution sparged with hydrogen and by supplying -0.1 V (Wang & Turner 2004).

4.5. Development of cell resistance

The study observed that with the current supplied being constant, the cell resistance increases with the increasing volume of the water treated (Fig 3.13) in both individual and combined experiments. The resistance in an electrochemical cell can be attributed to the anodic resistance, cathodic resistance, and resistance across the cation exchange membrane. Also, there is resistance within the solution media. Individual

resistances of a cathode, anode, and cation exchange membrane were not measured since the electrochemical cell was not connected to the potentiostat, which could have measured the voltages across these units. Instead, DC current was supplied directly to the cathode and anode. Therefore, only the overall cell voltages were measured from which the cell resistances were calculated. The existing data makes it difficult to predict which component of the electrochemical cell is the primary factor behind the increasing resistance in the cell. There was no fouling on the anode, and negligible fouling was observed on the cation exchange membrane. It can be hypothesized that the most significant contribution to the cell resistance would have come from the cathode. The depositions on the cathode make it difficult for the electrons to be supplied to the ions in the solution, which could lead to a buildup of resistance. A previous study based on a microbial cell with Fe3+ ions established cathode to be the main limiting factor and contributing up to 58% of the total internal cell resistance (Heijne et al. 2011). Also, as the volume of water is treated, the composition of the water matrix inside the cathode chamber and the cathode-solution interface changes. This could impact the resistance in the solution and at the interface, which increased in this case because of an increased presence of electroinactive species in the water and contributed to the overall cell resistance. Previous literature confirms the contribution of the resistances in electrolyte and electrolyte-electrode interface towards the cell resistance (MIT-OCW 2014). The difference in the cell resistance between the individual and combined experiments was also observed. However, further investigation is required to understand the root cause behind it.

4.6. Energy and economics

The energy consumption over the duration of the experiment can be calculated to ascertain the economics associated with integrating electrochemical reduction in the water treatment process. Energy in the form of kWh per unit volume (kWh/m^3) is calculated with the help of equation 1.10. From the equation, it is observed that for a constant current and flow rate, the energy consumed in the system is directly proportional to the voltage of the system. With an increase in the voltage of the system, energy consumption will also increase. The results showed that the voltage increases with increasing volumes of the treated effluent (Appendix .4). With the continuous operation of the electrochemical cell, the internal resistance of the system is increasing (Fig 3.13). This results in the increased voltage for the constant negative current supplied through the DC power source. Fig 4.6 shows the energy consumed (kWh/m^3) for Fe^{2+} and Mn^{2+} in the case of individual and combined experiments at pH 7. The general trend which emerges is that energy consumption increases with increasing volume of effluent treated. It is observed that the energy consumption in the case of individual Fe experiments increased by 17% when the volume of water treated reached 5.6 L. The energy consumed increased by 10% for Mn and 13% for combined experiments, respectively with the volume of water reaching 5.6 L. It is observed from Fig 4.6 that the maximum energy consumed by the system is 0.45 kWh/m^3. This value is considerably higher than energy per unit volume calculated in other electrochemical methods, such as 0.066 kWh/m^3 in electrochemical advanced oxidation processes (Rijsdijk 2022), 0.030 kWh/m^3 in horizontal embedded Fe-electrocoagulation, and 0.006 kWh/^{3} in Fe-electrocoagulation (Kraaijeveld 2021). However, since the current study was based on artificial water with extremely high concentrations of metal ions in it, the current density was kept high (30 A/m^2) to ensure sufficient cathodic deposits. In case of environmentally relevant concentrations associated with groundwater, a much lower current density should be applied.

In order to calculate the cost per unit volume for the electrochemical reduction method of treatment, the maximum capped price by the electricity usage as per the Dutch Government in 2023 (government.nl 2023), was considered, i.e. € 0.40 per kWh. Further, the maximum value of energy per unit volume, 0.45 kWh/m^3 was considered to account for the highest costs related to this method Fig 4.6. The maximum cost of treatment was calculated as €0.40 per kWh * 0.45 kWh/mm^3 = € 0.18/m^3.

However, this cost is only a part of operational expenditure (OPEX). Along with adding other cost heads related to OPEX such as manpower and administration charges, cathode cleaning, and deposition recovery costs. The treatment will also need to consider the costs associated with the capital expenditures, such as manufacturing plant-scale electrochemical reduction cell equipment (CAPEX). These costs, however, can be countered by the recovery of metal, which offers commercial benefits. Also, costs associated with managing and disposing of large amounts of sludge are saved through electrochemical reduction, which implies potential savings. In the end, the total economic burden of the electrochemical reduction process can be calculated using the formula:

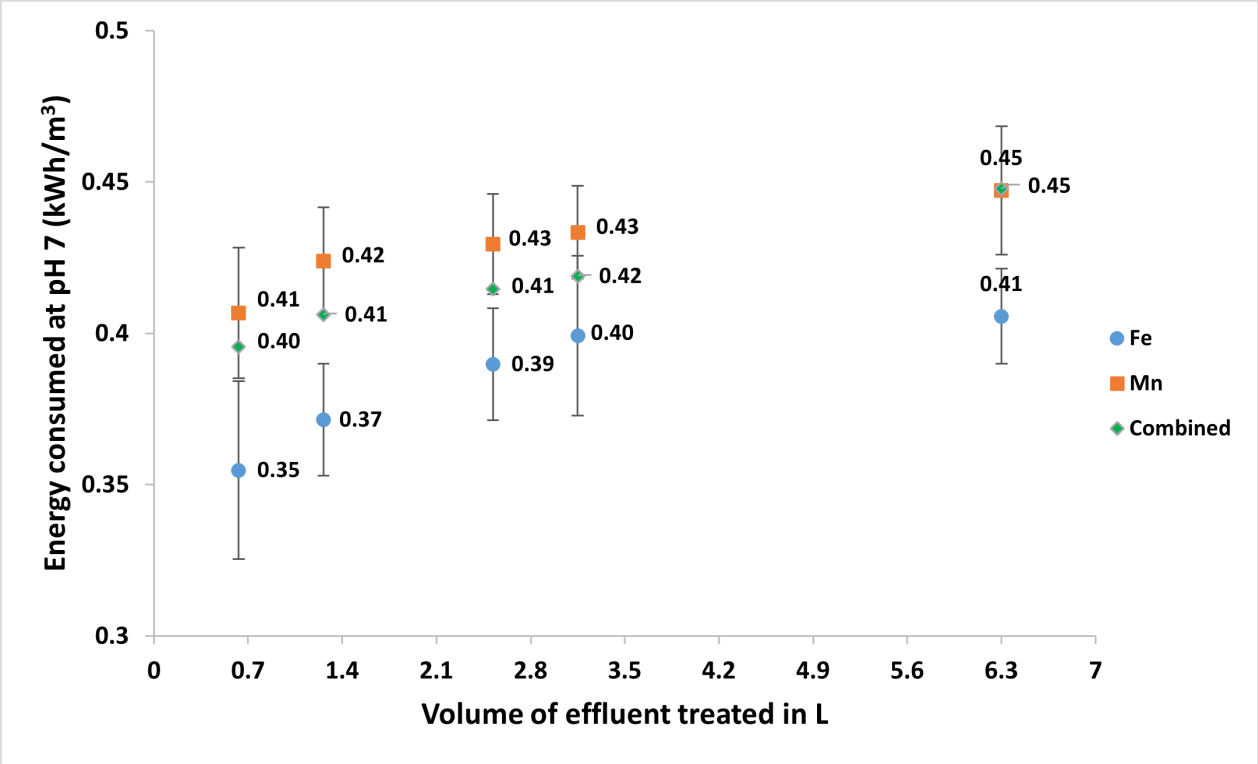

Figure 4.6: Energy consumption at pH 7

Cost = € 0.18/m3 + Remaining OPEX/m3 + CAPEX/m3 - Benefits from recovery of material/m3 - Cost of sludge disposal/m3 (4.5)

4.7. Maintaining cathode's performance and recovering the deposited metal

Once the metal is electrodeposited on the cathode, it needs to be collected for further utilization. Also, the build-up of deposits is detrimental to the performance of the cathode, so their removal is necessary before the next cycle. In this study, the focus was on studying how much 'recovery' of the metal is happening in terms of cathode deposits and not on actually recovering the deposited metal. The maintenance of the cathode was prioritized in order to have optimal performance in further experiments. Therefore, the deposits on the cathode were cleaned off by washing the cathode under water with soap and brush after each experiment. The results pf cleaning were found to be effective since the reused cathode was able to achieve similar effluent removal of the metal ions in the next iteration of the experiment. Also, the cell resistance for a given pH and cathode feed water composition did not change drastically after the cleaning. By cleaning the cathode, the diffusion process of the metal ions from the bulk to the cathode surface is improved as well as the transfer of electrons from the cathode to the metal ions is better. This improves the cathode's performance on reuse since the electrochemical reduction process at the cathode is rate limited by the diffusion of ions from the bulk solution to the cathode (Bard & Faulkner 1980). The surface behavior of the cathode can also be improved by activating the electrode surface with the help of switching of cathode and anode. It will result in the desorption of the adsorbed species on the previous cathode, causing them to move back into the bulk solution. This is because by switching, the direction of the current reverses and the electrode which was a cathode previously now becomes an anode, causing oxidation of the species adsorbed on its surface. The utilization of the switching experiment as a method of deposition removal has been discussed in the previous

studies (Bard & Faulkner 1980). Further information on the methodology for the switching experiment that can be followed is available in the Appendix (22).

In future studies, the recovery of the cathode deposits could be prioritized by applying different strategies. Mechanical scraping of the deposits at regular intervals to remove the electrodeposited metal has been found effective in separating metals. In one of the earliest studies in electrodeposition, silver was removed from the cathode with the help of wooden blades (Mosher 1934). The deposited metal and the cathode can have different thermal properties, such as melting point and the difference in melting point of a metal can be used for electrodeposition at high temperatures ensuring the electrodeposited metal melts and sinks to the bottom of the cathode while the cathode stays intact. Hydrometallurgical processes have been previously used to dissolve metals into solvents such as mineral acids, followed by their chemical precipitation (Jin & Zhang 2020). Nickel and copper can be dissolved in these acids and removed from the cathode. Another method that can be utilized is the use of seed cathodes. In this method, the cathode is made of the same material as the electrodeposited material, and post the cathodic reduction process, the cathode can be taken off. Further, cathodes such as rotating cathodes can prevent the deposition of the metal onto the cathode and result collection of the reduced material at the bottom of the cathode chamber (Bard & Faulkner 1980). Another method that has been found to be effective is the prevention of deposits onto the surface of the cathode by inducing agitation in the cathode chamber with the help of a stirrer or by deploying a rotating disc cathode (Bard & Faulkner 1980). In these cases, the depositions drop to the bottom of the cathode chamber and are easily collected. The rotating disc electrodes result in high rates of mass transport due to the turbulent flow regime, allowing metal deposition processes to take place at high speeds (Jüttner et al. 2000). In the present study, the design of the electrochemical cell was pre-determined and design modifications to induce agitation or aiding any other method of recovery on the cathode surface could not have been accommodated.

4.8. Translation case for environmentally relevant concentrations

In lieu of the removal rates for Fe and Mn obtained from the present study at extremely high concentrations, a theoretical case was developed for the removal of Fe and Mn present in groundwater in environmentally relevant concentrations. The concentrations were taken from a study by (Hamer et al. 2020), which is based on 32,000 groundwater samples taken from more than 4800 monitoring wells in Northern Germany. The median concentrations of Fe and Mn in samples taken from areas used as grasslands are 3.80 mg/L and 0.24 mg/L respectively. From the experiments, it was found that the maximum efficiencies for Fe, Mn, and combined removal were 35.05%, 14.90%, and 13.25% respectively. In the translation case, the combined case efficiency of 13.25% is considered. However, this 13.25% consists of an 11.5% efficiency for Fe and 1.75% efficiency for Mn.

The maximum allowed concentration as per health-based guidelines for Mn by World Health Organization is 0.08 mg/L (WHO 2023). However, as discussed previously, Fe and Mn compromise the utility of water at 0.3 mg/L and 0.02 mg/L. The removal is targeted at these concentrations. Further, the system settings from the study that are kept similar for the translation case are- the flow rate = 5.4 L/h, chamber volume = 200 cm^3, and the cathode area = 100 cm^2. Table 4.2 gives the results for the current that needs to be supplied for the required removal.

Contaminant	Removal to be achieved (mg/L)	Theoretical charge dosage (C/L)	Charge dosage required (C/L)
Fe	3.50	12.1	105.2
Mn	0.22	0.8	44.2

Table 4.2: Charge dosage required and current density to be supplied to achieve the desired concentrations

It is observed that in order to reach desired Fe^{2+} concentrations a current density of 15.8 A/m^2 is required while for Mn^{2+} concentrations current density of 6.6 A/m^2 is required. It shows that at environmentally relevant concentrations, for an influent flow rate of 5.4 L/h, much lower current densities are needed to achieve

the desired concentrations than the original current density of 30 A/m^2 supplied for this study. In this case, since the removal is happening for Fe and Mn combined, only one value of current density will be required, which could be the current density desired for Fe = 15.8 A/m^2. Assuming an average voltage of 7.5 V, at this current density, the energy requirement will be € 0.22 kWh/m^3. The energy costs will then be € 0.09 /m^3. This is already lower than the energy requirement and energy cost of 0.45 kWh/m3 and energy cost of € 0.18/m^3 established in this study.

Further, FE achieved in the current study has major scope for improvement by incorporating some of the recommendations which are mentioned in the forthcoming section (Recommendations 5.2). For instance, the maximum FE that was achieved across all the experiments in the current study was 35.05%. At this FE, the desired current densities for Fe and Mn removal are 5.18 A/m^2 and 0.33 A/m^2 respectively.

4.9. Applications and challenges of electrochemical reduction

4.9.1. Formation of hydrides through electrochemical reduction and their commercial potential

The presence of the element arsenic (As) in dissolved form As^{3+} has been detected in groundwater throughout the world (Nwankwo et al. 2020). Exposure to high levels of As for a prolonged time leads to adverse health conditions such as neurological disorders and cancer (KAPAJ et al. 2006). Therefore, the removal of As from water before its consumption is critical. Some of the currently used technologies for As removal from water includes ion exchange, coagulation and flocculation, adsorption on iron or alumina-based sorbents, electrocoagulation, and reverse osmosis (Mondal et al. 2013; Nicomel et al. 2016). These technologies rely on pre-oxidizing As^{3+} into a less toxic As^{5+} in an oxyanion form (H_2AsO_4 /$HAsO_4{}^2$) (Goren et al. 2020). Alhough reliable, these techniques have a challenge of the disposal of the toxic waste sludge produced after oxidation. The electrochemical reduction method offers a unique opportunity for removal of As^{3+} through its reduction at the cathode, resulting in the formation of elemental As depositions and arsine (AsH_3) production (Bejan & Bunce 2003; Salzberg & Goldschmidt 1960; Sengupta et al. 2010). The advantage of this method for As removal is that by reducing As^{3+} to pure element As and AsH_3, it forms two by-products that offer a commercial potential due to their widespread usage in the semiconductor industry. Also, it uses electrons as a reducing agent and therefore decreases the chemical usage. Hence, electrochemical reduction of arsenic offers the combined benefits of removal of toxic contaminant and recovery of valuable materials with economic benefits.

Fig 4.7 provides an overview of the setup, which can be used for the removal of As from water. The setup deploys the same system used in the current study except that the AsH_3 gas produced at the cathode is captured with the help of an adsorbing unit. Further, AsH_3 indicators and sensors can be used to ensure no leakage of this toxic gas occurs. Also, the experimental setup needs to have working conditions with a robust ventilation facility around such by the use of fumehood. The system can use cathodes with high hydrogen overpotentials, such as Cd and Pt-based cathodes, to maximize As^{3+} cathodic reduction and minimal side reactions ((Sáenz et al. 2012a)). This technique has proven to work effectively in both acidic and alkaline pH ranges ((Bejan & Bunce 2003)).

Further, the electrochemical reduction can also be used for the removal of phosphates from wastewater ((Nichols 2023; Snyder & Morales-Guio 2022)), disinfection by-products such as bromates ((Kishimoto & Matsuda 2009)), and heavy metals such as copper ((M. et al. 2013)).

The chemical reactions that this method will entail are provided below:

Cathode

$$2H^+ + 2e^- \rightarrow H_2 \uparrow \tag{4.6}$$

$$As^{5+} + 2e^- \rightarrow As3^+ \tag{4.7}$$

$$As^{3+} + 3e^- \rightarrow As \tag{4.8}$$

$$As + 3e^- \rightarrow AsH_3 \uparrow + 3H^+ \tag{4.9}$$

Anode

$$2H_2O - 2e^- \rightarrow \frac{1}{2}O_2 \uparrow + 2H^+ \tag{4.10}$$

$$Cl^- - e^- \rightarrow \frac{1}{2}Cl_2 \uparrow \tag{4.11}$$

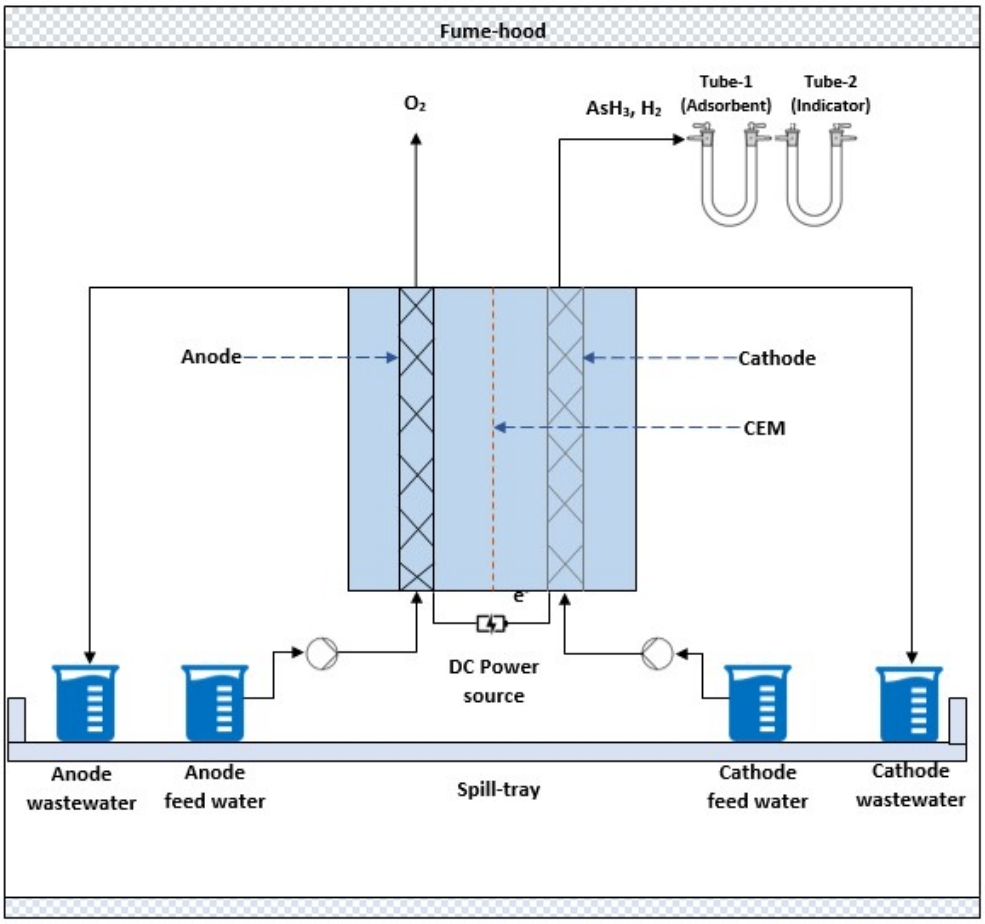

Figure 4.7: Experimental setup for electrochemical reduction of arsenic in water.

4.9.2. Development of magnetite semiconductor

Magnetite (Fe_3O_4 behaves as a useful semiconductor, with important properties such as a band gap of 0.1 eV, electronic conductivity around 200 $ohm^{-1}{\cdot}cm^{-1}$ at room temperature and reaching a maximum around 355 K, above which it shows a metallic behaviour (Teng 2008). Magnetic graphene oxide nanocomposites have been developed for multidimensional applications, including energy storage, water treatment, and drug delivery (Wang et al. 2013). Electrochemical reduction of oxic Fe-rich water can be used to produce Fe_3O_4 nanoparticles leading to cathodic deposition under mild conditions (Karimzadeh et al. 2018). The following cathodic reactions take place for the deposition:

$$2\,H_2O + 2\,e^- \rightarrow H_2 \uparrow + 2\,OH^- \tag{4.12}$$

$$2\,Fe^{3+}(aq) + 2\,Fe^{2+}(aq) + 8\,OH^- \rightarrow Fe_3O_4 + 4\,H_2O \tag{4.13}$$

4.9.3. Challenges in the utilization of electrochemical reduction method for water treatment

Given the high number of interconnected variables which were previously discussed (Table 1.1), it becomes extremely difficult to find the optimum system setting for the treatment of water containing multiple types of ions. In the study, it was found that the ions of Fe, Al, and Mn performed differently under the same set of conditions. Therefore, finding standard operational settings that can treat a vast majority of contaminants in the water is a research and engineering challenge.

The H_2 side reaction is a detrimental process and needs to be subverted. This can be achieved by using a cathodes such as Cd or Pt-based with high hydrogen overpotential (Sáenz et al. 2012a). However, these cathodes are expensive to procure and would have made the electrochemical reduction very expensive for water treatment. Further, the depositions of the electrochemically reduced material settles on the cathode resulting in a permanent morphological damage. Even after cleaning of the cathode, its surface is never the same.

In the study, direct DC current was supplied to the electrochemical cell for electrochemical reduction process. Since potentiostat was not used, the resistances developing in different components of the cell could not be determined.

5

Conclusion and Recommendations

5.1. Conclusion

The study shows that while Fe^{2+} and Mn^{2+} were electrochemically reduced in a wide range of the water matrices in different proportions, no apparent electrochemical reduction was observed in Al^{3+}. This implies that for the system settings established in the study, the electrochemical reduction was selective towards the removal of Fe^{2+} and Mn^{2+} and not for Al^{3+}. Further, Fe^{2+} removal was better than Mn^{2+} removal across all water matrices.

It was observed that the depositions of metals were strongly impacted by the pH of the cathode feedwater. The depositions on the cathode increased with the increasing pH. The Fe^{2+} depositions increased from 0.109 μm at pH 4 to 0.630 μm at pH 7 (by a factor of 5.8) and for Mn^{2+} it increased from 0.067 μm at pH 4 to 0.223 μm at pH 7 (factor of 3.3). While it was proposed initially that this study can be a field of interest for the treatment of acid mine drainage water due to high concentrations, the poor performance at low pH with the system settings in this study shows that more research is required for the process optimization, so that more apt system settings could be selected.

During the electrochemical reduction over the volume of the water treated, it was observed that the concentration of metal ions in the effluent decreased initially before increasing again. The effluent concentrations became equivalent to the influent concentrations (0.72 mmol/L) by the time the volume of water treated reached 6.3 L. It shows that the electrochemical reduction of the metal ions declined with the increasing volume of water treated.

The depositions were also affected by the ionic composition of the water. It was observed that the electrochemical reduction of a water matrix in the individual case performed better than the water matrix in the combined case. Henceforth, the depositions were higher in the individual experiments. For instance, at pH 7, it was observed that the faradaic efficiency of electrochemical reduction of Fe^{2+} declined from 35.05% in the individual experiments to 11.5% in the combined experiment. In the case of Mn^{2+} the decline was from 14.90% to 1.75%.

It was also observed that as the volume of water treated increases, the voltage of the cell increases. This is due to the increasing resistance of the cell which in turn depends on the resistances developing in anode, cathode, cation exchange membrane and the solution.

Electrochemical reduction can be utilized for treating water of contaminants impurities such as heavy metals, arsenic, and disinfection by-products like bromates; ensuring recovery of high-value products on the cathode and avoiding the production of excessive sludge with little economic value.

5.2. Recommendations for future research

This study was done with metal ions in extremely high concentrations of 0.72 mmol/L in the water matrix so that noticeable results in terms of metal ion removal and deposition build-up can be observed. The next step should be to perform these experiments on the concentrations which are found in the environment. Further, groundwater samples from the field can be taken for analysis.

Since Fe^{2+}, Mn^{2+}, and Al^{3+} had very different performances in the standardized settings for the study, more research is required towards alterations in the settings of current density and charge dosages to optimize the groundwater treatment process. Also, experiments could be carried out by connecting the electrochemical cell to a potentiostat in order to determine the potentials which are required to electrochemically reduce the dissolved species. A potentiostat can also help in determining the voltages developing on the cathode and anode and therefore, analyzing the contribution of the resistances developing in these components towards the total cell resistance.

An important outcome from the literature research done for this study was the impact that the material properties of the cathode have on the depositions. Hence, a study on the different cathode configurations in terms of material (Cd/Pt/Al/graphite-based), surface area, surface texture, and stationary and rotating type cathodes, could be undertaken. Performing experiments with the cathodes having high hydrogen overpotential (such as Cd or Pt electrodes) will help improve the FE and hence offer better removal of contaminants.

Since electrochemical reduction leads to the recovery of valuable depositions on the cathode, an investigation into finding methods to efficiently recover the deposits is required. Different methods such as manual scraping, chemical leaching, or experimental setup modification could be utilized for the research. A study based on a cathode-anode switching experiment can be a valuable method for removing depositions from the cathode, thus maintaining its performance. In this, a non-sacrificial cathode can be taken so that the cathode does not dissolve into the water on being switched to the anode.

Studies for arsenic and phosphate removal can be undertaken after taking adequate safety measures since the by-products from their cathodic reduction- arsine and phosphine respectively, have good commercial potential due to their requirements in the semiconductor industry. Further, a study to optimize system settings for the removal at low pH, for the treatment of acid mine drainage could also be developed.

The study had a challenge of delay between the electrochemical reduction experiment and its analysis through ICP-MS and SEM-EDS. This could have resulted in issues such as the oxidation of the deposits on the cathode once it was taken out of the electrochemical cell, for analysis in SEM-EDS. A study by utilizing in-situ and fast analytical methods such as X-ray fluorescence (XRF) or portable SEM can provide valuable real-time information on the deposits.

Bibliography

Ahmad, Z. (2006). *CHAPTER 2 - BASIC CONCEPTS IN CORROSION*. Butterworth-Heinemann. https://doi.org/https://doi.org/10.1016/B978-075065924-6/50003-9

Antony, H., Legrand, L., Maréchal, L., Perrin, S., Dillmann, P., & Chaussé, A. (2005). Study of lepidocrocite -feooh electrochemical reduction in neutral and slightly alkaline solutions at 25 °c. *Electrochimica Acta*, 51, 745–753. https://doi.org/10.1016/j.electacta.2005.05.049

Anubhav, J., Ong, S. P., Hautier, G., Richards, W. D., Chen, W., Dacek, S., Cholia, S., Gunter, D., Skinner, D., Ceder, G., & Persson, K. A. (n.d.). Commentary: The materials project: A materials genome approach to accelerating materials innovation. *Materials Project*.

Appleton, J. D., Fuge, R., & Mccall, G. (1996). *Groundwater geochemistry and health: an overview*. https://www.lyellcollection.org

Bard, A. J. & Faulkner, L. (1980). *Electrochemical Methods* (2 ed.). Wiley.

Bejan, D. & Bunce, N. J. (2003). Electrochemical reduction of as(iii) and as(v) in acidic and basic solutions. *Journal of Applied Electrochemistry*, 33, 483–489. https://doi.org/10.1023/A:1024491019960

Bigham, J. M. & Nordstrom, D. K. (2019). Iron and aluminum hydroxysulfates from acid sulfate waters. *Sulfate Minerals: Crystallography, Geochemistry, and Environmental Significance*, 40, 351–403. https://doi.org/10.2138/rmg.2000.40.7

Call, D. F., Merrill, M. D., & Logan, B. E. (2009). High surface area stainless steel brushes as cathodes in microbial electrolysis cells. *Environmental Science Technology*, 43, 2179–2183. https://doi.org/10.1021/es803074x. doi: 10.1021/es803074x

Cambridge (n.d.). Electrochemical and microengineering- undergraduate teaching notes. https://www.ceb.cam.ac.uk/research/groups/rg-eme/Edu/electrode-kinetics

Darband, G. B., Lotfi, N., Aliabadi, A., Hyun, S., & Shanmugam, S. (2021). Hydrazine-assisted electrochemical hydrogen production by efficient and self-supported electrodeposited ni-cu-p@ni-cu nano-micro dendrite catalyst. *Electrochimica Acta*, 382, 138335. https://doi.org/https://doi.org/10.1016/j.electacta.2021.138335

Deltares (2022). *Water security - focus on groundwater: Key to a sustainable and resilient world*. https://www.deltares.nl/app/uploads/2022/03/Water-security-focus-on-groundwater-Deltares.pdf

Durst, J., Siebel, A., Simon, C., Hasché, F., Herranz, J., & Gasteiger, H. A. (2014). New insights into the electrochemical hydrogen oxidation and evolution reaction mechanism. *Energy and Environmental Science*, 7, 2255 – 2260. https://doi.org/10.1039/c4ee00440j. Cited by: 1024; All Open Access, Green Open Access, Hybrid Gold Open Access

Díaz, S. L., Calderón, J. A., Barcia, O. E., & Mattos, O. R. (2008). Electrodeposition of iron in sulphate solutions. *Electrochimica Acta*, 53, 7426–7435. https://doi.org/https://doi.org/10.1016/j.electacta.2008.01.015. 7th International Symposium on Electrochemical Impedance Spectroscopy

EU (1998). Council directive 98/83/ec of 3 november 1998 on the quality of water intended for human consumption. *Official Journal of the European Communities*. https://eur-lex.europa.eu/legal-content/EN/TXT/PDF/?uri=CELEX:31998L0083&from=EN

Ezugbe, E. & Rathilal, S. (2020). Membrane technologies in wastewater treatment: A review. *Membranes*, 10, 89. https://doi.org/10.3390/membranes10050089

Felloni, L. (1968). The effect of ph on the electrochemicalbehaviour of iron in hydrochloric acid. *Corrosion Science*, 8, 133–148. https://doi.org/https://doi.org/10.1016/S0010-938X(68)80196-9

Ghernaout, D., Aichouni, M., & Touahmia, M. (2019). *Mechanistic insight into disinfection by electrocoagulation - a review*. https://doi.org/10.5004/dwt.2019.23457

Goren, A. Y., Kobya, M., & Oncel, M. S. (2020). Arsenite removal from groundwater by aerated electrocoagulation reactor with al ball electrodes: Human health risk assessment. *Chemosphere*, 251, 126363. https://doi.org/https://doi.org/10.1016/j.chemosphere.2020.126363

government.nl (2023). Price cap for gas, electricity and district heating. *Government of Netherlands, Energy Crisis*. https://www.government.nl/topics/energy-crisis/cabinet-plans-price-cap-for-gas-and-electricity

Grimm, J., Bessarabov, D., & Sanderson, R. (1998). *Review of electro-assisted methods for water purification*. https://doi.org/10.1016/S0011-9164(98)00047-2

Hamer, K., Gudenschwager, I., & Pichler, T. (2020). Manganese (mn) concentrations and the mn-fe relationship in shallow groundwater: Implications for groundwater monitoring. *Soil Systems*, 4. https://doi.org/10.3390/soilsystems4030049

Hao, F., Verma, A., & Mukherjee, P. P. (2019). Electrodeposition stability of metal electrodes. *Energy Storage Materials*, 20, 1–6. https://doi.org/https://doi.org/10.1016/j.ensm.2019.05.004

Hart, K. A., Kennedy, G. W., & Sterling, S. M. (2021). *Distribution, drivers, and threats of aluminum in groundwater in nova scotia, canada*. https://doi.org/10.3390/w13111578

Heijne, A. T., Liu, F., Rijnsoever, L. S. V., Saakes, M., Hamelers, H. V., & Buisman, C. J. (2011). Performance of a scaled-up microbial fuel cell with iron reduction as the cathode reaction. *Journal of Power Sources*, 196, 7572–7577. https://doi.org/10.1016/j.jpowsour.2011.04.034

Hessami, S. & Tobias, C. W. (1989). A mathematical model for anomalous codeposition of nickel-iron on a rotating disk electrode. *Journal of The Electrochemical Society*, 136, 3611. https://doi.org/10.1149/1.2096519

Hori, Y., Kikuchi, K., & Suzuki, S. (1985). *The chemical*.

Hori, Y., Wakebe, H., Tsukamoto, T., & Koga, O. (1994). Electrocatalytic process of co selectivity in electrochemical reduction of co2 at metal electrodes in aqueous media. *Electrochimica Acta*, 39, 1833–1839. https://doi.org/10.1016/0013-4686(94)85172-7

Hussain, J., Jónsson, H., & Skúlason, E. (2018). Calculations of product selectivity in electrochemical co2 reduction. *ACS Catalysis*, 8, 5240–5249. https://doi.org/10.1021/acscatal.7b03308. doi: 10.1021/acscatal.7b03308

Inc., B. T. (n.d.). What is passivation? how does passivation process work? how to passivate stainless steel parts? https://www.besttechnologyinc.com/passivation-systems/what-is-passivation/

Jartych, E., Jałochowski, M., & Budzyński, M. (2002). Influence of the electrodeposition parameters on surface morphology and local magnetic properties of thin iron layers. *Applied Surface Science*, 193, 210–216. https://doi.org/https://doi.org/10.1016/S0169-4332(02)00474-9

Jin, W. & Zhang, Y. (2020). Sustainable electrochemical extraction of metal resources from waste streams: From removal to recovery. *ACS Sustainable Chemistry Engineering*, 8, 4693–4707. https://doi.org/10.1021/acssuschemeng.9b07007. doi: 10.1021/acssuschemeng.9b07007

Jüttner, K., Galla, U., & Schmieder, H. (2000). Electrochemical approaches to environmental problems in the process industry. *Electrochimica Acta*, 45, 2575–2594. https://doi.org/https://doi.org/10.1016/S0013-4686(00)00339-X

Kang, N.-Y. & Lee, J.-H. (2023). Effects of bath composition and current density on the electrodeposition behavior of fe–ni invar alloy. *Electronic Materials Letters*. https://doi.org/10.1007/s13391-023-00413-8

KAPAJ, S., PETERSON, H., LIBER, K., & BHATTACHARYA, P. (2006). Human health effects from chronic arsenic poisoning–a review. *Journal of Environmental Science and Health, Part A*, 41, 2399–2428. https://doi.org/10.1080/10934520600873571. doi: 10.1080/10934520600873571

Karimzadeh, I., Aghazadeh, M., Doroudi, T., Ganjali, M. R., & Kolivand, P. H. (2018). Electrochemical preparation and characterization of chitosan-coated superparamagnetic iron oxide (fe3o4) nanoparticles. *Materials Research Innovations*, 22, 352–360. https://doi.org/10.1080/14328917.2017.1323991. doi: 10.1080/14328917.2017.1323991

Kaun, T. D., Cruse, T. A., & Krumpelt, M. (2004). *Chromium Poisoning of Cathodes by Ferritic Stainless Steel*. https://doi.org/https://doi.org/10.1002/9780470291184.ch58

Kelly, R., Scully, J., Shoesmith, D., & Buchheit, R. (2003). Electrochemical techniques in corrosion science and engineering. https://doi.org/10.1201/9780203909133

Kishimoto, N. & Matsuda, N. (2009). Bromate ion removal by electrochemical reduction using an activated carbon felt electrode. *Environmental Science Technology*, 43, 2054–2059. https://doi.org/10.1021/es803144w

Korshin, G. V. & Jensen, M. D. (2001). Electrochemical reduction of haloacetic acids and exploration of their removal by electrochemical treatment. *Electrochimica Acta*, 47, 747–751. www.elsevier.com/locate/electacta

Kovendhan, M., Kang, H., Jeong, S., Youn, J. S., Oh, I., Park, Y. K., & Jeon, K. J. (2019). Study of stainless steel electrodes after electrochemical analysis in sea water condition. *Environmental Research*, 173, 549–555. https://doi.org/10.1016/j.envres.2019.03.069

Kraaijeveld, E. (2021). *Horizontally embedded fe(0) electrocoagulation to enhance as(iii) removal in biologically active rapid sand filters for drinking water treatment*. https://repository.tudelft.nl/islandora/object/uuid%3Ab2e70821-9804-405b-a98f-0ff6542945d6

Li, Q., Jensen, J. O., & Bjerrum, N. (2009). *Chemistry, electrochemistry, and electrochemical applications | aluminum*. https://doi.org/10.1016/B978-044452745-5.00951-5

LibreTexts (2021). Standard reduction potential libretexts chem. https://chem.libretexts.org/Bookshelves/Analytical_Chemistry/Supplemental_Modules_(Analytical_Chemistry)/Electrochemistry/Redox_Chemistry/Standard_Reduction_Potential

Lotfi, N., Shahrabi, T., Yaghoubinezhad, Y., & Darband, G. B. (2019). Electrodeposition of cedar leaf-like graphene oxide@ni–cu@ni foam electrode as a highly efficient and ultra-stable catalyst for hydrogen evolution reaction. *Electrochimica Acta*, 326. https://doi.org/10.1016/j.electacta.2019.134949. Cited by: 43

M., E., F.C., V., & Matencio, T. (2013). *Metallic and oxide electrodeposition*. https://doi.org/10.5772/55684

M, T. & H, G. (2019). High-resolution sem and edx characterization of deposits formed by ch+ar dbd plasma processing in a packed bed reactor. *Nanomaterials (Basel)*.

Ma, M. C., Li, G., Chen, X., Archer, L. A., & Wan, J. (2021). *Suppression of dendrite growth by cross-flow in microfluidics*. https://www.science.org

McFarland, M. L. & Dozier, M. C. (2023). *Drinking water problems: Iron and manganese*. https://texaswater.tamu.edu/resources/factsheets/l5451ironandman.pdf

MIT-OCW (2014). *Lecture 2: Basic physics of galvanic cells electrochemical energy conversion*. https://ocw.mit.edu/courses/10-626-electrochemical-energy-systems-spring-2014/ca1416c480deca1321a5edd1aa971557_MIT10_626S14_Lec2.pdf

Mondal, P., Bhowmick, S., Chatterjee, D., Figoli, A., & der Bruggen, B. V. (2013). Remediation of inorganic arsenic in groundwater for safe water supply: A critical assessment of technological solutions. *Chemosphere*, 92, 157–170. https://doi.org/https://doi.org/10.1016/j.chemosphere.2013.01.097

Mosher, M. A. (1934). *Volume 106 - papers - refining - miscellaneous - recovery of precious and secondary metals from electrolytic copper refining*.

Mostad, E., Rolseth, S., & Thonstad, J. (2008). Electrowinning of iron from sulphate solutions. *Hydrometallurgy*, 90, 213–220. https://doi.org/https://doi.org/10.1016/j.hydromet.2007.07.014

Mustafa, A., Lougou, B. G., Shuai, Y., Wang, Z., Razzaq, S., Zhao, J., & Tan, H. (2020). Theoretical insights into the factors affecting the electrochemical reduction of co2. *Sustainable Energy Fuels*, 4, 4352–4369. https://doi.org/10.1039/D0SE00544D

Myung, S.-T., Kumagai, M., Asaishi, R., Sun, Y.-K., & Yashiro, H. (2008). Nanoparticle tin-coated type 310s stainless steel as bipolar plates for polymer electrolyte membrane fuel cell. *Electrochemistry Communications*, 10, 480–484. https://doi.org/https://doi.org/10.1016/j.elecom.2008.01.001

Müller, C. I., Sellschopp, K., Tegel, M., Rauscher, T., Kieback, B., & Röntzsch, L. (2016). The activity of nanocrystalline fe-based alloys as electrode materials for the hydrogen evolution reaction. *Journal of Power Sources*, 304, 196–206. https://doi.org/https://doi.org/10.1016/j.jpowsour.2015.11.008

Nichols, E. M. (2023). Electrochemistry cracks the p–o bond: Sustainable reduction of phosphates to phosphorus. *ACS Central Science*, 9, 343–345. https://doi.org/10.1021/acscentsci.3c00056. doi: 10.1021/acscentsci.3c00056

Nicomel, N. R., Leus, K., Folens, K., Van Der Voort, P., Du Laing, G., Naidu, R., & Rahman, M. M. (2016). Technologies for arsenic removal from water: Current status and future perspectives. *International Journal of Environmental Research and Public Health*, 13, 0062. https://doi.org/10.3390/ijerph13010062

Nwankwo, C. B., Hoque, M. A., Islam, M. A., & Dewan, A. (2020). Groundwater constituents and trace elements in the basement aquifers of africa and sedimentary aquifers of asia: Medical hydrogeology of drinking water minerals and toxicants. *Earth Systems and Environment*, 4, 369–384. https://doi.org/10.1007/s41748-020-00151-z

Qasem, N., Mohammed, R., & Lawal, D. (2021). *Removal of heavy metal ions from wastewater: a comprehensive and critical review*. https://doi.org/10.1038/s41545-021-00127-0

Qiu, R., Zheng, J. Y., Cha, H., Jung, M.-H., Lee, K., & Kang, Y. (2012). One-dimensional ferromagnetic dendritic iron wire array growth by facile electrochemical deposition. *Nanoscale*, 4, 1565–1567. https://doi.org/10.1039/c2nr11780k

Radjenovic, J., Bagastyo, A., Rozendal, R. A., Mu, Y., Keller, J., & Rabaey, K. (2011). Electrochemical oxidation of trace organic contaminants in reverse osmosis concentrate using ruo2/iro2-coated titanium anodes. *Water Research*, 45, 1579–1586. https://doi.org/https://doi.org/10.1016/j.watres.2010.11.035

Rijsdijk, S. (2022). *Exploring electrochemical advanced oxidation processes as novel method for arsenic removal from dune water*. https://repository.tudelft.nl/islandora/object/uuid%3Ad6e89818-d818-46fa-8408-ea752c2c09d8

Rossmeisl, J., Chan, K., Skúlason, E., Björketun, M. E., & Tripkovic, V. (2016). On the ph dependence of electrochemical proton transfer barriers. *Catalysis Today*, 262, 36–40. https://doi.org/10.1016/j.cattod.2015.08.016

Ruj, D. B., Chakrabortty, D. S., Nayak, D. J., & Chatterjee, R. (2021). Treatment of arsenic sludge generated from groundwater treatment plant: A review towards a sustainable solution. *South African Journal of Chemical Engineering*, 37, 214–226. https://doi.org/https://doi.org/10.1016/j.sajce.2021.06.003

Salzberg, H. W. & Goldschmidt, B. (1960). Arsine evolution and water reduction at an arsenic cathode. *Journal of The Electrochemical Society*, 107, 348. https://doi.org/10.1149/1.2427692

Sengupta, M. K., Sawalha, M. F., Ohira, S. I., Idowu, A. D., & Dasgupta, P. K. (2010). Green analyzer for the measurement of total arsenic in drinking water: Electrochemical reduction of arsenate to arsine and gas phase chemiluminescence with ozone. *Analytical Chemistry*, 82, 3467–3473. https://doi.org/10.1021/ac100604y

Sirés, I., Brillas, E., Oturan, M. A., Rodrigo, M. A., & Panizza, M. (2014). *Electrochemical advanced oxidation processes: today and tomorrow. a review.* https://doi.org/10.1007/s11356-014-2783-1

Snyder, N. A. & Morales-Guio, C. G. (2022). Perspective on the electrochemical recovery of phosphate from wastewater streams. *Electrochemical Science Advances*, n/a, e2200010. https://doi.org/https://doi.org/10.1002/elsa.202200010. https://doi.org/10.1002/elsa.202200010

Subbaiah, T., Vijetha, P., Marandi, B., Sanjay, K., & Minakshi, M. (2022). Ionic mass transfer at point electrodes located at cathode support plate in an electrorefining cell in presence of rectangular turbulent promoters. *Sustainability*, 14. https://doi.org/10.3390/su14020880

Sáenz, M., Fernández, L., Domínguez, J., & Alvarado, J. (2012a). Electrochemical generation of volatile lead species using a cadmium cathode: Comparison with graphite, glassy carbon and platinum cathodes. *Spectrochimica Acta Part B: Atomic Spectroscopy*, 71-72, 107–111. https://doi.org/https://doi.org/10.1016/j.sab.2012.03.009

Sáenz, M., Fernández, L., Domínguez, J., & Alvarado, J. (2012b). Electrochemical generation of volatile lead species using a cadmium cathode: Comparison with graphite, glassy carbon and platinum cathodes. *Spectrochimica Acta Part B: Atomic Spectroscopy*, 71-72, 107–111. https://doi.org/https://doi.org/10.1016/j.sab.2012.03.009. COLLOQUIUM SPECTROSCOPICUM INTERNATIONALE XXXVII (CSI XXXVII)

Tawfik, H., Hung, Y., & Mahajan, D. (2007). Metal bipolar plates for pem fuel cell—a review. *Journal of Power Sources*, 163, 755–767. https://doi.org/https://doi.org/10.1016/j.jpowsour.2006.09.088

Teng, C.-L. (2008). *Investigation of electrodeposited magnetite films: Formation and characterization.*

Tkalenko, M. D., Tkalenko, D. A., & Kublanovs'kyi, V. S. (2002). *Change in the ph of solutions and the cathodic passivation of metals under the conditions of electrochemical protection in aqueous media o 2 + 2 h 2 o + 4 e = 4 oh.*

Tufano, K. J. & Fendorf, S. (2008). *Confounding impacts of iron reduction on arsenic retention.* https://doi.org/10.1021/es702625e

UNESCO (2022). *The united nations world water development report 2022 groundwater making the invisible visible facts and figures.* https://en.unesco.org/wwap.

United, N. (2023). *The 17 goals.* https://sdgs.un.org/goals

USBR.gov (2023). *Water facts - worldwide water supply.* https://www.usbr.gov/mp/arwec/water-facts-ww-water-sup.html

van Genuchten, C. M., Addy, S. E. A., Peña, J., & Gadgil, A. J. (2012). *Removing arsenic from synthetic groundwater with iron electrocoagulation: An fe and as k-edge exafs study.* https://doi.org/10.1021/es201913a. doi: 10.1021/es201913a

Vik, E. A., Carlson, D. A., Eikum, A. S., & Gjessing, E. T. (1984). *Electrocoagulation of potable water.* https://doi.org/10.1016/0043-1354(84)90003-4

Wang, G., Chen, G., Wei, Z., Dong, X., & Qi, M. (2013). Multifunctional fe3o4/graphene oxide nanocomposites for magnetic resonance imaging and drug delivery. *Materials Chemistry and Physics*, 141, 997–1004. https://doi.org/10.1016/j.matchemphys.2013.06.054

Wang, H. & Turner, J. (2004). Ferritic stainless steels as bipolar plate material for polymer electrolyte membrane fuel cells. *Journal of Power Sources*, 128, 193–200. https://doi.org/10.1016/j.jpowsour.2003.09.075

WHO (1997). *Aluminium in drinking-water background document for development of who guidelines for drinking-water quality.* https://apps.who.int/iris/bitstream/handle/10665/75362/WHO_SDE_WSH_03.04_53_eng.pdf?se

WHO (2022). *Fourth edition incorporating the first and second addenda guidelines for drinking-water quality.* https://www.who.int/publications/i/item/9789240045064

WHO (2023). *Guidelines for drinking-water quality: fourth edition incorporating the first and second addenda. corrigenda (24 may 2023).* https://cdn.who.int/media/docs/default-source/wash-documents/water-safety-and-quality/dwq-guidelines-4/9789240045064_corrigenda_rev-gdwq-2-addenda.pdf?sfvrsn=c95453c4_3

wirecloth, C. (n.d.). Measure wire mesh open area. http://www.wirecloth.com/cwc-inc/ptrslts.htm?measure=2&value1=0.26&value2=30&Submit=Calculate

Wołowiec, M., Komorowska-Kaufman, M., Pruss, A., Rzepa, G., & Bajda, T. (2019). Removal of heavy metals and metalloids from water using drinking water treatment residuals as adsorbents: A review. *Minerals*, 9. https://doi.org/10.3390/min9080487

WQA (2022). *What is manganese? manganese fact sheet.* 26/10/2022https://wqa.org/wp-content/uploads/2022/09/20220614_ConsumerContent_Manganese.pdf

Xie, L. & Shang, C. (2006). A review on bromate occurrence and removal strategies in water supply. *Water Science and Technology: Water Supply*, 6, 131–136. https://doi.org/10.2166/ws.2006.960

Yao, F., Yang, Q., Zhong, Y., Shu, X., Chen, F., Sun, J., Ma, Y., Fu, Z., Wang, D., & Li, X. (2019). Indirect electrochemical reduction of nitrate in water using zero-valent titanium anode: Factors, kinetics, and mechanism. *Water Research*, 157, 191–200. https://doi.org/10.1016/j.watres.2019.03.078

Zaghdoudi, M., Fourcade, F., Soutrel, I., Floner, D., Amrane, A., Maghraoui-Meherzi, H., & Geneste, F. (2017). Direct and indirect electrochemical reduction prior to a biological treatment for dimetridazole removal. *Journal of Hazardous Materials*, 335, 10–17. https://doi.org/10.1016/j.jhazmat.2017.04.028

Zhang, Y., Tang, J., Ni, Z., Zhao, Y., Jia, F., Luo, Q., Mao, L., Zhu, Z., & Wang, F. (2021). Real-time characterization of the fine structure and dynamics of an electrical double layer at electrode–electrolyte interfaces. *The Journal of Physical Chemistry Letters*, 12, 5279–5285. https://doi.org/10.1021/acs.jpclett.1c01134. doi: 10.1021/acs.jpclett.1c01134

Zou, X., Gu, S., Lu, X., Xie, X., Lu, C., Zhou, Z., & Ding, W. (2015). Electroreduction of iron(iii) oxide pellets to iron in alkaline media: A typical shrinking-core reaction process. *Metallurgical and Materials Transactions B*, 46, 1262–1274. https://doi.org/10.1007/s11663-015-0336-8

Appendix

.1. Laboratory Set-up

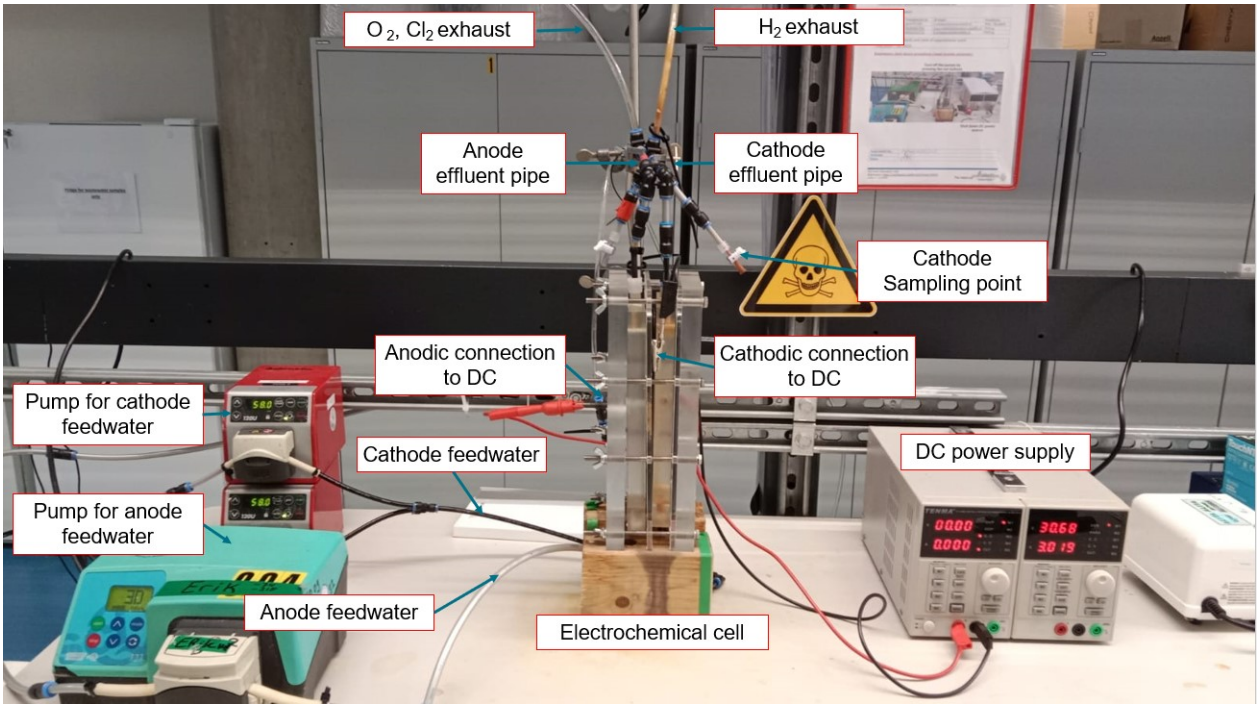

Figure 1: Lab Set-up for the study

.2. Calculations for depositions

The thickness of deposition was calculated with the help of the measurements of the concentrations in the effluent and the flow rate at a given time. This gives the number of moles of an element present in the deposit. Next, the mass of the deposit can be found with the help of density/mol data available on the metal. The manufacturer has provided the dimensions of the cathode which were further cross-checked in the lab. With this information, the average thickness of the deposit on the cathode surface area is found. Below are the calculations involved:

Length of the stainless steel cathode mesh = 20 cm
Width of the stainless steel cathode mesh = 5 cm
Diameter of wire, d = 0.26 mm
Mesh opening size, s = 0.586 mm ((wirecloth nd), Kingdelong Wiremesh Co. Ltd.)
Open area = $s^2/(s^2 + d^2)$ = 48% ((wirecloth nd))
Mesh area, A = 10404.12678 mm2 = 104.04 cm2
Density, D = 7870 mg/cm3
Volume, V = Concentrations * Volume of effluent treated
Mass, M = V * D
Thickness (calculated in μm) = V / A

pH	Mass Deposited, M (mg)	Volume (cm3)	M/Area	Thickness of deposit (cm)	Thickness of deposit (µm)
4	8.90E+00	1.13E-03	8.55E-02	1.09E-05	0.109
6	2.47E+01	3.14E-03	2.37E-01	3.02E-05	0.302
7	5.16E+01	6.56E-03	4.96E-01	6.30E-05	0.630
8	5.24E+01	6.66E-03	5.04E-01	6.40E-05	0.640

Table 1: Fe depositions over 70 minutes of electrochemical reduction for the individual case.

pH	Mass Deposited, M (mg)	Volume (cm3)	M/Area	Thickness of deposit (cm)	Thickness of deposit (µm)
4	9.45E-02	1.32E-05	9.08E-04	1.265E-07	0.001
6	2.27E+00	3.16E-04	2.18E-02	3.0361E-06	0.030
7	1.59E+01	2.22E-03	1.53E-01	2.1337E-05	0.213

Table 2: Mn depositions over 70 minutes of electrochemical reduction for the individual case.

.2.1. Deposits from electrochemical reduction of Fe^{2+} and Mn^{2+} individually

.2.2. Deposits of Fe, Mn from combined case with electrochemical reduction

pH	Mass Deposited, M (mg)	Volume (cm3)	M/Area	Thickness of deposit (cm)	Thickness of deposit (µm)
4	5.48E+00	6.96E-04	5.27E-02	6.69E-06	0.067
6	1.24E+01	1.57E-03	1.19E-01	1.51E-05	0.151
7	1.82E+01	2.32E-03	1.75E-01	2.23E-05	0.223

Table 3: Fe depositions over 70 minutes of electrochemical reduction for the combined case.

pH	Mass Deposited, M (mg)	Volume (cm3)	M/Area	Thickness of deposit (cm)	Thickness of deposit (µm)
4	0.00E+00	0.00E+00	0.00E+00	0.00E+00	0.000
6	8.51E-01	1.18E-04	8.17E-03	1.14E-06	0.011
7	2.52E+00	3.51E-04	2.42E-02	3.37E-06	0.034

Table 4: Mn depositions over 70 minutes of electrochemical reduction for the combined case.

.3. Combined experiments over pH 4 and pH 6 results

In the case of Mn for pH 4 (2b) and pH 6 (2d), the effluent concentrations are as high as the influent concentration of 0.72 mmol/L. It is apparent that the cathodic reduction of Fe^{2+} exceeds the cathodic reduction of Mn^{2+} across all pH and timestamps. This implies that the standard system settings for the study were less conducive towards Mn^{2+} reduction. Also, for Mn^{2+}, the cathodic reduction was most observed in pH 7, followed by pH 6, and for pH 4 it was the least. This was similar to the result obtained for the cathodic reduction of Fe^{2+}.

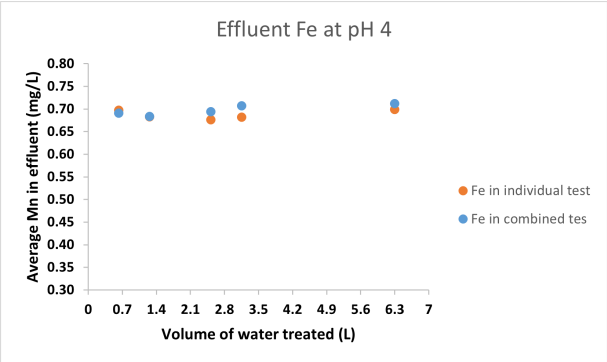

(a) Fe in pH 4

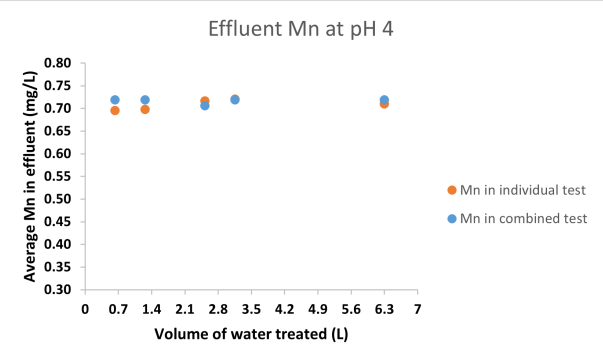

(b) Mn in pH 4

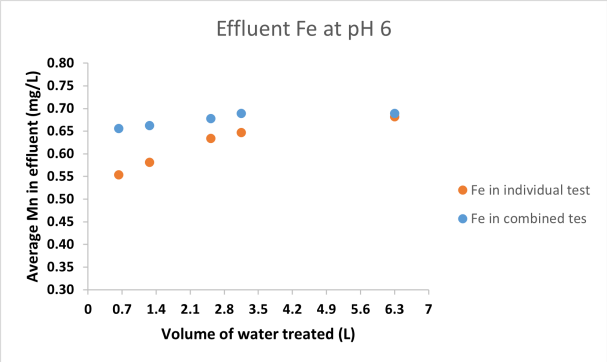

(c) Fe in pH 6

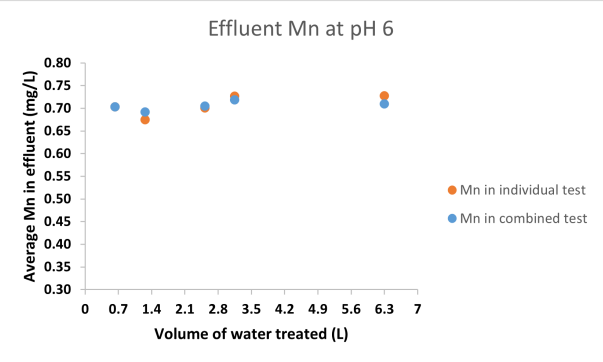

(d) Mn in pH 6

Figure 2: Comparison of metal ions in the effluent in the individual experiment with metal ions in the combined experiment with respect to the volume of water treated

.4. Voltages across all pH

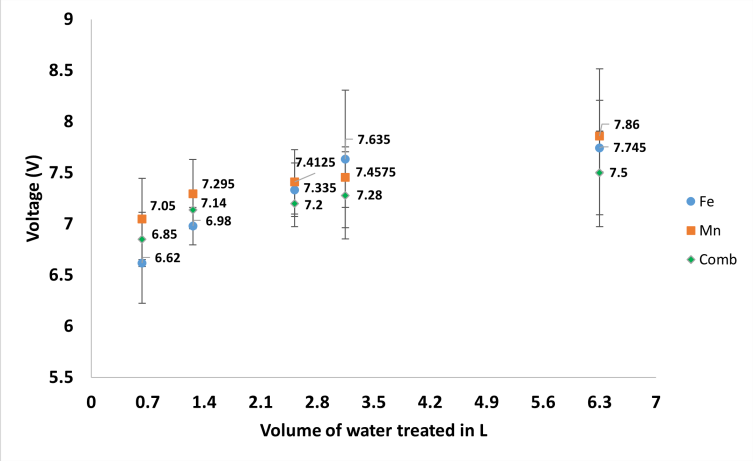

Figure 3: Voltage of the system at pH 4

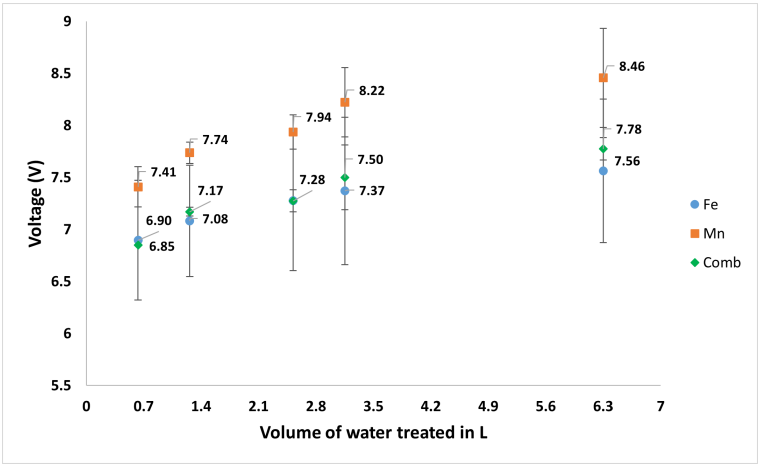

Figure 4: Voltage of the system at pH 6

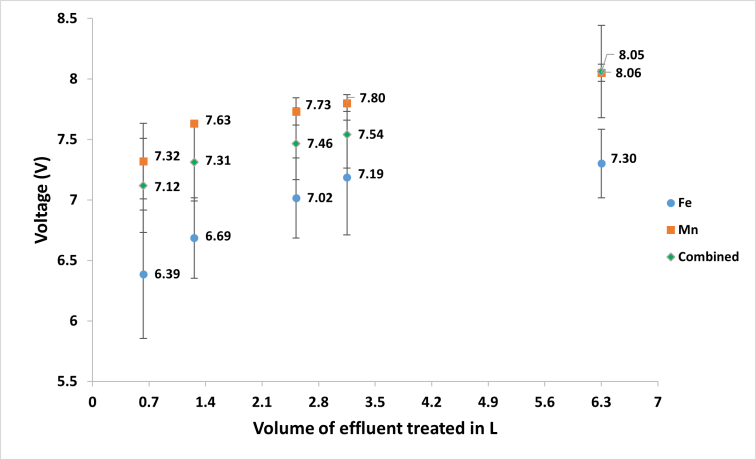

Figure 5: Voltage of the system at pH 7

.5. pH of the effluent

The pH is declining for Fe and Mn individual experiments, while it is rising for the combined experiments. The pH of the effluent for the experiments with a water matrix of pH 7 was analyzed to understand the pH changes in the effluent collected during the functioning of the electrochemical cell to treat water. However, there was a lack of clear trends in the effluent pH. With H_2 side reaction at the cathode, the concentration of OH^- ions rises, increasing the pH of the system. In this study when the electrochemical reduction of the metal ions increases, the FE increases, and the H_2 side reaction declines. This is because both metal and H^+ ions are competing for the electrons supplied at the cathode. Therefore, the increase in the effluent pH is subverted when the electrochemical reduction of metal ions is high. As the volume of water treated is increasing, the electrochemical reduction of the metal ions changes, which in turn affects the pH. Further, the effluent pH is affected due to the purging of CO_2 and N_2 in order to keep the cathode feedwater anoxic in this study. Both CO_2 and N_2 are capable of impacting the pH of a system, and while efforts were made to ensure the cathode feedwater pH stays constant, there were still small deviations because of less control. It can be deduced that multiple variable affect the effluent pH and henceforth no clear trend is observed. It calls for further study.

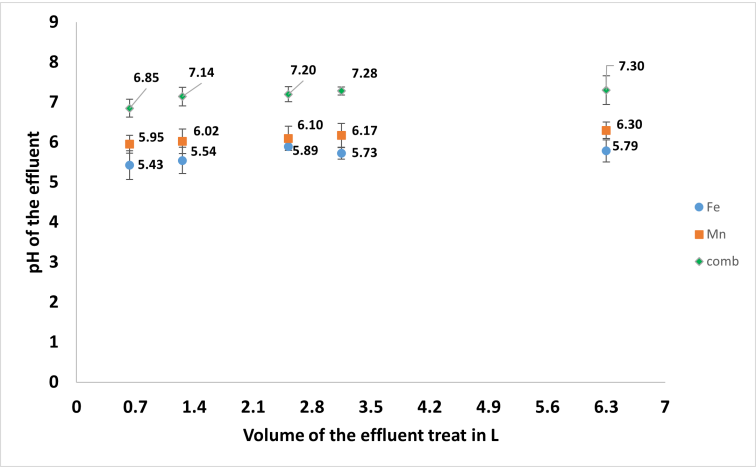

Figure 6: Change in effluent pH with influent pH 4

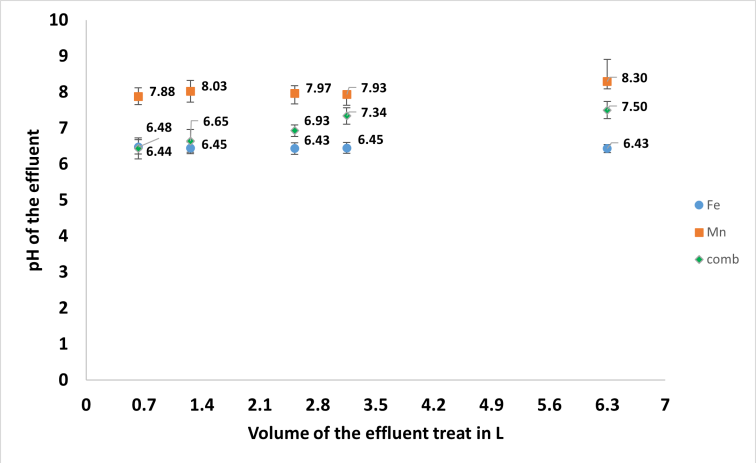

Figure 7: Change in effluent pH with influent pH 6

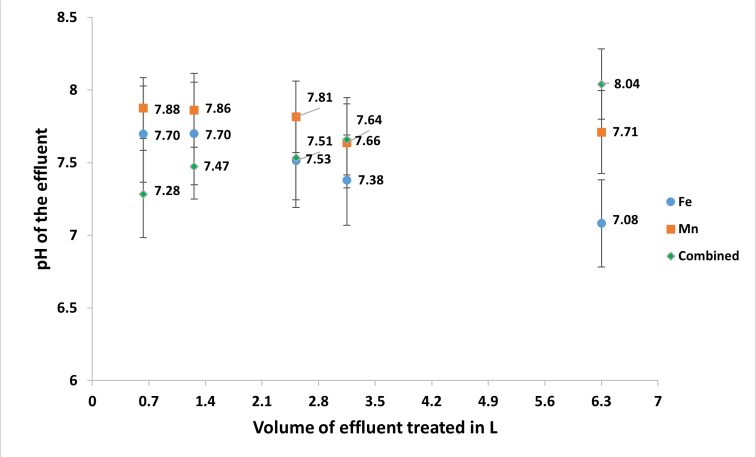

Figure 8: Change in effluent pH with influent pH 7

.6. SEM-EDS point scan element composition results

This section provides the elemental analysis for the 3 points selected on the cathode for each experiment (both individual and combined).

.6.1. Fe point scan

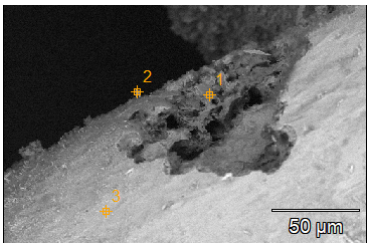

Figure 9: Point scan for Fe

Weight %

	C	O	Na	Al	Si	S	Cl	Cr	Mn	Fe	Ni	Mo
Fe1(1)_pt1	6.49	17.94	1.02	4.85	0.51		0.28	12.54		53.16	2.58	0.63
Fe1(1)_pt2	12.02	14.40	1.14	5.23	0.48			9.82	0.77	53.64	2.49	
Fe1(1)_pt3	1.34	2.63	0.29	1.75	0.15	0.09		14.82	4.35	73.03	1.55	

Table 5: Point-scan for Fe (element weight percentage)

Atom %

	C	O	Na	Al	Si	S	Cl	Cr	Mn	Fe	Ni	Mo
Fe1(1)_pt1	17.12	35.54	1.41	5.69	0.58		0.25	7.65		30.17	1.39	0.21
Fe1(1)_pt2	29.73	26.72	1.48	5.76	0.51			5.61	0.42	28.52	1.26	
Fe1(1)_pt3	5.43	7.98	0.62	3.14	0.26	0.13		13.84	3.84	63.48	1.29	

Table 6: Point-scan for Fe (element atom percentage)

Compound %

	C	O	Na	Al	Si	S	Cl	Cr	Mn	Fe	Ni	Mo
Fe1(1)_pt1	6.49	17.94	1.02	4.85	0.51		0.28	12.54		53.16	2.58	0.63
Fe1(1)_pt2	12.02	14.40	1.14	5.23	0.48			9.82	0.77	53.64	2.49	
Fe1(1)_pt3	1.34	2.63	0.29	1.75	0.15	0.09		14.82	4.35	73.03	1.55	

Table 7: Point-scan for Fe (element compound percentage)

.6.2. Mn point scan

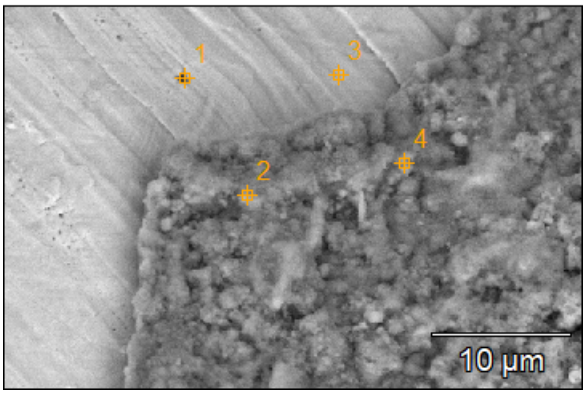

Figure 10: Point scan Mn

Weight %

	C	O	F	Mg	Al	Si	S	Cl	Ca	V	Cr	Mn	Fe	Ni	As	Mo
Mn(1)_pt 1	2.31	6.54			0.16	0.40				0.15	17.50	4.77	57.37	8.84	0.09	1.86
Mn(1)_pt 2	3.38	35.43	7.34		0.05	0.12			0.06		0.28	53.34				
Mn(1)_pt 3	1.71	0.59		0.04		0.48					16.67	1.57	67.01	9.78		2.14
Mn(1)_pt 4	5.75	43.54	0.00		0.07	0.20	0.03	0.05	0.07		0.42	49.86				

Figure 11: Element percentage by weight

Atom %

	C	O	F	Mg	Al	Si	S	Cl	Ca	V	Cr	Mn	Fe	Ni	As	Mo
Mn(1)_pt 1	8.57	18.20			0.26	0.64				0.13	14.98	3.87	45.73	6.70	0.05	0.86
Mn(1)_pt 2	7.28	57.28	9.99		0.04	0.11			0.04		0.14	25.11				
Mn(1)_pt 3	7.35	1.90		0.08		0.89					16.56	1.48	61.98	8.61		1.15
Mn(1)_pt 4	11.59	65.90	0.00		0.06	0.17	0.02	0.04	0.05		0.20	21.98				

Figure 12: Element percentage by no of atoms

Compound %

	C	O	F	Mg	Al	Si	S	Cl	Ca	V	Cr	Mn	Fe	Ni	As	Mo
Mn(1)_pt 1	2.31	6.54			0.16	0.40				0.15	17.50	4.77	57.37	8.84	0.09	1.86
Mn(1)_pt 2	3.38	35.43	7.34		0.05	0.12			0.06		0.28	53.34				
Mn(1)_pt 3	1.71	0.59		0.04		0.48					16.67	1.57	67.01	9.78		2.14
Mn(1)_pt 4	5.75	43.54	0.00		0.07	0.20	0.03	0.05	0.07		0.42	49.86				

Figure 13: Element percentage by compounds

.6.3. Al point scan

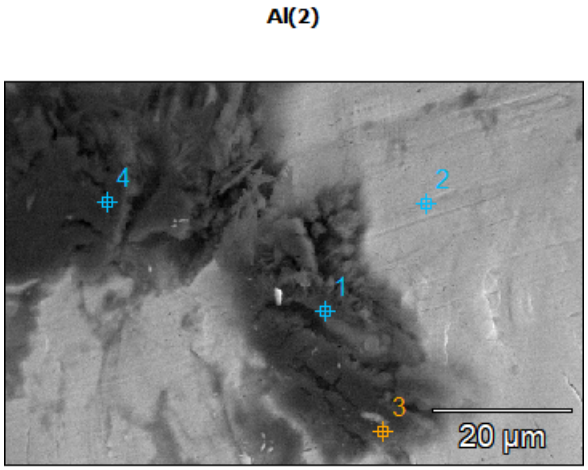

Figure 14: Point scan Al

Weight %

	C	O	F	Na	Al	Si	Cl	K	Cr	Mn	Fe	Ni	Mo
Al(2)_pt1	1.04	5.46	0.00	10.94	0.24	3.43	0.16	0.11	13.78	1.11	55.26	7.16	1.30
Al(2)_pt2	1.22	1.79		1.45	0.41	0.42			16.60	1.03	65.99	9.40	1.70
Al(2)_pt3	1.37	3.45		5.26	0.36	0.66			15.77	1.40	63.28	7.42	1.05
Al(2)_pt4	0.66	5.02		11.20	0.05	1.35			14.05	1.15	57.41	8.00	1.12

Figure 15: Element percentage by weight

Atom %

	C	O	F	Na	Al	Si	Cl	K	Cr	Mn	Fe	Ni	Mo
Al(2)_pt1	3.53	13.92	0.00	19.40	0.36	4.98	0.19	0.12	10.81	0.83	40.34	4.98	0.55
Al(2)_pt2	5.05	5.59		3.15	0.75	0.74			15.93	0.93	58.98	7.99	0.89
Al(2)_pt3	5.18	9.82		10.43	0.60	1.07			13.82	1.16	51.65	5.76	0.50
Al(2)_pt4	2.31	13.22		20.53	0.08	2.02			11.39	0.88	43.33	5.74	0.49

Figure 16: Element percentage by no of atoms

Compound %

	C	O	F	Na	Al	Si	Cl	K	Cr	Mn	Fe	Ni	Mo
Al(2)_pt1	1.04	5.46	0.00	10.94	0.24	3.43	0.16	0.11	13.78	1.11	55.26	7.16	1.30
Al(2)_pt2	1.22	1.79		1.45	0.41	0.42			16.60	1.03	65.99	9.40	1.70
Al(2)_pt3	1.37	3.45		5.26	0.36	0.66			15.77	1.40	63.28	7.42	1.05
Al(2)_pt4	0.66	5.02		11.20	0.05	1.35			14.05	1.15	57.41	8.00	1.12

Figure 17: Element percentage by compounds

.6.4. Combined point scan

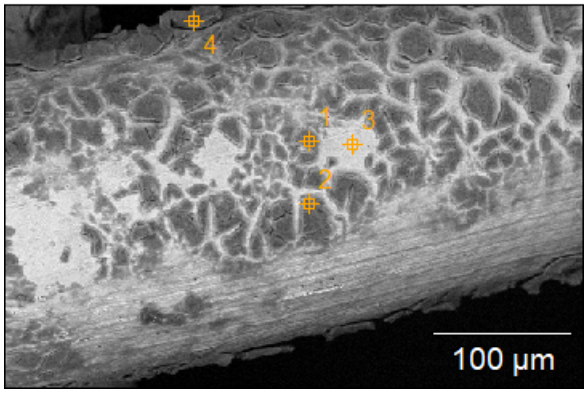

Figure 18: Point scan combined

Weight %

	C	O	F	Na	Al	Si	S	Cl	Cr	Mn	Fe	Ni	Mo
Com(1)_pt1	1.56	20.85	0.00	2.15	11.54	0.13	1.66	1.07	5.68	15.37	38.36	1.63	
Com(1)_pt2	0.77	7.73	0.00	0.76	2.98	0.26		0.24	14.22	3.37	59.43	8.28	1.96
Com(1)_pt3	0.74	2.12			0.56	0.32			16.13	3.15	65.98	9.42	1.58
Com(1)_pt4	2.81	4.31	0.00	0.28	1.28	0.06	0.19	0.27	0.84	35.59	54.35		

Figure 19: Element percentage by weight

Atom %

	C	O	F	Na	Al	Si	S	Cl	Cr	Mn	Fe	Ni	Mo
Com(1)_pt1	4.12	41.45	0.00	2.98	13.60	0.15	1.64	0.96	3.47	8.89	21.84	0.88	
Com(1)_pt2	2.83	21.31	0.00	1.46	4.88	0.41		0.30	12.06	2.70	46.93	6.22	0.90
Com(1)_pt3	3.16	6.78			1.06	0.57			15.90	2.94	60.52	8.22	0.85
Com(1)_pt4	10.56	12.16	0.00	0.55	2.15	0.10	0.27	0.34	0.73	29.23	43.91		

Figure 20: Element percentage by no of atoms

Compound %

	C	O	F	Na	Al	Si	S	Cl	Cr	Mn	Fe	Ni	Mo
Com(1)_pt1	1.56	20.85	0.00	2.15	11.54	0.13	1.66	1.07	5.68	15.37	38.36	1.63	
Com(1)_pt2	0.77	7.73	0.00	0.76	2.98	0.26		0.24	14.22	3.37	59.43	8.28	1.96
Com(1)_pt3	0.74	2.12			0.56	0.32			16.13	3.15	65.98	9.42	1.58
Com(1)_pt4	2.81	4.31	0.00	0.28	1.28	0.06	0.19	0.27	0.84	35.59	54.35		

Figure 21: Element percentage by compounds

.7. Anode and Cathode switching experiment

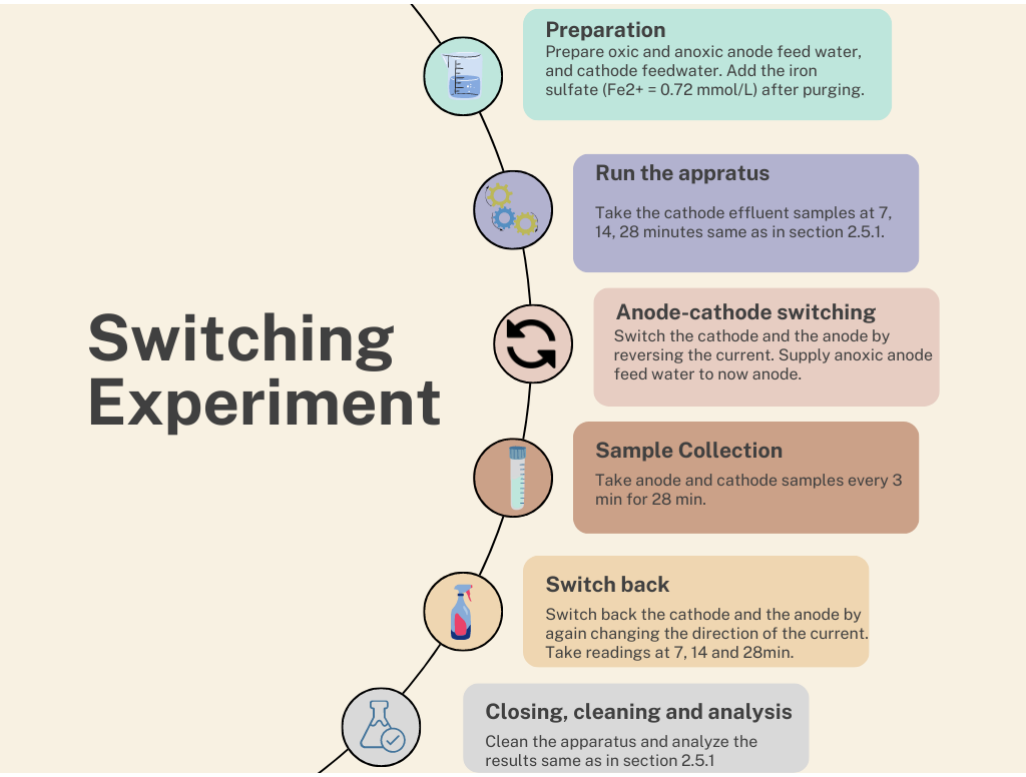

Figure 22: Step-wise methodology for the switching experiment

In this experiment, the objective was to investigate the impact of switching the anode (chamber 1) and cathode (chamber 2) of the electrochemical cell. The switching of the cathode to the anode would have led to the release of the metal depositions formed over it due to the reduction process. This, in turn, would theoretically result in the presence of the metal concentration in the effluent of now 'anode' (chamber 2). The stainless steel mesh electrodes were used for both the anode and the cathode. The anode chamber (chamber 1) was filled with oxic anode feed water containing, while the cathode chamber (chamber 2) was filled with anoxic cathode feed water containing 0.72 mmol/L concentration Fe^{2+} in the form of $Fe_2SO_4.7H_2O$. The charge dosage was set at 200 C/L, and the current density was maintained at 30 A/m_2. Initially, the effluent at chamber 2 was collected at timestamps of 7 min, 14 min, and 28 min. After this, the cathode and anode of the system were reversed by changing the direction of the current from the DC power current supply. After changing the current direction, the cathode feed water in chamber 2 was stopped and instead, the now anode chamber (chamber 2) was supplied with anoxic anode feed water containing only NaCl and $NaHCO_3$ to prevent oxidation and settlement of the depositions. The effluent samples from chamber 1 and chamber 2 were taken every 2 minutes for 14 minutes. After 14 minutes, the current was switched back, restoring the

anode in chamber 1 and the cathode in chamber 2. Cathode feed water containing Fe^{2+} was also restored in chamber 2. Effluent readings at 7 min, 14 min, and 28 min intervals were taken from chamber 2 to compare them with the readings obtained in the first step. Tests were performed on the collected effluent samples to determine the presence of Fe and Cl_2.

.8. Pourbaix diagrams for Fe, Mn and Al

Fig 23 shows the pourbaix diagram of Fe for pH 4-8, it can be seen that Fe (s) has a very big window of formation. Further, Fe^{2+} needs the lower absolute value of negative potential to be supplied (-0.44 V vs SHE), which makes its chances of electrochemically reducing high. It was observed throughout the experiment with Fe^{2+} electrochemically reduced more effectively compared to Mn^{2+}. In the case of Mn in Fig 24, it is observed that it can be reduced at a broad pH range the absolute value of the negative potential to be supplied is much higher (-1.18 V vs SHE) than that of Fe^{2+}. This impacts Mn^{2+} reduction performance in comparison to Fe^{2+}. Additionally, beyond the potential supplied, other factors also impact electrochemical reduction which may have resulted in the performance differences in Fe and Mn electrochemical reduction. The pourbaix diagrams also indicate the inactivity of Al^{3+}. In Fig 25, it is clearly visible that Al(s) has a very low window of formation and it gets much lesser in the case of pH 7, which was the sampling point for SEM-EDS.

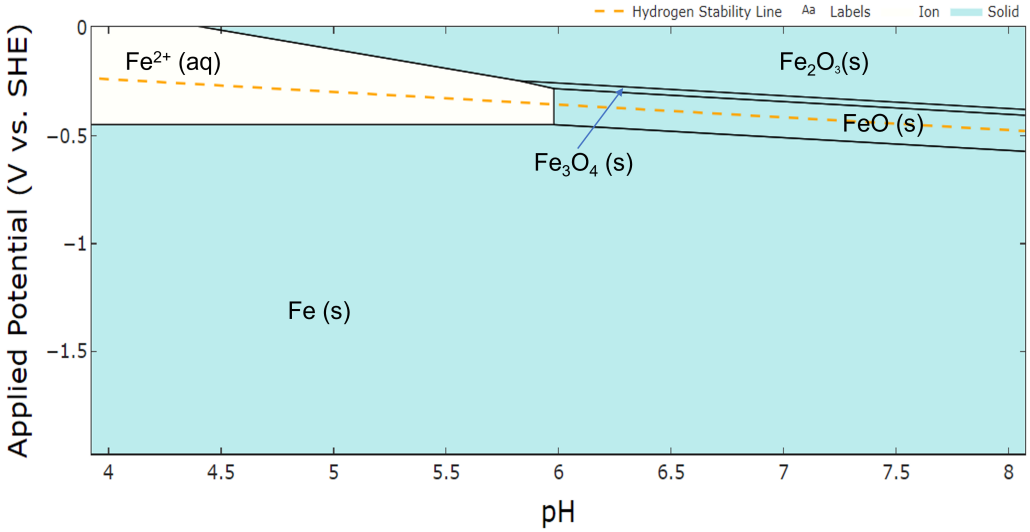

Figure 23: Pourbaix diagram for Fe^{2+}

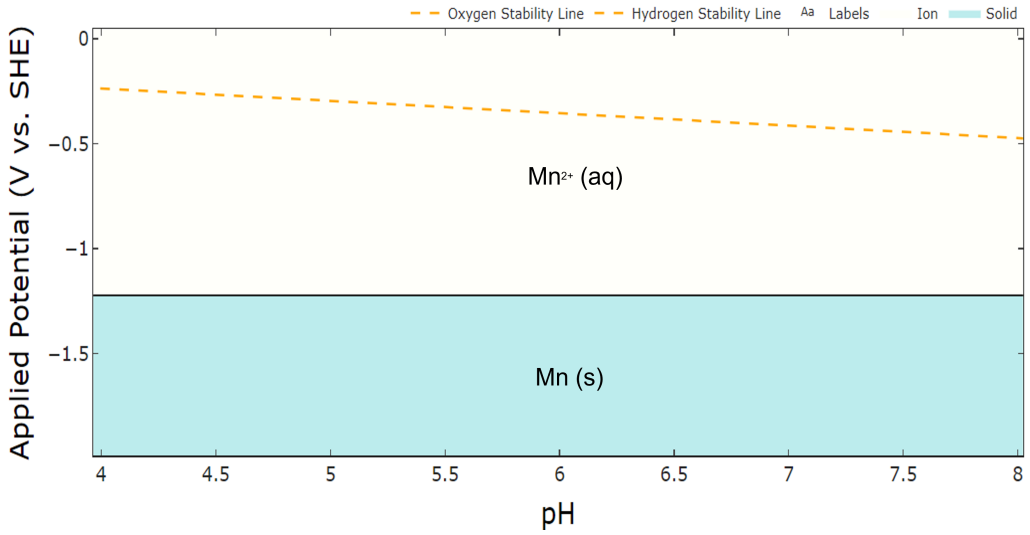

Figure 24: Pourbaix diagram for Mn^{2+}

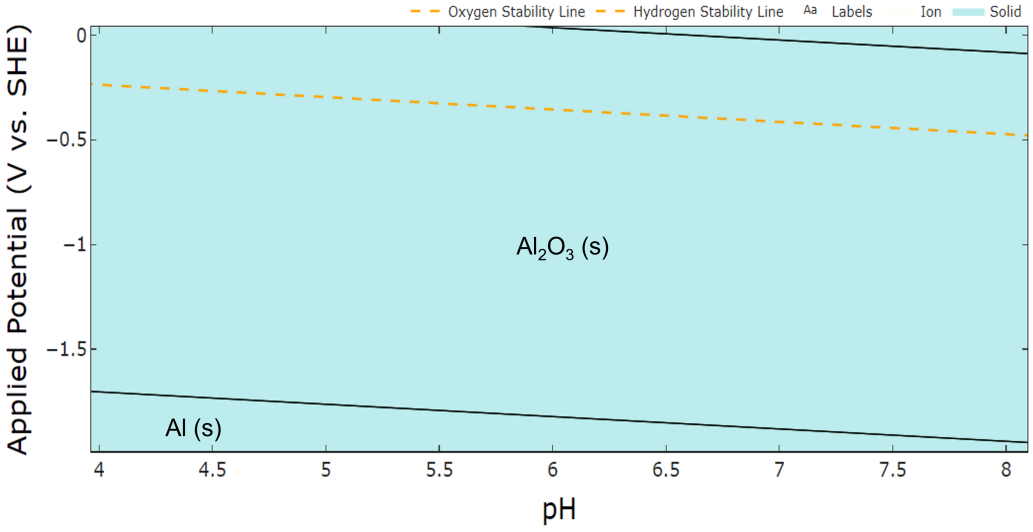

Figure 25: Pourbaix diagram for Al^{3+}

.9. PHREEQC simulations

.9.1. PHREEQC Al

```
DATABASE WATEQ4F.DAT
SOLUTION  1 Input reactor
-units    mmol/l
-temp     19
pH        7
Alkalinity 2.143 as HCO3
Na        11.54
Cl        9.402 as NaCl
Al        0.5578 as Al2(SO4)3.14H2O
S(6)      0.7162
-water    10000 gram
END
```

Figure 26: Al PHREEQC code at pH 7

```
------------------------------Saturation indices---------------------------------

  Phase               SI** log IAP   log K(292 K,   1 atm)

  Al(OH)3(a)           1.76     12.96   11.20  Al(OH)3
  Basaluminite        11.77     34.47   22.70  Al4(OH)10SO4
  Boehmite             3.95     12.96    9.01  AlOOH
  CO2(g)              -5.10     -6.50   -1.39  CO2
  Diaspore             5.71     12.96    7.25  AlOOH
  Gibbsite             4.50     12.96    8.45  Al(OH)3
  H2(g)              -22.00    -25.12   -3.12  H2
  H2O(g)              -1.67     -0.00    1.67  H2O
  Halite              -5.63     -4.06    1.57  NaCl
  Jurbanite           -1.16     -4.39   -3.23  AlOHSO4
  Mirabilite          -5.92     -7.32   -1.40  Na2SO4:10H2O
  Nahcolite           -7.27     -7.87   -0.60  NaHCO3
  Natron             -11.70    -13.25   -1.55  Na2CO3:10H2O
  O2(g)              -41.26    -44.11   -2.85  O2
  Thenardite          -7.15     -7.32   -0.17  Na2SO4
  Thermonatrite      -13.41    -13.24    0.17  Na2CO3:H2O
  Trona              -20.59    -21.12   -0.52  NaHCO3:Na2CO3:2H2O
```

Figure 27: Al PHREEQC output on the different SI at pH 7

```
------------------------------Saturation indices---------------------------------

  Phase               SI** log IAP   log K(292 K,   1 atm)

  Al(OH)3(a)         1.90     13.10    11.20  Al(OH)3
  Basaluminite      14.34     37.04    22.70  Al4(OH)10SO4
  Boehmite           4.09     13.10     9.01  AlOOH
  CO2(g)            -1.38     -2.78    -1.39  CO2
  Diaspore           5.85     13.10     7.25  AlOOH
  Gibbsite           4.65     13.10     8.45  Al(OH)3
  H2(g)            -20.00    -23.12    -3.12  H2
  H2O(g)            -1.67     -0.00     1.67  H2O
  Halite            -5.63     -4.06     1.57  NaCl
  Jurbanite          0.97     -2.26    -3.23  AlOHSO4
  Mirabilite        -5.94     -7.34    -1.40  Na2SO4:10H2O
  Nahcolite         -4.55     -5.15    -0.60  NaHCO3
  Natron            -9.98    -11.53    -1.55  Na2CO3:10H2O
  O2(g)            -45.26    -48.11    -2.85  O2
  Thenardite        -7.17     -7.34    -0.17  Na2SO4
  Thermonatrite    -11.69    -11.53     0.17  Na2CO3:H2O
  Trona            -16.16    -16.68    -0.52  NaHCO3:Na2CO3:2H2O
```

Figure 28: Al PHREEQC output on the different SI at pH 6

.9.2. PHREEQC Mn

```
DATABASE WATEQ4F.DAT
SOLUTION  1 Input reactor
-units    mmol/l
-temp     19
pH        8
Alkalinity 2.143 as HCO3
Na        11.54
Cl        9.402 as NaCl
Mn(2)     0.7162 as MnSO4.H2O
S(6)      2.1486
-water    10000 gram
end
```

Figure 29: Mn PHREEQC code at pH 8

```
-----------------------------Saturation indices-------------------------------

Phase               SI** log IAP   log K(292 K,   1 atm)

Birnessite        -7.15     36.45   43.60  MnO2
CO2(g)            -3.02     -4.41   -1.39  CO2
H2(g)            -24.00    -27.12   -3.12  H2
H2O(g)            -1.67     -0.00    1.67  H2O
Halite            -5.65     -4.08    1.57  NaCl
Hausmannite       -1.18     61.36   62.54  Mn3O4
Manganite         -0.89     24.45   25.34  MnOOH
Mirabilite        -5.50     -6.90   -1.40  Na2SO4:10H2O
MnCl2:4H2O       -10.16     -7.71    2.45  MnCl2:4H2O
MnSO4             -9.35     -6.45    2.90  MnSO4
Nahcolite         -4.19     -4.80   -0.60  NaHCO3
Natron            -7.63     -9.18   -1.55  Na2CO3:10H2O
Nsutite           -6.11     36.45   42.56  MnO2
O2(g)            -37.26    -40.11   -2.85  O2
Pyrochroite       -2.75     12.45   15.20  Mn(OH)2
Pyrolusite        -5.91     36.45   42.36  MnO2
Rhodochrosite      2.37     -8.73  -11.11  MnCO3
Rhodochrosite(d)   1.66     -8.73  -10.39  MnCO3
Thenardite        -6.73     -6.90   -0.17  Na2SO4
Thermonatrite     -9.35     -9.18    0.17  Na2CO3:H2O
Trona            -13.45    -13.98   -0.52  NaHCO3:Na2CO3:2H2O
```

Figure 30: Mn PHREEQC output on the different SI at pH 8

.9.3. PHREEQC Fe

```
DATABASE WATEQ4F.DAT
SOLUTION  1 Input reactor
-units    mmol/l
-temp     19
pH        8
Alkalinity 2.143 as HCO3
Na        11.54
Cl        9.402 as NaCl
Fe(2)     0.7162 as FeSO4.7H2O
S(6)      0.7162
-water    10000 gram
END
```

Figure 31: Fe PHREEQC code at pH 8

```
-----------------------------Saturation Indices---------------------------------

  Phase               SI** log IAP   log K(292 K,   1 atm)

  CO2(g)            -2.98     -4.38   -1.39  CO2
  H2(g)            -24.00    -27.12   -3.12  H2
  H2O(g)            -1.67     -0.00    1.67  H2O
  Halite            -5.64     -4.07    1.57  NaCl
  Melanterite       -4.54     -6.83   -2.28  FeSO4:7H2O
  Mirabilite        -5.95     -7.35   -1.40  Na2SO4:10H2O
  Nahcolite         -4.15     -4.76   -0.60  NaHCO3
  Natron            -7.58     -9.13   -1.55  Na2CO3:10H2O
  O2(g)            -37.26    -40.11   -2.85  O2
  Siderite           2.25     -8.60  -10.85  FeCO3
  Siderite(d)(3)     1.85     -8.60  -10.45  FeCO3
  Thenardite        -7.18     -7.35   -0.17  Na2SO4
  Thermonatrite     -9.30     -9.13    0.17  Na2CO3:H2O
  Trona            -13.36    -13.89   -0.52  NaHCO3:Na2CO3:2H2O
```

Figure 32: Fe PHREEQC output on the different SI at pH 8

.10. Cathode composition

Item	Chemical Composition											Physical Property	
Grade	C	Si	Mn	P	S	Cr	Ni	Mo	Cu	Pb	Sn	T.S.Mpa	EL. %
AISI 316	0.01	0.360	1.180	0.019	0.001	17.160	11.900	2.050	0.03	0.001	0.001	640	54

Figure 33: Composition of stainless steel woven mesh cathode made of AISI 316 material. (Kingdelong Wiremesh Co. Ltd.)

.11. Initial Tests

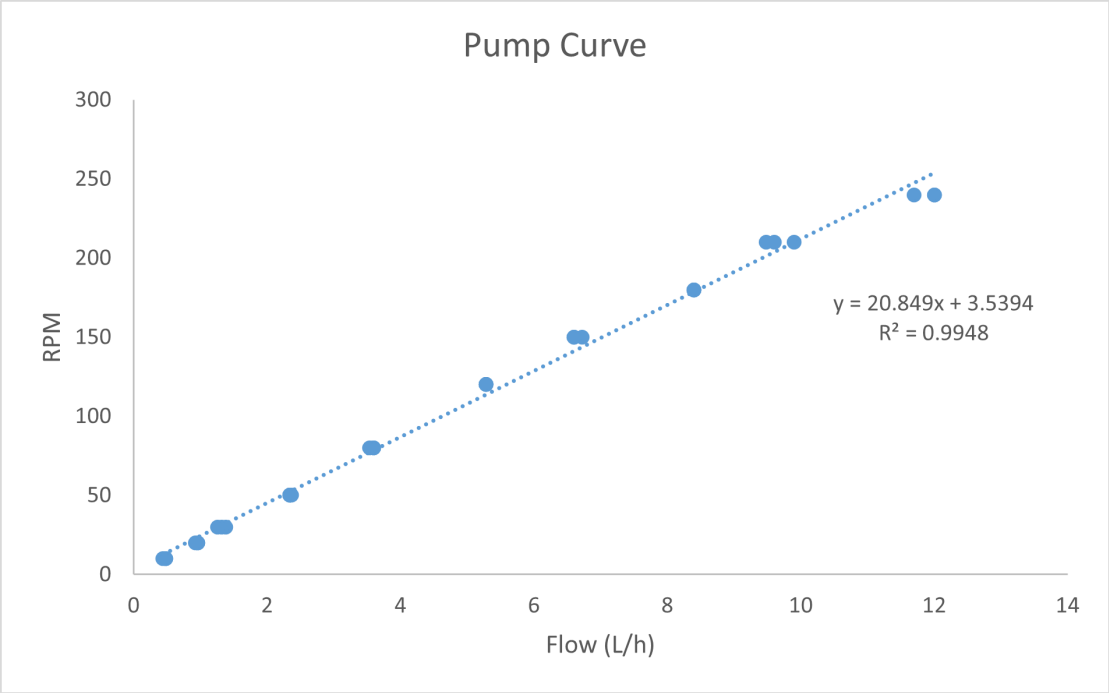

Figure 34: Pump curve for flowthrough experiments

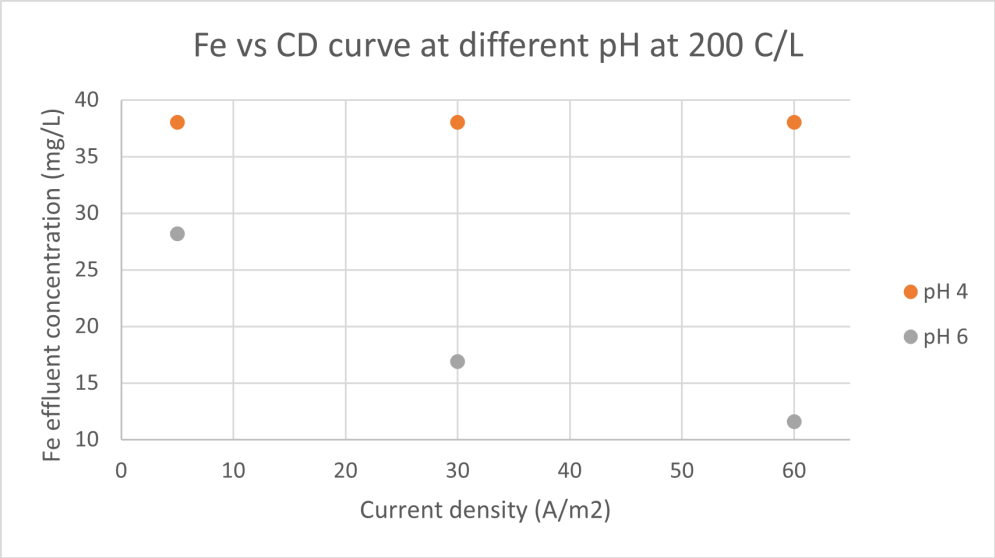

Figure 35: Variable current density experiments

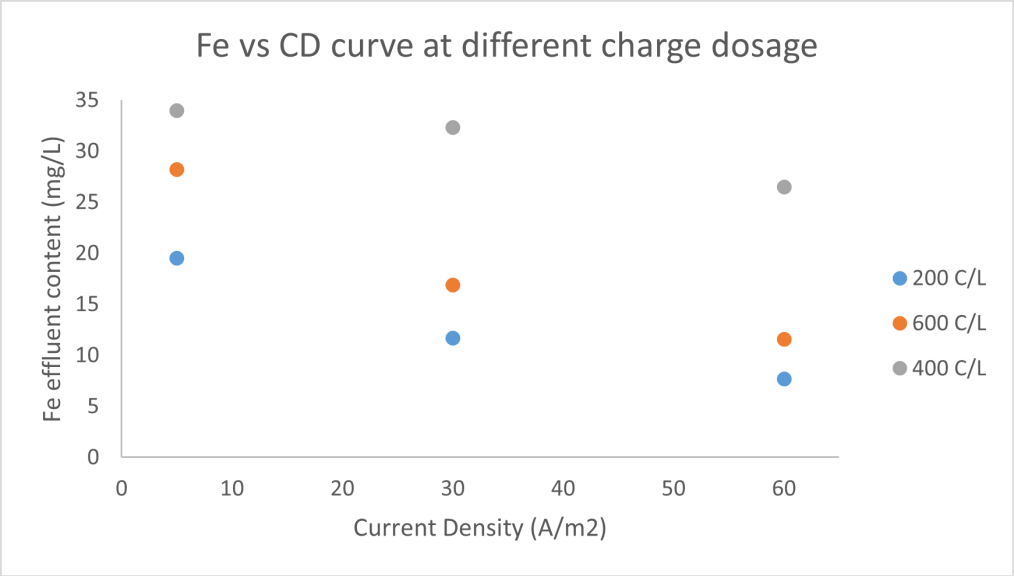

Figure 36: Variable charge dosage experiments

.12. Mechanism of electrochemical reduction and important parameters

In electrochemical reduction, the reactant moves from the bulk region to the electrode surface region and gains externally supplied electrons from the cathode's surface. The movement of the reactant in and out of the cathode-electrolyte interface is important for predicting the current flow. The transport of the reactant i.e. mass transport, can occur by diffusion, convection, and migration. These can influence the electrochemical reduction (Cambridge nd). Taking into consideration a cathodic reaction:

$$O + ne^{-} \rightarrow R \tag{1}$$

A series of steps convert the dissolved O (metal ions) into a reduced form R. The current (or electrode reaction rate) is governed by the rates of processes given by:

- Mass transfer from the bulk solution to the electrode surface.
- Electron transfer at the surface of the electrode.
- Chemical reactions on the electrode surface preceding or following the electron transfer.
- Surface reactions, such as adsorption, desorption, or electrodeposition (Bard & Faulkner 1980).

.12.1. Important information related to electrochemical reduction

Electrode material

The electrode material selected must have high activation energies for undesired side reactions. For instance, cathode material such as Pb, Cd has high overpotential for H_2 evolution, which helps in more reduction of metal ions and avoids the wastage of electrical energy (Sáenz et al. 2012b), i.e. target higher faradaic efficiencies for the reduction of metals. In this study, the electrodes should ideally have high hydrogen overpotential so that the side-reaction of H_2 production at the cathode should be minimized and Fe, Mn, and Al production is maximized. Further, an ideally designed electrode has high surface roughness for a larger surface area, high exchange current densities, and steep Tafel slopes. In a previous study, multiple cathodes were tried to find out the cathodes with the highest hydrogen overpotential, and Pt, graphite-based cathodes seemed to

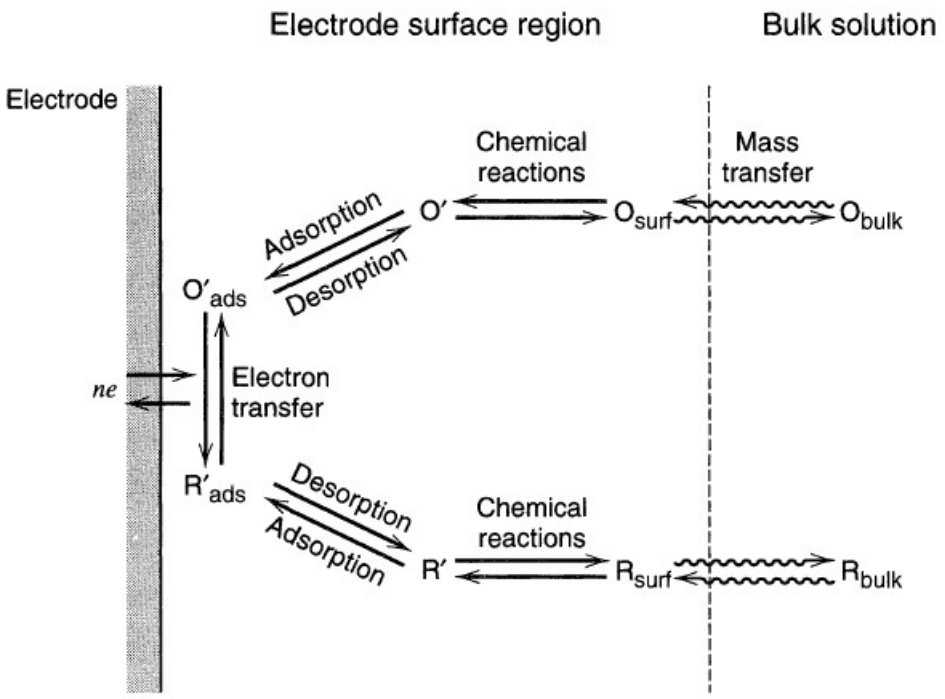

Figure 37: Reaction pathway for electrochemical reduction. Source: (Bard & Faulkner 1980)

perform the best (Sáenz et al. 2012a). This results in a high electron transfer rate i.e. higher current and lower voltage. The overpotential for hydrogen evolution on the specific cathodic material is related to the binding of hydrogen on the surface. A good cathode for the H_2 reaction is characterized by having a high exchange rate which is based on the low binding energy of hydrogen onto the surface and minimal barriers for the surface reactions (Durst et al. 2014).

Electric Double Layer

When a metal is dipped in an electrolyte, an electric double layer is formed. The electric double layer- which is a thin electrolyte layer, is located adjacent to the surface of the electrode. It is responsible for determining the potential of the metal (Bard & Faulkner 1980). Here, the ions are able to move in a solution and so the electrostatic interactions are in competition with Brownian motion. The passage of electric current through metal–electrolyte interface results in the transformation of constituents of the electrolyte on the electrode's surface resulting in the consumption of initial reagents and the accumulation of reduction products on the cathode. In electrochemical reduction, the reactant moves from the bulk region to the electrode surface region and gains externally supplied electrons from the cathode's surface. The movement of the reactant in and out of the cathode-electrolyte interface is important for predicting the current flow. The transport of the reactant i.e. mass transport, can occur by diffusion, convection, and migration. These can influence the electrochemical reduction (Cambridge nd; Hao et al. 2019). The concentration changes and pH of the thin electrolyte layer in the course of electrolysis affects the cathodic deposition process (Tkalenko et al. 2002). The adsorption of H production is already detrimental to the metal recovery due to reduction in FE, it also gets adsorbed onto the cathode. This impacts the cathode's performance by blocking the cathode surface so that the reaction only occurs at the uncovered part of the cathode and it also affects the composition of the electrode surface region. However, it needs to be noted that SEM-EDS is not capable of capturing H. Therefore, other analytical techniques, such as XPS, could have worked better to investigate this issue (M & H 2019). The ions in the interface layer interact with the cathode through nonspecific adsorption, where long-range electrostatic forces unsettle the distribution of ions near the electrode surface and specific adsorption, in which a strong interaction between the ions and the electrode material causes the formation of a layer

(partial or complete) on the electrode surface (Bard & Faulkner 1980)

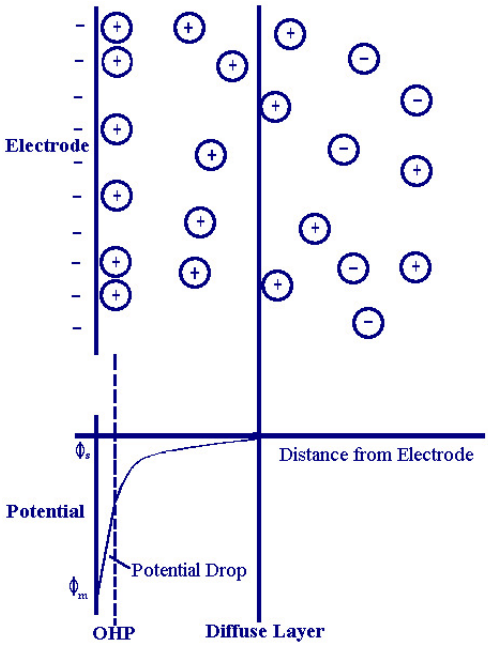

Figure 38: Cathode-bulk solution interface or electric double layer. The attracted ions are thought to approach the electrode surface and create a layer that balances the electrode charge. The distance of the approach is restricted by the ion's radius. Source: (Cambridge nd)

Metal Hydroxides at high pH

The pH of the cathode water can affect the reduction since the availability of the free metal ions (M^{n+}) changes. At higher pH in the case of Fe, there is the formation of Fe-based hydroxide species which participate in the reduction process (Díaz et al. 2008). Further, these hydroxide species impact the cathode-electrolyte interface and can generate non-faradaic processes such as adsorption-desorption. It is also observed that reduction at the cathode leads to an increase in the alkaline local pH values cathode-electrolyte interface (Grimm et al. 1998). As the pH of the cathode-electrolyte interface of the electrolyte increases, there will be deposition of the formation of hydroxides or basic salts of metals on the surface of the cathode. Other factors the combination of the electrodes (Sengupta et al. 2010; Sáenz et al. 2012b), pH of the cathode water (Felloni 1968), current density applied (Tkalenko et al. 2002) and type of ions in the cathode water (Antony et al. 2005).

E (reversible potential difference across the cathode-solution interface) is calculated with the help of the following equation:

$$E = Eo - \frac{RT}{nF} * ln(K) \tag{2}$$

where E is the potential applied in volts (V), Eo is the standard reversible potential (potential for the unit activity of all reactants and products), and K is the reaction quotient for the reaction in consideration. It can also be understood from the above equation that rate constant K for the electron transfer is proportional to the exponential of the potential applied (Cambridge nd).